Spectroscopy of indoles in argon matrices at 20K, with 1La origin identification
by Bruce Jonathon Fender

A thesis submitted in partial fulfillment of the requirements for the degree of Doctor of Philosophy in Chemistry
Montana State University
© Copyright by Bruce Jonathon Fender (1997)

Abstract:
The first site selected UV spectra (with polarization) of matrix isolated indole, 3-methylindole, 5-methylindole, 2-methylindole, 1-methylindole, 2,3-dimethyl indole, and 4-fluoroindole in argon at 20K were obtained. The main thrusts of this research is to locate the true 1La origin, and to characterize the fluorescence and the phosphorescence.

The true 1La origin for indole lies 1100-1300 cm^-1 (split) above the 1Lb origin and the true 1La origin was distinguished from its false 1La origin at 455 and 480 cm^-1 (jet). The fluorescence was identified as 1Lb and sharp (10 cm^-1) phosphorescence was obtained giving the Franck-Condon factors for La emission. The 1La origin for 3-methylindole was 260 cm^-1 (unsplit) above the 1Lb origin, which was verified both by fluorescence anisotropy and 2-photon measurements. The fluorescence was identified as 1Lb. For 2,3-dimethylindole the combined perturbation of the two methyl groups causes the inversion of states with the 1La being 190 cm^-1 below the 1Lb. This was verified by 1La fluorescence identification and by 2-photon measurements. The 1La fluorescence can be distinguished from its 1Lb counterpart.

The rest of the mono-methylated indoles emit from the 1Lb state and the 1La origin lies above the 1Lb as follows: 5-methylindole (1800 cm^-1), 2-methylindole (400-600 cm^-1), 1-methylindole (430-600 cm^-1). For 4-fluoroindole the 1La origin lies 1520 cm^-1 above the 1Lb and the fluorescence is characterized by a long Franck-Condon progression of the 26°1 mode.

Also included in this work is indole and 3-methylindole in N2 at 30K, 3-methylindole in ethanol at 15K, and 3-methylindole complexed with H2O and methanol in a supersonic jet.

This information will facilitate the use of tryptophan as a spectroscopic probe molecule in the understanding of protein structure and dynamics.

SPECTROSCOPY OF INDOLES IN ARGON MATRICES AT 20K, WITH 1La ORIGIN IDENTIFICATION

by

Bruce Jonathon Fender

A thesis submitted in partial fulfillment
of the requirements for the degree

of

Doctor of Philosophy

in

Chemistry

MONTANA STATE UNIVERSITY
Bozeman, Montana

July, 1997

D378
F3522

APPROVAL

of this thesis submitted by

Bruce Jonathon Fender

This thesis has been read by each member of the thesis committee and has been found to be satisfactory regarding content, English usage, format, citations, bibliographic style, and consistency, and is ready for submission to the College of Graduate Studies.

July 23, 1997
Date

Patrick R Calli
Chairperson, Graduate Committee

Approved by the Major Department

July 24, 1997
Date

David McDorley
Head, Major Department

Approved for the College of Graduate Studies

7/27/97
Date

Graduate Dean

STATEMENT OF PERMISSION TO USE

In presenting this thesis in partial fulfillment of the requirement for a doctoral degree at Montana State University, I agree that the library shall make it available to borrowers under rules of the library. I further agree that copying of this thesis is allowable only for scholarly purposes, consistent with "fair use" as prescribed in the U. S. Copyright Law. Requests for extensive copying or reproduction of this thesis should be referred to University Microfilm International, 300 North Zeeb Road, Ann Arbor, Michigan 48106, to whom I have granted "the exclusive right to reproduce and distribute my dissertation in and from microform along with the non-exclusive right to reproduce and distribute my abstract in any format in whole or in part."

Signature 

Date 7/23/97

ACKNOWLEDGMENTS

I wish to thank Professor Patrik Callis for his guidance, support, and insight, which has kept me on track during my graduate career. I thank the Callis group, especially Dr. Pedro Muino, Kurt Short, and David Hahn, for their advice and assistance during my stay in the group.

I also wish to thank Professor Lee Spangler and his group for their willingness to give a helpful word of advice or the lending of equipment.

I would also like to thank the rest of the members of my graduate committee, Dr. Reed Howald, Dr. Jan Sunner, Dr. Eric Grimsrud, and Dr. Myles Watts for their time and commitment.

And a final word of thanks goes to my family (to my Mom and Dad, to my brother and his family, and to my sister) for their constant love and support through the years.

TABLE OF CONTENTS

Page

LIST OF TABLES vii

LIST OF FIGURES viii

ABSTRACT xii

1. INTRODUCTION 1

Background 4
Statement of Problem 11

2. THEORY 14

Emission Anisotropy 14
The Onsager-Mataga-Lippert Model 16
Herzberg-Teller Coupling 18
Fermi Resonance 20
Site Selective Spectroscopy 21
Phosphorescence 25
Principles of Supersonic Jet Spectroscopy 28
Two-Photon Spectroscopy 29

3. EXPERIMENTAL SECTION 34

Matrix Isolation 34
Absorption Measurements 39
Phosphorescence Measurements 41
Two-Photon Spectroscopy 41
Formation of the Matrices 42
Supersonic Jet Instrument 45

4. RESULTS AND DISCUSSION 49

Indole in an Argon Matrix 49
Fermi Resonance 56

TABLE OF CONTENTS-Continued

Page

Herzberg-Teller 59
The ^1L_a Origin 60
Site Structure 63
Phosphorescence 68
3-Methylindole 74
5-methylindole 84
2,3-Dimethylindole 86
2-Methylindole 96
1-Methylindole 98
Phosphorescence 104
4-Fluoroindole 106
Phosphorescence 118
Comparison Of Properties 120
Nitrogen 124
Indole in N_2 at 30K 124
3-Methylindole in N_2 at 30K 129
3-Methylindole in Ethanol at 15K 131
3-Methylindole Complexes in a Supersonic Jet 135
Water Complex 135
Methanol Complex 139

5. SUMMARY 146

REFERENCES 148

LIST OF TABLES

Table		Page
1.	The two-photon values of the argon matrix and the jet spectra	54
2.	Indole Phosphorescence	73
3.	1-Methylindole phosphorescence	105
4.	4-Fluoroindole phosphorescence	119
5.	The energy difference for the ^1L_a and ^1L_b states of substituted indoles relative to indole	121
6.	The frequencies of modes 28, 27, 26	121
7.	Site energies for the S_1, S_2, T_1 states of indole in argon at 20K	122
8.	Indole + H_20	139
9.	Indole + Methanol	142

LIST OF FIGURES

Figures		Page
1.	Tryptophan	3
2.	Indole with numbering system	3
3.	Excitation to the ^1L_a and ^1L_b states, where r is a distortion along a general coordinate that takes the geometry from the ^1L_b minimum to the ^1L_a minimum	5
4.	Schematic diagram for determining the emission anisotropy	15
5.	Site structure of the supersonic jet environment, (a), argon matrix environment, (b), and solution environment, (c)	23
6.	Phosphorescence (Ph) and fluorescence (Fl)	27
7.	Supersonic jet expansion	28
8.	One and two-photon spectroscopy	30
9.	Matrix isolation experimental setup	35
10.	Transmittance experimental setup	40
11.	Jet experimental setup	48
12.	Transmittance spectrum of indole in argon at 20K, with 0.2 cm^{-1} bandpass	50
13.	The 26^0_1 line excited at 285.84, 285.85, 285.86, 285.87, 285.88 nm, with a 2 cm^{-1} bandpass	51
14.	Supersonic jet fluorescence excitation spectrum of indole (with Ω values), (a), simulated matrix spectrum, (b), fluorescence excitation spectrum of indole in argon at 20K, (c), and the fluorescence anisotropy, (d)	53

LIST OF FIGURES-Continued

Page

15. Two-photon spectrum of the ^1L_b origin, (a), 26^1_0, (b), and 28^1_0, (c), of indole in argon at 20K 55

16. Fermi resonance of the 29^1_0 and the $41^1_0 42^1_0$ lines 59

17. Fluorescence spectrum of indole in argon at 20K (500-800 cm^{-1}), (a), and fluorescence anisotropy, (b) 61

18. Fluorescence spectrum of indole in argon at 20K, (a), and the stick spectrum, (b) 64

19. Fluorescence excitation spectra (200-1400 cm^{-1}) of indole in argon at 20K from site 1, (a), site 2, (b), site 5, (c), and site 3, (d) 67

20. The phosphorescence decay, (a), and the log plot, (b) 68

21. The phosphorescence spectra of indole in argon at 20K from site 1, (a), site 5, (b), and site 2, (c) 71

22. The phosphorescence spectrum of indole in argon at 20K from site 5, (a) and the stick spectrum 72

23. Transmittance spectrum of 3MI in argon at 20K, with a 0.2 cm^{-1} bandpass 75

24. Supersonic jet fluorescence excitation spectrum of 3MI (with Ω value), (a), fluorescence excitation spectrum of 3MI in argon at 20K, (b), and fluorescence anisotropy, (c) 78

25. Two-photon spectrum of the ^1L_a and ^1L_b origin region (-50-400 cm^{-1}) of 3MI in argon at 20K 79

26. Dispersed fluorescence spectrum of 3MI in argon at 20K 82

27. Dispersed phosphorescence spectrum of 3MI in argon at 20K, with ^1L_b origin excitation at 288.78 nm 83

LIST OF FIGURES-Continued

Page

28. Supersonic jet fluorescence excitation spectrum of 5MI (with Ω values), (a), fluorescence excitation spectrum of 5MI in argon at 20K, (b), and fluorescence anisotropy, (c) 87

29. Dispersed fluorescence spectrum of 5MI in argon at 20K 88

30. Dispersed phosphorescence spectrum of 5MI in argon at 20K, with ^1L_b origin excitation at 291.75 nm 89

31. Fluorescence excitation spectrum of 2,3DMI in argon at 20K, (a), and the fluorescence anisotropy, (b) 93

32. Dispersed fluorescence spectrum of 2,3DMI in argon at 20K 94

33. Dispersed phosphorescence spectrum of 2,3DMI in argon at 20K, with ^1L_a origin excitation at 288.66 nm 95

34. Transmittance spectrum of 2MI in argon at 20K, with a 0.2 cm^{-1} bandpass 99

35. Fluorescence excitation spectrum of 2MI in argon at 20K, (a), and the fluorescence anisotropy, (b) 100

36. Dispersed fluorescence spectrum of 2MI in argon at 20K 101

37. Dispersed phosphorescence spectrum of 2MI in argon at 20K, with ^1L_b origin excitation at 286.07 nm 102

38. Transmittance spectrum of 1MI in argon at 20K, with a 0.2 cm^{-1} bandpass 107

39. Fluorescence excitation spectrum of 1MI in argon at 20K, (a), and the fluorescence anisotropy, (b) 108

40. Dispersed fluorescence spectrum of 1MI in argon at 20K 109

41. Dispersed phosphorescence spectrum of 1MI in argon at 20K, with ^1L_b origin excitation at 291.55 nm, and stick spectrum, (b) 110

LIST OF FIGURES-Continued

Page

42. Transmittance spectrum of 4FI in argon at 20K, with a 0.2 cm^{-1} bandpass 114

43. Fluorescence excitation spectrum of 4FI in argon at 20K, (a), and fluorescence anisotropy, (b) 115

44. Dispersed fluorescence spectrum of 4FI in argon at 20K 116

45. Dispersed phosphorescence spectrum of 4FI in argon at 20K, with ^1L_b origin excitation at 281.89 nm, (a), and the stick spectrum, (b) .. 117

46. Energies of the ^1L_a and ^1L_b states 123

47. The fluorescence excitation spectrum of indole in N_2 at 30K, (a), and the fluorescence anisotropy, (b) 126

48. Fluorescence spectra of indole in N_2 at 30K, (a), and N_2 at 15K, (b) ... 127

49. The phosphorescence spectrum of indole in N_2 at 30K 128

50. Transmittance spectra of 3MI in argon at 20K, (a) and N_2 at 30K, (b) .. 130

51. Fluorescence spectra of 3MI in ethanol at 300K, (a), 15K, (b), and red-edge excitation (307 and 303.5 nm) at 15K, (c) 134

52. The fluorescence excitation spectrum of 3MI$(H_2O)_1$ in a supersonic jet (with Ω values) 137

53. Two-photon spectrum of 3MI$(H_2O)_1$ complex origin (with Ω values) 138

54. The fluorescence excitation spectrum of 3MI(methanol)$_1$ in a supersonic jet (with Ω values) 143

55. Two-photon spectra of the bare 3MI origin, (a), and 3MI(methanol)$_1$ complex origin, (b), (withΩvalues) 144

56. Two-photon spectra of the first quanta at -268.3 cm^{-1}, (a), and the second quanta at -247.2 cm^{-1}, (b), (with Ω values) 145

ABSTRACT

The first site selected UV spectra (with polarization) of matrix isolated indole, 3-methylindole, 5-methylindole, 2-methylindole, 1-methylindole, 2,3-dimethylindole, and 4-fluoroindole in argon at 20K were obtained. The main thrusts of this research is to locate the true ^1L_a origin, and to characterize the fluorescence and the phosphorescence.

The true ^1L_a origin for indole lies 1100-1300 cm^{-1} (split) above the ^1L_b origin and the true ^1L_a origin was distinguished from its false ^1L_a origin at 455 and 480 cm^{-1} (jet). The fluorescence was identified as ^1L_b and sharp (10 cm^{-1}) phosphorescence was obtained giving the Franck-Condon factors for L_a emission. The ^1L_a origin for 3-methylindole was 260 cm^{-1} (unsplit) above the ^1L_b origin, which was verified both by fluorescence anisotropy and 2-photon measurements. The fluorescence was identified as ^1L_b. For 2,3-dimethylindole the combined perturbation of the two methyl groups causes the inversion of states with the ^1L_a being 190 cm^{-1} below the ^1L_b. This was verified by ^1L_a fluorescence identification and by 2-photon measurements. The ^1L_a fluorescence can be distinguished from its ^1L_b counterpart.

The rest of the mono-methylated indoles emit from the ^1L_b state and the ^1L_a origin lies above the ^1L_b as follows: 5-methylindole (1800 cm^{-1}), 2-methylindole (400-600 cm^{-1}), 1-methylindole (430-600 cm^{-1}). For 4-fluoroindole the ^1L_a origin lies 1520 cm^{-1} above the ^1L_b and the fluorescence is characterized by a long Franck-Condon progression of the 26^0_1 mode.

Also included in this work is indole and 3-methylindole in N_2 at 30K, 3-methylindole in ethanol at 15K, and 3-methylindole complexed with H_20 and methanol in a supersonic jet.

This information will facilitate the use of tryptophan as a spectroscopic probe molecule in the understanding of protein structure and dynamics.

Chapter 1

INTRODUCTION

Proteins are one of the basic building blocks of life consisting of chains of amino acids linked together through amide bonds. One amino acid is distinguished from another by its side chain. Protein chemistry is quite complex; the sequence and conformation of amino acids of proteins are needed to completely understand its functionality. There are many ways of understanding protein conformation: from a theoretical standpoint using molecular modeling and dynamic simulations or from an experimental standpoint using NMR, X-ray crystallography, and spectroscopy. A common technique, X-ray diffraction, obtains a three-dimensional structure but requires the protein to be crystalline, which is quite difficult to nearly impossible for certain proteins. Furthermore, since the protein is not in its natural environment, the information gained is questionable when extended to living systems. This technique is also unable to study conformational changes in proteins due to environmental changes.

Spectroscopic techniques, where light is used to interact with an environmentally sensitive probe molecule, revealing structural and environmental information about the protein in vivo (living systems), offers useful complementary information. Three amino acids could be used as natural

spectroscopic probes in proteins when monitoring fluorescence with UV excited light: tyrosine, tryptophan, and phenylalanine. However, tyrosine is insensitive to its local environment and phenylalanine has a poor quantum yield. Furthermore, if tryptophan was present in the residue, then observing the fluorescence from either tyrosine or phenylalanine would be difficult. Tryptophan, on the other hand, is a more sensitive probe because of its low-lying ^1L_a excited state, whose large permanent dipole interacts strongly with its local environment[1,2]. Tryptophan can also be selectively excited on the long-wavelength absorption edge. For these reasons tryptophan has served as a spectroscopic probe molecule in proteins for over 30 years[1]. The structure of tryptophan in its zwitterion state is shown in Figure 1.

Tryptophan is naturally incorporated in many proteins, and it may be inserted by point mutations if needed. Indole, the chromophore of the amino acid tryptophan, accounts for much of the UV absorption of proteins. The structure of indole and its numbering system is shown in Figure 2. Indole has two low lying $\pi\pi^*$ singlet excited states, labeled ^1L_a and ^1L_b, using Platt notation[3]. The overlap of these nearly degenerate states causes the absorption spectrum to be quite complicated. A considerable amount of experimental and theoretical data on indole exists[1,2,4-19,21-23], but because of its complicated nature, its spectroscopic properties are still not fully known. Consequently, a more comprehensive picture of the electronic structure of indole is needed.

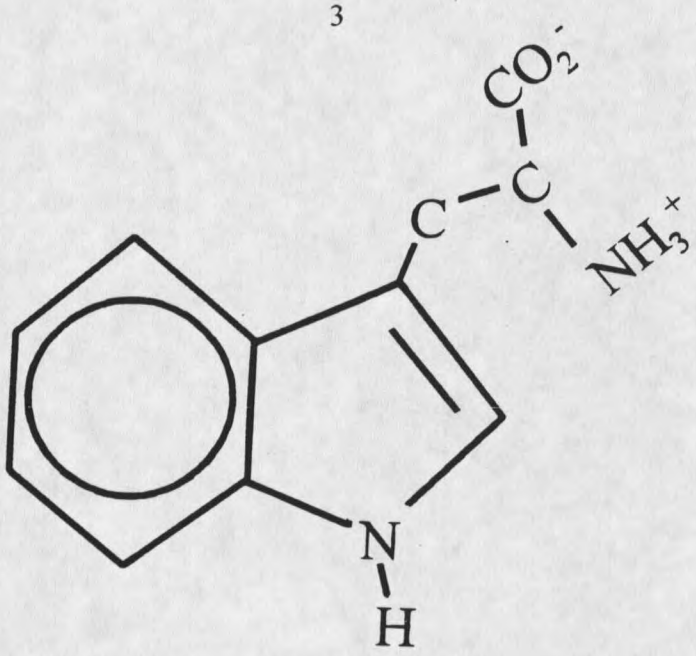

Figure 1. Tryptophan

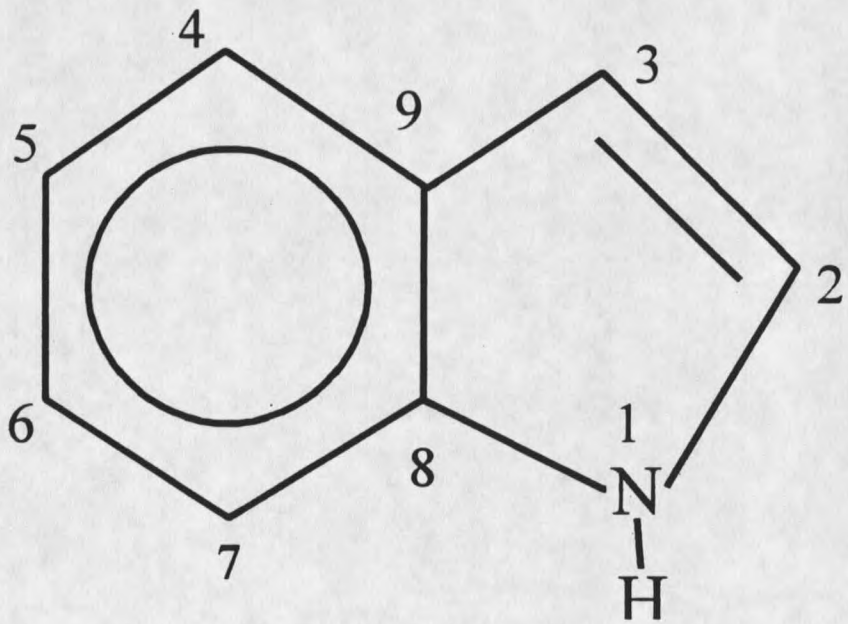

Figure 2. Indole with numbering system.

Background

In 1976, Valeur and Weber completed work on indole in propylene glycol at -58^0 C with polarized emission[4]. They concluded from the emission anisotropy that the 280 nm band consisted of two excited states, ^1L_a and ^1L_b, whose transition moments lie in the plane of the molecule at approximately 90^0 relative to each other (see Figure 3). They went on to separate and resolve the two excited states using the anisotropy. However, their experiment lacked resolution, so they could not resolve individual vibrational lines.

The ^1L_b state of indole is known to have a smaller geometry change upon excitation and a permanent dipole similar to the ground state[5]. Therefore, the ^1L_b state is less perturbed by its local environment and can be recognized by its relatively sharp structure. The ^1L_b state is the S_1 state for indole, 5-methylindole (5MI), and 3-methylindole (3MI) in a nonpolar (low-interacting) environment.

The ^1L_a state, on the other hand, has a large permanent dipole because its transition involves charge transfer, where electron density is shifted from the 5-member ring to the 6-member ring[5,72]. This increase in dipole causes its fluorescence to be red-shifted and broadened by large Stokes shifts because of the larger interaction between its permanent dipole and the environment. These two factors cause the ^1L_a state in solution to be recognized by its broad structure. In a polar environment, the ^1L_a state will be the S_1 state for indole, 3MI, and 2,3-dimethylindole (2,3DMI). 5MI is one exception and emits from

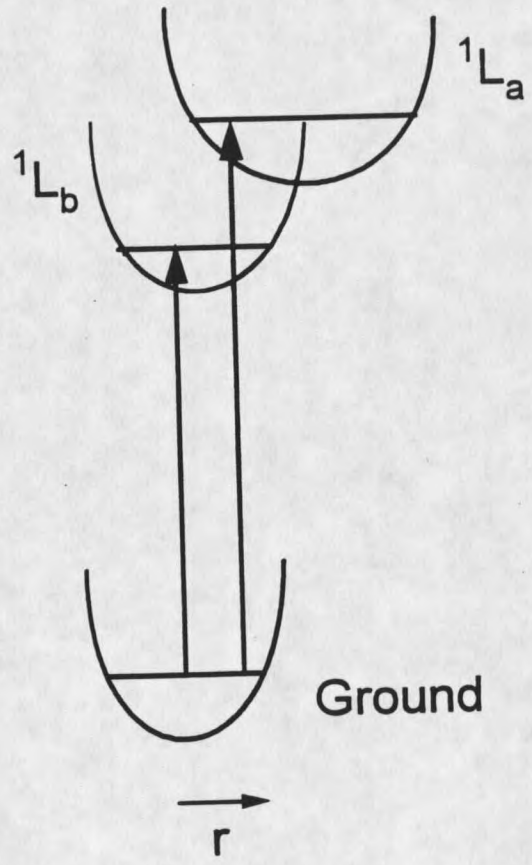

Figure 3. Excitation to the ^1L_a and ^1L_b states, where r is a distortion along a general coordinate that takes the geometry from the ^1L_b minimum to the ^1L_a minimum.

both states in a polar environment [6].

Comparing vapor phase spectra and partially resolved room temperature solution spectra, Strickland *et al.*[7,8] have given evidence for these two electronic states in indole and indole derivatives (3MI and 2,3DMI). The ^1L_a lines were distinguished from the ^1L_b lines by differential solvent shifts due to their differences in permanent dipole and differences in dispersion interactions. The ^1L_a origin of indole was postulated to lie 1460 cm^{-1} above the ^1L_b origin in the vapor. They first noted that methylation in the 3-position caused significant changes to the absorption spectrum; the ^1L_a origin was found to be extremely sensitive to this methylation, drastically red-shifting to 680 cm^{-1} above the ^1L_b origin in vapor and 340 cm^{-1} in perfluorohexane. The Callis group verified the latter result with a value of 300 cm^{-1} in perfluorohexane, using a 2-photon technique[9]. By the addition of a second methyl group to indole in the 2-position producing 2,3DMI, further red-shifts the ^1L_a origin. Strickland *et.al.*[7] concluded that the ^1L_a and the ^1L_b origins nearly overlap both in vapor and in perfluoromethylcyclohexane. This evidence points toward substitutions and solvation playing an important role in the photophysics of indole.

Utilizing supersonic jet spectroscopy, Wallace and coworkers have done extensive spectroscopy on indole and indole derivatives as isolated molecules or molecular complexes[10-16]. They used a variety of experimental techniques in their thorough investigation of indole: nanosecond fluorescence excitation, picosecond 2-photon resonant ionization, lifetime measurements via picosecond

excitation, and dispersed emission. Extensive lifetime measurements of the excited state were made and attempts were made to use lifetimes as a method to distinguish ^1L_b states with longer lifetimes from ^1L_a states with shorter lifetimes. This method reveals lifetimes, but lifetime measurements cannot be used as a positive means of identifying the state. There tends to be a general connection between the ^1L_a-^1L_b energy gap and the lifetimes, where smaller ^1L_a-^1L_b energy gaps produce shorter lifetimes and vice versa. These experiments simply tuned the ^1L_a-^1L_b energy gap of indole by methylation and/or complexation. Through this work, Wallace *et al.*[13,16], and Lami and Glasser [84,65] suggested that the ^1L_a state is a nonradiative state through dissociation of the N-H bond. However, this nonradiative mechanism was later experimentally proven incorrect [17].

Callis and coworkers made huge strides in the development of a 2-photon technique, which had the ability to separate ^1L_a lines from ^1L_b lines through the absorption event. The two photon technique used the preferential absorption of circular versus linear polarized light, where the polarization ratio Ω can be measured, where Ω=intensity using circular polarized light/intensity using linear polarized light. For an ^1L_b transition the Ω~1.5 and for an ^1L_a transition the Ω~0.5[9,18,21]. The absorption of the two photons happens on the femtosecond time scale; therefore, this technique can be used under nonrigid conditions such as liquids and gases because the two photons absorb before the molecule loses its orientation due to rotational motion. This method has had profound ability to separate ^1L_a and ^1L_b states in the excited state manifold, except vibronically

coupled lines. The method was first applied to indole and indole derivatives in various solvents at room temperature[18] and subsequently used on indole vapor [19,20] and 3MI vapor [20], where the ^1L_a intensity was found 1454cm^{-1} above the ^1L_b origin for indole and 400 cm^{-1} for 3MI.

The recent expansion of supersonic jet spectroscopy, and in conjunction with this two-photon technique gave the experimenter the highest resolution and the clearest picture of the two excited states. The Callis group completed many experiments on a variety of indoles (indole, 3MI, (d_1-3MI), and 5MI); the positions of the ^1L_a and ^1L_b lines were located and identified, and a picture was made between methylation and the ^1L_a and ^1L_b states. For the first time, a more definitive statement could be made concerning these two states.

Indole had two small lines at 455 and 480 cm^{-1} above the ^1L_b origin that gave an ^1L_a signature, but most of the ^1L_a intensity sat 1000 cm^{-1} higher in energy. It was first speculated that these two lines were in fact the ^1L_a origin and were split (25 cm^{-1} splitting) by coupling to the nearby ^1L_b origin, but there was much hesitation about this assignment. First, the combined intensity of these two lines was much lower than the intensity of the ^1L_b origin. This result was later contradicted by theory [5]. Second, it was theorized that these lines were not the ^1L_a origin, but vibronically coupled ^1L_b lines. Bickel *et al.* [10] performed extensive dispersed fluorescence experiments on indole in a jet, using ground state assignments, then assigning the corresponding excited state frequencies; the 480 cm^{-1} line was assigned 28^1_0 and the 455 cm^{-1} line was assigned $39^1_0 41^1_0$.

These lines were not assigned to a different origin. Later experiments involving hydrogen bonded complexes in the jet were completed to shed light on this assignment[21]. It was postulated that the ^1L_a lines should have a greater red-shift upon complexation than corresponding ^1L_b lines due to their difference in permanent dipole. Upon complexation (methanol, H_2O, and D_2O), the 480 cm^{-1} and 455 cm^{-1} lines of indole did not red-shift relative to the complexes' origin, but the intensities of the lines varied. The lines not red-shifting gave evidence for vibronic coupling, and the line intensity variation gave evidence for Fermi resonance.

The ^1L_a origin of 3MI lies in several lines between 300-900 cm^{-1} above the ^1L_b origin, with no discernable prominent ^1L_a origin. The ^1L_a origin is split due to coupling to the ^1L_b manifold. Also, the methyl rotor is inactive on excitation. For 5MI, the ^1L_a intensity lies approximately 1400 cm^{-1} above the ^1L_b origin, and the methyl rotor is active upon excitation with a 60^0 conformational change of the methyl group[22]. This coupling lowers the line intensity because the intensity is distributed over the entire methyl rotor structure.

Due to the popularity of using tryptophan as a spectroscopic probe, currently several tryptophan analogues are being used as optical probes in proteins in replacement of tryptophan[23-26]. One of these analogues is 4-fluorotryptophan (4-FT), where 4-fluoroindole (4FI) replaces indole as the chromophore[23]. The purpose of this change is to select the desired emission characteristics by selecting the desired chromophore. 4-FT was selected

because it could be naturally incorporated into proteins in the place of tryptophan did not change the functionality of the protein, and would not fluoresce. In practice, one or more of the tryptophan(s) in a protein containing multiple tryptophans could in essence be "turned off" with the goal of unraveling a complex fluorescence spectrum by selectively deleting emitters. Because of this characteristic, there is a renewed interest in understanding fluorinated indoles[27,28].

Low temperature glasses/matrices have been studied for the last several decades. Low temperature matrices have given experimenters the ability to study reactive species, radicals, and ions[29-31], which would be nearly impossible to study otherwise. In recent years, there has been a renewed interest in matrix isolated spectroscopy with the advent of narrow band laser excitation sources, which selectively excite molecules that are in a narrow range of energy, giving site selection capabilities. The matrix material ranges from noble gases (as in this thesis) to various hydrocarbons made popular by Shpol'skii[32,33].

Indole has also been studied in low temperature glasses. As mentioned earlier, Valeur and Weber studied indole and various related compounds in propylene glycol at -58^{0}C. Kawski *et al.*[34] did room temperature study on indole incorporated in a poly(vinyl alcohol) film, with polarized fluorescence and phosphorescence. Illich *et al.* studied indole in an argon matrix at 10K, but was unable to select from a single site[35]. This experiment gave a blurred excitation spectrum that consisted of several spectra on top of one another.

The research that influenced our decision to explore indole in argon was completed by Gutmann *et al.*[36], who studied naphthalene and octadeutonapthalene in argon at 12K, with both one and two-photon techniques. They could produce extremely sharp lines, some as narrow as 4 cm^{-1}, which could compete with the resolution of the jet. Gupiapati *et al.*[37] later studied anthracene and pyrene in argon with polarized emission measurements. These experiments gave us the evidence we needed: argon matrices can produce sharp lines and polarized emission.

Statement Of The Problem

Previous research has positively identified ^1L_a transitions in various indoles; the two-photon technique incorporated with jet expansion has given a high resolution picture of the excited state manifold of various indoles. Still, there has been no positive identification of the ^1L_a origin for indole, 3MI, d_3-3MI, and 5MI, using 2-photon spectroscopy because it cannot distinguished between true ^1L_a lines and vibronically coupled ^1L_b lines.

In indole, there is speculation that the 480 cm^{-1} and 455 cm^{-1} lines do not constitute the true ^1L_a origin, but a split false origin. For 3MI, there is no discernable prominent ^1L_a origin; instead the intensity is spread over several lines spanning 400 cm^{-1}. For 5MI, the ^1L_a origin is well above the ^1L_b origin, but the exact location has not been found. For 2,3DMI the ^1L_a origin is supposed to be near the ^1L_b origin, and for 2MI, 1MI, and 4FI the ^1L_a origins are completely

unknown.

In proteins there is some uncertainty with fluorescence, because of two possible fluorescent states of indole. For indole, polar environment favors ^1L_a emission, and nonpolar favors ^1L_b emission; however, proteins lie somewhere between these extremes. A question remains about the existence of sharp ^1L_a fluorescence and its structure. Fluorescence monitoring is an experimental aid in the understanding of protein chemistry, and there is a common practice: if the fluorescence is sharp then it is considered to be ^1L_b, but if the fluorescence is diffuse then it is considered to be ^1L_a fluorescence. This assumption may be flawed. There is no fundamental reason there could not be sharp ^1L_a fluorescence, except that the conditions that are conducive to producing ^1L_a fluorescence, i.e. polar environments, are also conducive to broadening it. If an incorrect fluorescence assignment of a protein is made, then false information about the protein environment is given. Theoretical results have shown some significant differences between ^1L_a and ^1L_b emission due to differences in Franck-Condon factors between the two excited state potentials and the ground state potential[38], but experimental verification is needed.

This research will use site selective matrix isolation of indole, 3MI, 5MI, 2,3DMI, 2MI, 1MI, and 4FI to unravel the complex photophysics of indole. Site selection produces sharp lines, and matrix isolation produces a rigid trapping environment, where photoselection leads to anisotropic emission. This method incorporates a small-bandpass laser in conjunction with a small-bandpass

monochromator, giving the experimenter the ability to produce sharp fluorescence excitation, fluorescence, and phosphorescence spectra. This technique can distinguish between ^1L_a and ^1L_b states by emission anisotropy and by differential solvent shift. The differential shift will be able to separate false ^1L_a lines (vibronically coupled lines) from true ^1L_a lines. This technique can help complete the picture painted by the jet and positively identify the true ^1L_a origins, identify the emission, and examine the phosphorescence. This data will also give pertinent information as to how substitutions to the indole ring affect both the electronic energies of the ^1L_a and ^1L_b states and normal modes frequencies.

Chapter 2

THEORY

Emission Anisotropy

The emission anisotropy measurements are critical to the experiments carried out in this thesis. The discussion will follow the theory laid out by Kawski[39] and will depend on these four basic assumptions:

1) Considering the case of linear polarized excitation of a dilute fluorophore in a rigid environment, where rotation between excitation and emission is impossible.

2) There is no phase relation between the exciting light and the emitting light.

3) The direction of the emission transition dipole, relative to the molecular axis, does not depend on the excitation, but only on the molecular states between which the transition occurs.

4) No other depolarizing factors will be taken into account.

Consider the case of an excitation vector, E, vertically polarized along the x-axis, see Figure 4.

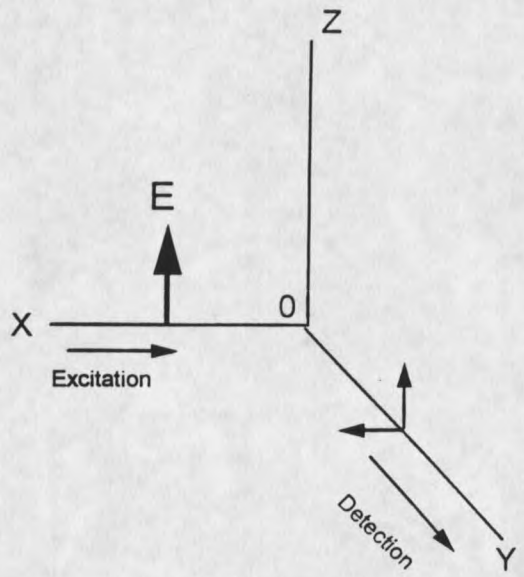

Figure 4. Schematic diagram for determining the emission anisotropy.

According to Jablonski[41], the anisotropy of the emission, r, for the emission field can be defined as:

$$r = \frac{I_{\parallel} - I_{\perp}}{I_{\parallel} + 2I_{\perp}} \qquad (1)$$

Equation 1 is used in the laboratory to calculate the anisotropy of the emission. The denominator is proportional to the total emission intensity. The perpendicular term can be factored out using the following relation $I_{\perp}=(I-I_{\parallel})/2$ giving Equation 2:

$$r = \frac{3}{2} \cdot \frac{I_{\parallel}}{I} - \frac{1}{2} . \qquad (2)$$

Equation 2 is expanded to incorporate the angular dependence of the absorption and emission moments on the anisotropy giving the Perrin equation[40]:

$$r(\beta) = \frac{2}{5}\left[\frac{3}{2}\cos^2\beta - \frac{1}{2}\right], \qquad (3)$$

where β is the angle between the absorption and emission moments. For a complete discussion see Kawski[39]. The first part of Equation 3 is the maximum anisotropy due to photoselection, 2/5, and the second part in brackets is the angular dependence of anisotropy. The emission anisotropy (r) will have values ranging from -0.2 to 0.4, for $\beta = 90^0$ and $\beta = 0^0$, respectively. These are the theoretical values and the experimental values will deviate somewhat due to depolarization in the experiment. If depolarization does occur, then it is important check for the anisotropy values be at the proper ratio (2:-1).

The Onsager-Mataga-Lippert Model

The Onsager-Mataga-Lippert Model[42-49] will be used as a method of calculating spectral shifts that result from the solute molecule placed in a medium with a constant dielectric constant (ϵ). This model is based on the Onsager reaction field. The model is used to calculate the energy correction for absorption in vacuum compared with absorption in a solvent. The model is based on the representation of the solute molecules as point dipoles, with both the ground state dipole, u_g, and the excited state dipole, u_e, in a solvent sphere

with a radius (a), a static dielectric constant (ϵ), and a refractive index (n), see Equation 4.

$$hc\Delta\bar{\nu}_{ground} = -(\mu_g)^2\frac{2}{a^3}\left[\frac{\epsilon-1}{2\epsilon+1} - \frac{n^2-1}{2n^2+1}\right] - (\mu_g)^2\frac{2}{a^3}\left[\frac{n^2-1}{2n^2+1}\right] \quad (4)$$

Equation 4 is broken into two terms, the first term corrects the energy due to the reaction field caused by the reorientation of the solvent. This does not change during excitation period of the solute, analogous to the Born-Oppenheimer approximation. This first term does not play a factor in the matrix experiments, because the matrix material does not have a permanent dipole and can be removed from the Equation 4. Even if there was a permanent dipole, the temperature and/or the rigidity of the matrix would not allow for this type of reorientational motion of the matrix.

The second term corrects the energy due to electronic polarizability of the solvent molecules. Since electrons are small, this electronic term is in equilibrium with the solvent molecules during the excitation period. The energy difference of excitation from the ground state to an excited state can be calculated as follows[21,86]:

$$\Delta\bar{\nu}(cm^{-1}) = \frac{(\mu_e^2 - \mu_g^2)}{2}\frac{2}{a^3}\left[\frac{n^2-1}{2n^2+1}\right]*5035 , \quad (5)$$

where the numerical constant 5035 converts the energy change into cm^{-1} units[86]. The first term is divide by two so that the free energy change is calculated and the equation requires the actual dipole[86]. This model will be used to calculate the theoretical energy (free energy) shifts for the two excited states ^1L_a and ^1L_b, by the differences in their actual permanent dipoles.

This model is better suited for systems in polar solvents. For the argon matrix, this model is incomplete because it only deals with the more tangible permanent dipole difference and does not include a dispersion term. For molecules that do not have a permanent dipole by symmetry, these dispersion forces alone are responsible for the shifts. They can be quite large and are proportional to the polarizability of the solvent[50]. The ^1L_a state of napthalene and anthracene is known to red-shift about 500 cm^{-1} more than the ^1L_b state in hydrocarbon solvent[52]. Anthracene's ^1L_a state is known experimentally to red-shift 500-700 cm^{-1} by going into solid argon[51] and red-shifts 1200 cm^{-1} further by incorporation into fluorene[53]. It would be reasonable to expect part of the red-shift seen in the argon matrix to come from dispersion forces.

Herzberg-Teller Coupling

The intensity of a transition or the probability that a transition between two state occurs is proportional to the square of the transition dipole

$$I \propto |\bar{M}_{ge}|^2, \tag{6}$$

where I is the intensity of the transition and M_{ge} is the transition dipole between the ground state and the excited state. The transition dipole can be written explicitly:

$$\bar{M}_{ge} = \int\int \Psi_g(r,Q)\Phi_g(Q)\ \bar{M}\ \Psi_e(r,Q)\Phi_e(Q)drdQ, \tag{7}$$

and can be rearranged

$$\bar{M}_{ge} = \int \Phi_g(Q)\left[\int \Psi_g(r,Q)\ \bar{M}\ \Psi_e(r,Q)dr\right]\Phi_e(Q)dQ, \tag{8}$$

where Ψ is the electronic wavefunction and Φ is the nuclear wavefunction, the subscripts g and e refer to the ground and excited states, respectively, and, r refers to the electronic coordinates and Q to the nuclear coordinates. The term in the square brackets is dependent on the nuclear coordinates and is constant under the Condon approximation. Herzberg-Teller vibronic coupling occurs when there is a failure of the Condon approximation and the term in the bracket needs to be expanded:

$$\bar{M}_{ge} = \int \Phi_g(Q)\left[\bar{M}^o_{ge} + \sum_a \frac{\partial \bar{M}_{ge}}{\partial Q_a} Q_a + \cdots\right]\Phi_e(Q)dQ, \tag{9}$$

where the first term is the transition dipole at the equilibrium position, and the second term has the vibronic coupling constants and is a function of nuclear

motion. Therefore, nuclear motion can couple intensity into a transition through this term.

Herzberg-Teller coupling occurs when a vibronic transition that is forbidden due to no displacement of the potential well, is observed due to nuclear displacement along a normal coordinate that comes from zero point vibrational motion of a ground state normal mode. If one of these modes has a non zero coupling constant, then the vibronic transition will be observed.

Fermi Resonance

Fermi resonance occurs when two vibrations are nearly degenerate in energy and in proper symmetry. This coupling occurs due to anharmonic behavior of the vibrations; one vibration interferes with the other, because they are not displaying 100% normal mode behavior. If they meet the proper symmetry conditions, then a perturbation can occur that mixes the two levels. This mixing causes intensity redistribution and splitting of these two levels, which depends on the energy separation and the interaction between the levels.

Fermi resonance can most easily be explained using the variation method rather than perturbation theory, because the interaction is typically beyond the perturbation limit. Fermi resonance can be explained by two cases of the variation method. In case 1 the energy levels are degenerate ($\alpha_1 - \alpha_2 = 0$) and in case 2 the energy separation is on the order of the interaction between the two states ($\alpha_1 - \alpha_2 \approx \beta$), where α_1 and α_2 are the energies of levels 1 and 2,

and β is the interaction between the levels. In case 1 there is an equal state mixing and in case 2 there is unequal state mixing. The wavefunction that describes the mixed states is a combination of the original wavefunctions. Through this mechanism, intensity can be redistributed from strongly allowed state and given to a weakly allowed state. Spectroscopists widely use Fermi resonance in data interpretation.

Site Selective Spectroscopy

Site selective spectroscopy is the technique used in these experiments to improve the spectral data. It is a method of acquiring spectral data from a matrix embedded sample that achieves the sharpest lines possible. This occurs because all the absorption and emission are from only one site, which sharpens and simplifies the spectra.

In a chemical system all molecules are perturbed by their local environment, the environment actually produces an electric field that the molecule senses. This field can interact with any changes made in the molecule, especially in the absorption and emission of photons. For a simple example, let us only consider a single electronic transition. The energy of such a transition will be designated by a vertical line in Figure 5. If the solvent field is oriented in such a way to facilitate the electronic transition, then the energy for the transition will red-shift to lower energy, but if the solvent field is opposed to the transition, the energy will blue-shift to higher energy. In solution there is a

"gaussian" distribution of environments; therefore, there is a "gaussian" distribution of perturbed molecules leading to broadening of the spectra, see Figure 5c. In the jet expansion there is a much smaller distribution of environments; the molecules are vibrationally and rotationally cold and isolated in a vacuum, see Figure 5a. This leads to narrow spectra. In the argon matrix at 20K there are several sites within the matrix, which are highly populated by the guest molecules, see Figure 5b. This can lead to narrow spectra. The term "site" selection is commonly used, but in actuality the correct term is "energy difference" selection or just "energy" selection.

First, site selection requires the guest molecule to be incorporated into a host matrix at a temperature well below the melting point of the host material. This low temperature of the matrix produces a rigid trapping environment for the guest molecule, where rotational structure and hot bands (hot bands are transitions caused by thermally excited molecules in the ground state.) are eliminated. The concentration of the guest molecule is kept low to reduce guest molecule/guest molecule interactions, so all environmental electronic influences come exclusively from the host matrix. Interaction (induced electric field) can be controlled, by controlling the polarizability of the matrix material. A less polarizable matrix should in theory interact less with the guest molecule and vice versa.

The basis behind site selection is that the guest molecule will occupy particular sites within the host matrix. Small guest molecules occupy interstitial

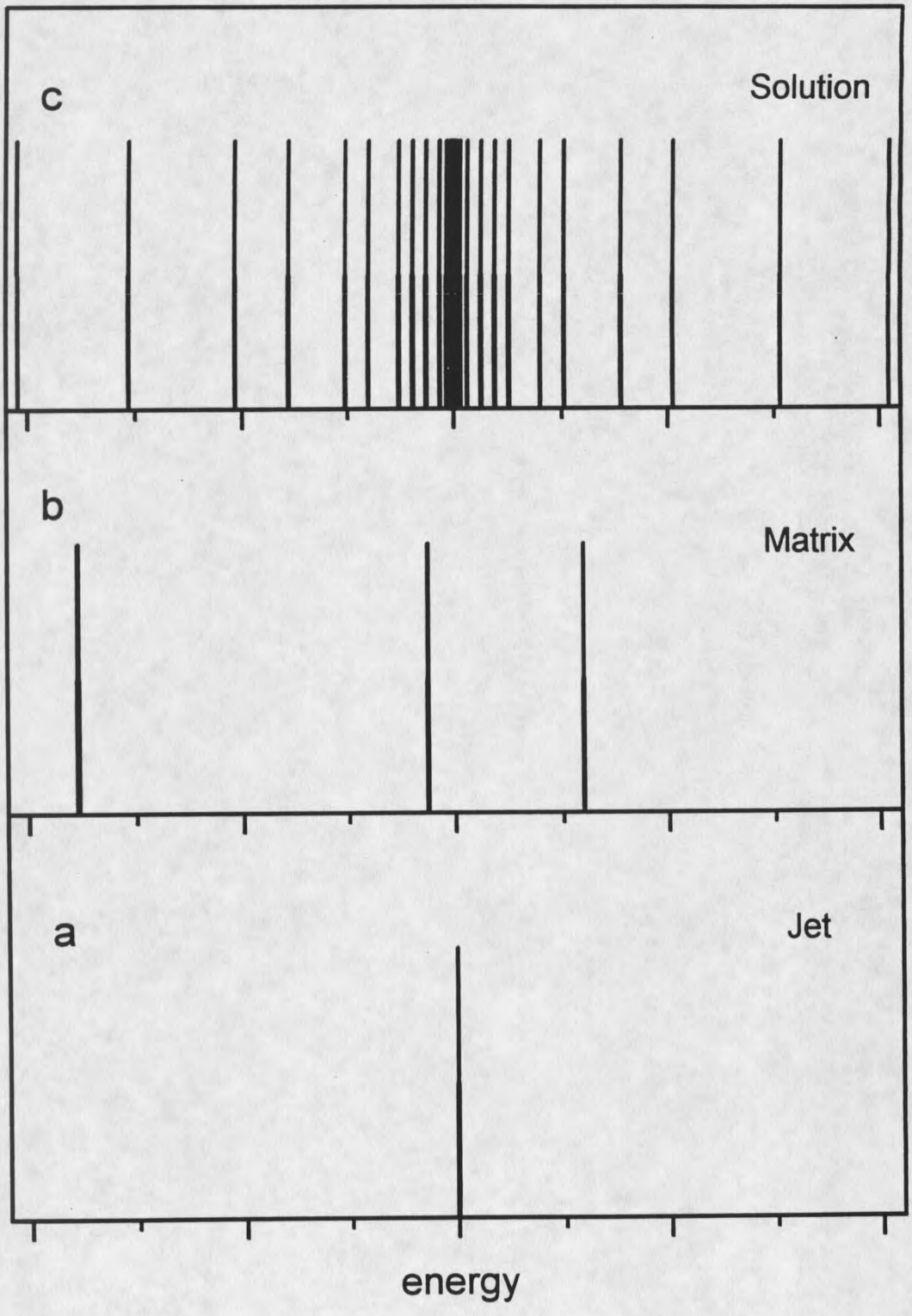

Figure 5. Site structure of the supersonic jet environment, (a), argon matrix environment, (b), and solution environment, (c).

holes (sites) that are analogous to those of the host molecules, and larger guest molecules occupy sites formed by actual displacement of one or more of the host atom(s) or molecule(s). In theory, these sites should be highly populated, with a large number of molecules sitting in a similar site (solvent cage) produced by a similar matrix arrangement around the guest molecules, producing similar molecular energies. There is extensive evidence of noble gas matrices having multiple sites in which aromatic molecules display transition energies differing about 100 cm^{-1}, which leads to band congestion in a conventional absorption spectroscopy. The reproducibility of the site structure in argon suggests that the argon matrix is indeed polycrystalline and indole fits into lattice planes within argon's the face center cubic (FCC) lattice structure by the removal of several argon atoms.

Second, to achieve site selection, the energy spacing between the sites must be far enough apart so that sites can be independently excited by a small bandpass laser, while monitoring a single vibrational line in the emission or vice versa. A small bandpass laser in conjunction with a small bandpass monochromator has the capabilities of producing sharp fluorescence excitation, dispersed fluorescence, and phosphorescence spectra. Because of this arrangement, there is an intensity limitation on the experiment because only a small portion of the emission is collected.

There is also an intrinsic problem that arises for site selection if the sites are closer than either the laser bandwidth or the spectral linewidth. This spectral

overlap is problematic because the phonon wing extends at least 100 cm^{-1} to the blue of the zero-phonon band. The zero-phonon band is strictly a molecular transition, where the lattice absorbs none of the photon's energy, whereas the phonon wing is caused by a slightly higher energy photon causing a molecular transition plus lattice excitation. For indole, there are 6 sites within 213 cm^{-1}, for 2MI 4 sites within 55 cm^{-1}, and for 4FI 6 sites within 117 cm^{-1}. These closely spaced sites can lead to site contamination in the spectra due to overlapping spectra, with a major contribution from one site and minor contributions from other sites.

The term "sharp site" will refer to sites in which indole gives an energy width of about 10 cm^{-1} through transmittance measurements. Likewise, any site giving an energy width greater than 20 cm^{-1} will be referred to as a "broad site." In addition, fluorescence excitation, fluorescence and phosphorescence lines will also be referred to in the same manner, any line around 10 cm^{-1} will be considered "sharp" and any line greater than 20 cm^{-1} will be considered "broad", regardless as to the site in which it sits. The general statement usually holds: sharp sites produce sharp spectra and broad sites produce broad spectra.

Phosphorescence

Phosphorescence is light emitted from the lowest triplet state (T_1) to the ground state (S_0). Due to Hund's rule the triplet state (T_1) state always lies lower in energy than the first singlet state (S_1). The T_1 state is very difficult to populate

by direct excitation from the ground state manifold, because it is spin forbidden and therefore has a small oscillator strength. The T_1 state is therefore populated indirectly through the S_1 state, see Figure 6. The energy transfer from the S_1 state to the T_1 state is denoted as intersystem crossing (ISC). For this to occur, the S_1 and the T_1 must have a common intersection point between their two potential wells, and there must be some mechanism for unpairing two electrons spins. If these two requirements are met, then ISC can occur and some of the population of the S_1 state can drain into the T_1 state.

The mechanism of spin-orbit coupling is the mechanism by which the spin conversion is made possible. Phosphorescence is enhanced in solids because of reduced diffusional quenching of the triplet, which means, the quenching agent can not diffuse to the excited chromophore in the solid lattice, therefore reducing quenching. Also, ISC is enhanced in the presence of heavier atoms, which have greater coupling between their orbital and spin angular momenta. This makes the cryogenic matrices ideal for the production of phosphorescence and heaver atoms can be used to increase the phosphorescence signal if it is desired.

For Indole phosphorescence, the transition dipole direction is perpendicular to the plane of the molecule and the phosphorescence occurs exclusively from the T_1 state[1].

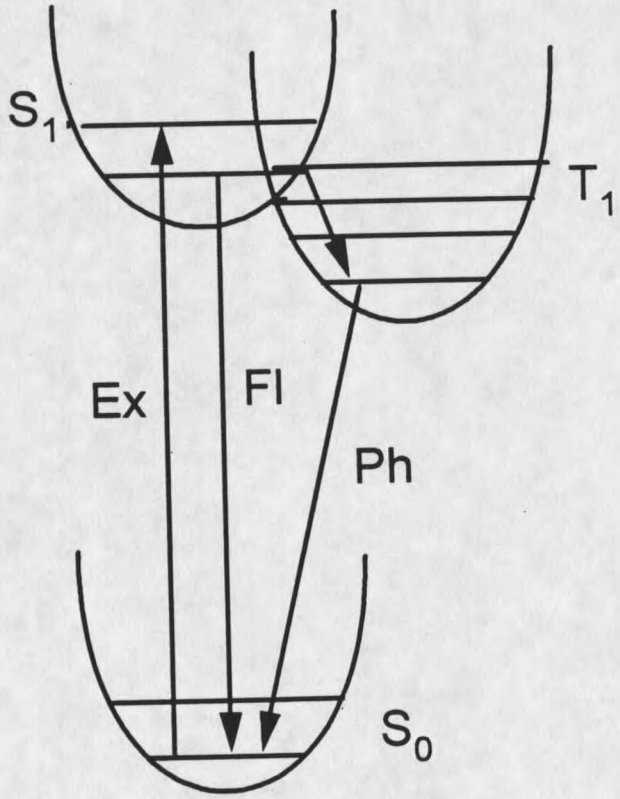

Figure 6. Phosphorescence (Ph) and fluorescence (Fl).

Principles Of Supersonic Jet Spectroscopy

Supersonic jet expansion is an experimental method by which molecules are collisionally cooled to cryogenic temperatures. These temperatures are achieved when sample molecules and carrier gas from a pressurized region (3-10 atmospheres) are expanded through a nozzle, diameter 0.5 to 1.0 mm, into an evacuated chamber, 10^{-5} to 10^{-6} torr, and collisions occur between the carrier gas and the sample molecules in the nozzle region. The sample molecule's energy in the form of vibrational, rotational, or other degrees of freedom is transformed into a large translational energy in the evacuated chamber. In the evacuated chamber, the molecules are in a collisionless environment as they move along their trajectories, see Figure 7. Therefore, all excitations occur from the zero vibrational level in the ground state; eliminating most hot bands and simplifying the spectrum.

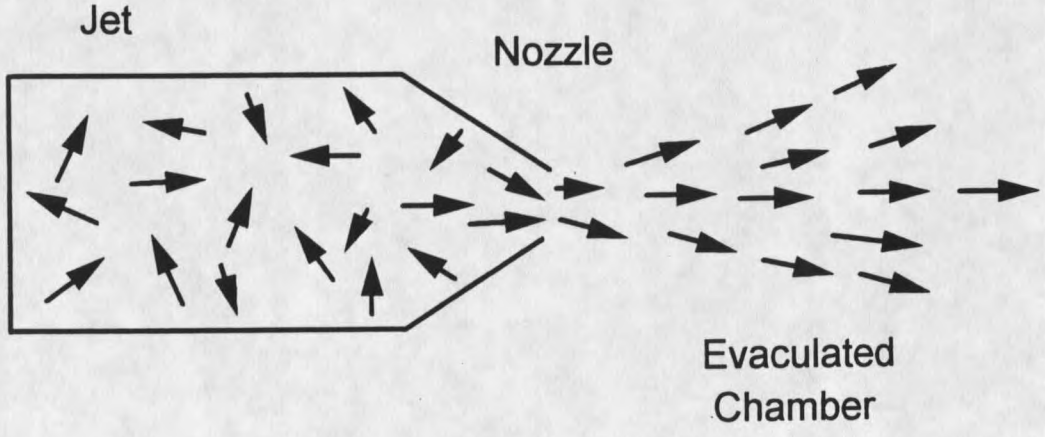

Figure 7. Supersonic jet expansion.

Two-Photon Spectroscopy

The traditional method of spectroscopy, is known as one-photon spectroscopy, which is the main focus of the matrix isolation work. The energy of the single photon absorbed exactly equals the energy difference needed to place the molecule into resonance--reach an excited energy level of the molecule. The simple equation is used:

$$\Delta E = h\nu \tag{10}$$

where h is Planck's constant and v is the frequency of the photon, and ΔE is the energy difference between the states.

In the 1960's, with the advent of high powered lasers, a second type of spectroscopy was developed known as two-photon spectroscopy, where two photons absorb simultaneously to achieve resonance energy of the molecule. The energy of the two photons add together using the modified energy formula:

$$\Delta E = h\nu_1 + h\nu_2 \tag{11}$$

where ν_1 and ν_2 are the frequencies the first and second photons respectively. This allows for two general types of two photon spectroscopy: one-color where the photons have the same frequency and two-color where the photons have different frequencies. The first photon that absorbs excites the molecule to a virtual state (non-resonant state) and the second photon further excites the molecule from the virtual state to the final resonant state, see Figure 8.

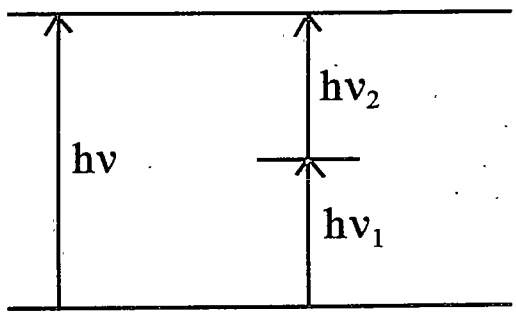

Figure 8. One and two-photon spectroscopy.

Consequently, the photons must be absorbed almost simultaneously (within about a femtosecond (10^{-15} s)) or the first photon is emitted as scattered light. Today with the advent of high-powered ultra-short pulsed lasers (picosecond to femtosecond pulses) three or more-photon absorption is possible and experiments have been completed.

Experimentally, a useful aspect of two-photon spectroscopy is its ability to probe the excited state through photoselection, where the information gained is conserved in the system regardless of vibrational relaxation or internal conversion in the system. It is strictly an absorption event. Since the photons absorb simultaneously, rotational motion of the molecule is meaningless. Therefore, this method can be used on gas and solution phase systems, where

there is continual motion, and can likewise be used on static systems, such as, the argon matrix.

The theory of two-photon spectroscopy was first deduced by Goppert-Mayer in 1939[54] using perturbation theory. The two-photon absorption process is a second-order perturbation and requires a high flux of laser light. However, as frequently happens in science, experiments were not yet feasible until a much later time with the advent of lasers.

McClain[55-57] has done extensive work on the theory of two-photon absorption spectroscopy. For absorption of two identical photons the rate of absorption (R) is proportional to the following equation:

$$R \propto | \mu \cdot S \cdot \mu |^2 I^2 \qquad (12)$$

where μ is the unit polarization vector of the exciting light, S is the two-photon absorptivity tensor, and I is the intensity of the exciting laser light. The equation stipulates that the rate of absorption is proportional to the square of the laser light intensity. This square dependence is a good check for 2-photon absorption; the absorption intensity must be proportional to the square of the laser intensity. The two-photon tensor is given in Cartesian coordinates by a 3 x 3 matrix:

$$S_{ab} = \sum_i \frac{a_{fi} \cdot b_{ig}}{\nu_{ig} - \nu_{laser}} \qquad (13)$$

where a,b are x, y, and z and the summation is over all the states of the molecule, including the ground states and the excited state (a complete set). There is also a direct connection between the relative directions of the two photons and the intensity of the fluorescence due to photoselection. From McClain's[55] work, the expression for fluorescence intensity (I_f) for the absorption of two identical photons with isotropic emission is

$$I_f = \sum_{i,j=1}^{4} P_i M_{ij} Q_j , \qquad (14)$$

where P_i are geometric factors which depend on the orientation of the polarization vectors of the exciting and emitting light, the Q_j factor depends on the molecular two-photon tensor (see Equation 12) and the fluorescence transition dipole, and M_{ij} is a matrix that binds the P_i factor and the Q_j factor. The important point to mention here is the direct link between the direction of polarization of the photons and the resulting fluorescence intensity; therefore, polarization changes will change fluorescence intensity.

Also from McClain's work[55] two other parameters are defined:

$$\delta_F = \sum_{a,b} S_{aa} S_{bb}^{*} \qquad (15)$$

From these two parameters another important parameter, Ω, the two-photon

$$\delta_G = \sum_{a,b} S_{ab} S_{ab} . \quad (16)$$

polarization ratio, can be defined. Ω is the ratio of intensities of the emission using linearly and circularly polarized light

$$\Omega = \frac{I_{circular}}{I_{linear}} = \frac{3 - \delta_F/\delta_G}{2 + \delta_F/\delta_G} . \quad (17)$$

The value of Ω can range from 0.0 to 1.5[58]. The experimental results are in good agreement with theoretical results[58]; the Ω value for the ^1L_b state is ~1.5 and the Ω value of the ^1L_a state is ~0.5. The ^1L_a state preferentially absorbs two parallel photons and the ^1L_b state preferentially absorbs two perpendicular photons; therefore, we have a means of differentiating between the two states by preferential absorption.

Chapter 3

EXPERIMENTAL SECTION

Matrix Isolation

The experimental apparatus, shown in Figure 9, consists of a Janis Research Company closed cycle helium refrigerator (CCS-650) integrated with a Lakeshore autotuning temperature controller. The cold head portion of the unit was kept under vacuum at a pressure of 10^{-5} to 10^{-6} torr, maintained by a Knotes glass diffusion pump (# 924785) that was backed by a mechanical roughing pump. The temperature of the cold head was kept constant at 20K (Ar) and 30K (N_2) throughout the experiment. The sample was layered on a sapphire window bolted to the cold head; thermal grease was used to maintain good thermal contact between the cold head and the sapphire window. The sapphire window was tilted to achieve a 45-degree angle with the excitation beam.

The matrices were prepared using a bulk tank of an ultra-pure (99.99999%) matrix gas, argon or nitrogen, which was fed through a regulating system containing a sample chamber, a toggle valve, and a metering valve. The matrix gas/sample mixture was produced by sending the matrix gas (with a backing pressure of 2 to 3 PSI) through the sample chamber where gaseous sample molecules were transported along with the matrix gas. The matrix

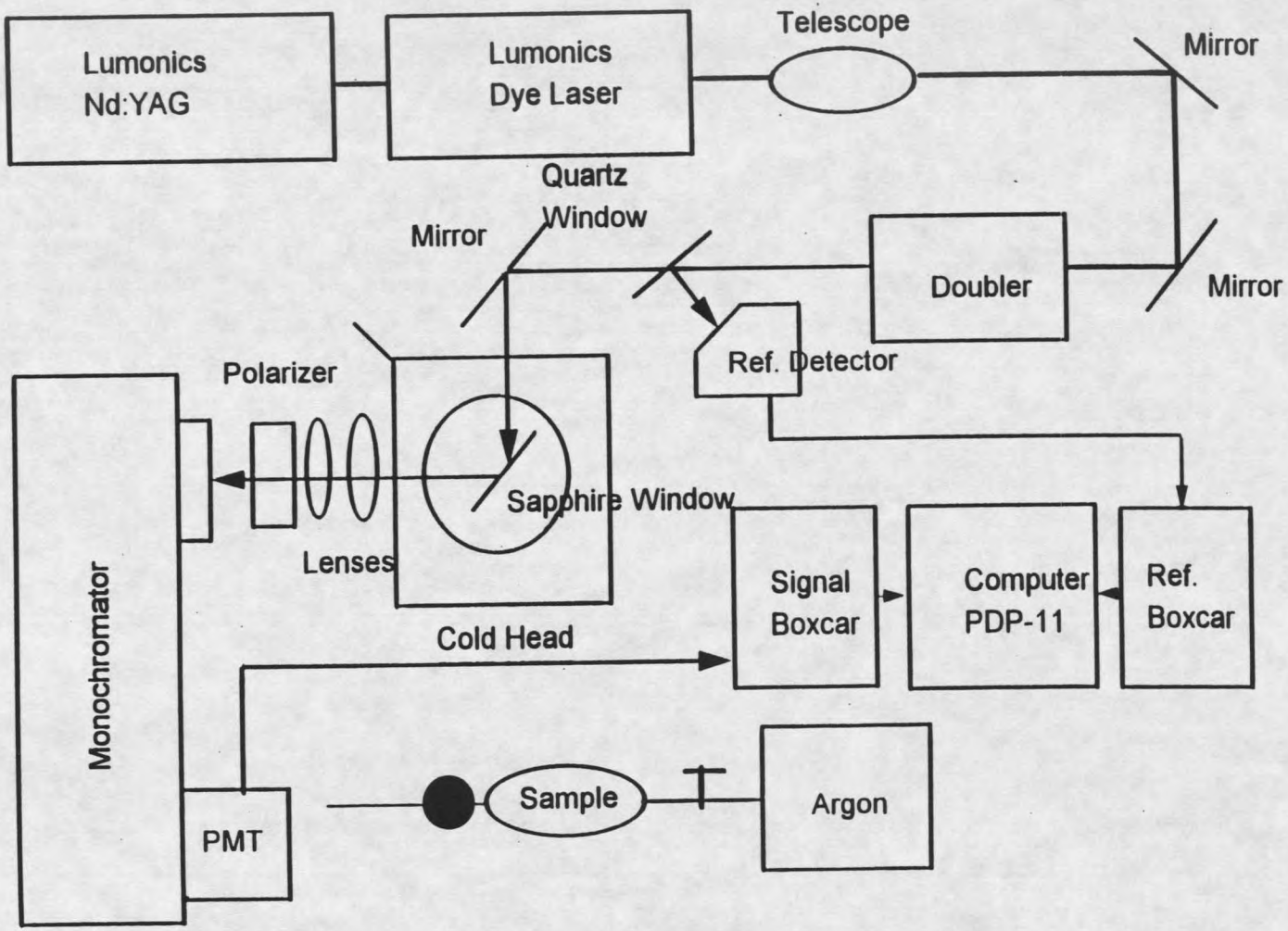

Figure 9. Matrix isolation experimental setup.

gas/sample mixture finally arrived at a small 1/16 in. capillary, shot through the vacuum, and deposited on the window at the prescribed temperature. The temperature of the sample chamber was increased for less volatile 2,3-DMI crystals, using heating tape (60V). This increase in temperature resulted in an increased sample concentration. The regulating system noted above, controlled the layering speed of the matrix. All crystalline samples were placed in the sample chamber as described, except for 1MI because it was a liquid, and required a special handling procedure. This procedure required a small amount of 1MI being placed in the sample chamber, with any excess being removed. The sample chamber was then purged with argon, so only a film of 1MI was left on the wall of the sample chamber. This simple procedure worked well to reduce the amount of 1MI in the matrix.

The chemicals were obtained from Aldrich and were used without further purification: indole (99+%, Lot # 03231AZ), 3-methylindole (98%, Lot # 11822CF), 5-methylindole (99%, Lot # 06701HX), 2,3-dimethylindole (99%, Lot # 092767), 2MI (98%, Lot # 08019EG), 1MI (97%, Lot # 09327EZ), and 4FI (99%, Lot # 24H0685).

The sample was irradiated with UV laser light for one-photon experiments. The laser light was produced by a pulsed Q-switched Lumonics Nd:YAG (HY-200) laser and later by a Continuum Surelite III-10 laser, that pumped a Lumonics (HD-300) tunable dye laser. For wavelengths between 566nm and 600nm, a dye combination of Rhodamine 590 (53 mg/l) and Rhodamine 610

(7mg/l) was pumped with the second-harmonic of the YAG, 532nm. For wavelengths between 523nm and 586nm, Coumarin 540A dye (1082 mg/l) was used and was pumped with the third-harmonic of the YAG, 355 nm. The beam coming from the dye laser was expanded to 8mm by a 4X Galilean telescope, which consists of two lenses: 120mm f.l. convex and a -30 mm f.l. concave (Oriel). The beam was expanded to reduce damage to the directing mirrors. The laser light was then doubled into the UV wavelength using an Inrad Autotracking II frequency doubler. The UV light coming from the doubler was horizontally polarized and was converted to vertical polarization by a depolarizing wedge followed by a glan polarizer oriented to pass vertically polarized light. The laser excitation linewidth was 0.20 cm^{-1}.

The fluorescence was collected at 90^0 from the exciting beam, collimated using an Esco S1-UV grade lens (d=50.8mm, fl=76.2mm), and then focused onto the entrance slit of the monochromator using an Esco S1-UV grade lens (d=50.8mm, fl=305mm). The f/number of the collecting lens was chosen to collect a large solid angle of emission, and the f/number of the focusing lens was matched, as closely as possible, to the f/7 optics of the monochromator, in order to maximize the focusing of the fluorescence onto the gratings. If the experiment required polarization measurements of the emission, a polacoat sheet polarizer was placed in front of the entrance slit of the monochromator, and the polarizer could be oriented to pass vertically and horizontally polarized light. A quartz depolarizing wedge was also mounted in front of the entrance slit to avoid

spurious polarization, due to the polarization dependent transmission of the gratings. The emission light was dispersed using a Spex 1404 double monochromator (grating 2400 gr/mm, fl=0.85). The monochromator's linear dispersion was 0.2nm/mm for the above grating, and the slit widths used for the 1-photon experiments varied from 70 μm to 200 μm (1.5-4 cm^{-1} bandpass) and for 2-photon experiments from 2 mm to 3 mm (40-60 cm^{-1} bandpass). The light was collected using a Hammamatsu R928 PMT cooled to -25^0 C using a Product For Research thermally cooled PMT housing (TE177RF.005).

The signal was amplified and gated using Evans Associates circuitry in conjunction with a boxcar built by Anderson and Callis[59]. The boxcar was triggered by two photodiodes and its gating was set for 200 usec. The signal was digitally converted using a Data Translation A/D converter and the data was stored on a PDP-11 computer.

The computer program that controls the laser, the polarizer, and data collection was written by former group members Anderson, Callis, Jones, Rehms, Theiste, and Williams, and was later modified by Sammeth and Muino. I have since modified this program to control the monochromator, the emission polarizer, and the anisotropy calculation.

The fluorescence excitation scan was completed by scanning the laser across the excitation manifold while monitoring a strong line in the emission, usually the 26^0_1 line. The fluorescence spectra was obtained by exciting a strong line in the excited state, usually the 26^1_0 line, while scanning the

monochromator. This method allows for selective monitoring at specific sites.

Absorption Measurements

The absorption measurements of the origin regions of the spectra were made using a broadband Xe lamp excitation source, see Figure 10. The lamp sat directly across from the monochromator and the exciting light directly impinged on the Ar sample on the cold finger. Between the light source and the sample sat a 3mm thick UG-11 filter (transmit 400-250 nm) which allowed only the UV light to pass. The resulting light was focused into the monochromator through small slits, using the lens system mentioned earlier, while the monochromator was scanned over the origin region of the spectrum. This set up produced a transmittance spectrum and the spectrum could be transformed into an absorption spectrum, if desired. A Laboratory Photometer model 11 powered the phototube and amplified the resulting signal. The amplified signal was then sent to an X-Y recorder and a hard copy was later digitized by hand.

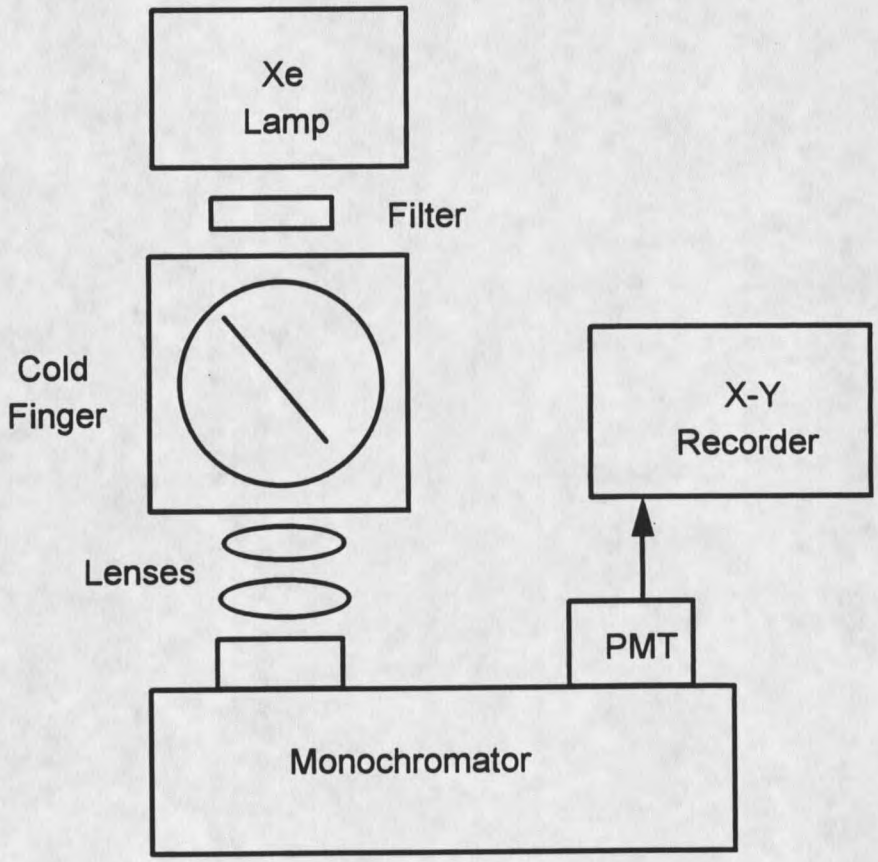

Figure 10. Transmittance experimental setup.

Phosphorescence Measurements

The phosphorescence spectra were not taken in the same fashion as the fluorescence measurements, because the lifetimes of the phosphorescence was nearly 10 second, which was outside the limits of our gated electronics. The measurements were taken using the same detection system used in the absorption measurements, except the source of excitation was the laser tuned to the S_1 origin of the sample.

Two-Photon Spectroscopy

The same system used for the one-photon measurements was modified for use in two-photon spectroscopy measurements. The Inrad II frequency doubler was removed and replaced by several optical components capable of producing linear and circular polarized light, without altering the spatial position of the laser beam. To accomplish this, the laser light coming from the dye laser passed first through a Glan-Foucault polarizer to ensure 100% vertically polarized light. The light then passed through a series of three Fresnel rhombs, consisting of a double rhomb and a single rhomb. If the double rhomb was not rotated, relative to the axis of the rhomb, then the light passing through the system remains vertically polarized. If the double rhomb was rotated by 22.5^0, with respect to the plane of the incident laser light, then the E vector of the light exiting the double rhomb was rotated by 45^0, by 4 internal reflections. This light

then entered the single rhomb at an angle of 45^0 and was converted to circular polarized light by two internal reflections. Therefore, both types of polarized light were produced by simple rotation of the double rhomb, which was controlled by a stepping motor. To ensure accurate data acquisition, back to back linear and circular measurements were made for each laser step and the signal was normalized by dividing by the square of the laser intensity.

Since 2-photon absorption requires strong laser intensity, focusing of the laser beam by a focusing lens might be required to increase the laser intensity. The jet data was taken using a Esco focusing lens (d= 50.8 mm, f.l.= 700 mm) placed at the front of the jet, and no focusing lens was used in the argon matrix experiment.

The total emission was collected during the jet two-photon experiments, and to reduce scattered light from hitting the phototube in the jet, a 3mm UG-11 filter, a saturated $NiSO_4$ solution, and a 5 mm diaphragm was used. For two-photon spectroscopy using the matrix isolation setup, the monochromator was locked onto the strongest emission line and the monochromator's slits were open 2 to 3 mm (40-60 cm^{-1}). To reduce scattered light from entering the monochromator a 1 mm UG-11 filter was placed at the entrance slit of the monochromator, allowing only 400-250 nm light to pass.

Formation Of The Matrices

The success of these experiments hinges on the quality of the matrix.

Here are some guidelines for producing good matrices. The matrix should be layered at a relatively slow rate for two important reasons: to produce a more uniform matrix[60,61] and to control the temperature load on the cold finger. The rate of deposition should be kept around 4 millimoles matrix gas/hr. The matrix layering speed should be controlled to limit the heating of the cold finger to no more than 0.20K. This was especially critical with argon, because argon forms extremely brittle matrices[62], where only a minor temperature change (±.30K) caused the matrix to shatter. This was less critical for nitrogen, but still was important. Cracking was the process by which the matrix relieved strain, but left the matrix unusable for polarization measurements. This cracking can also be caused by the thickness of the matrix, due to temperature gradients within the matrix.

These experiments require fine temperature control of the cold finger. The cold head has two small built in heaters that are cycled electronically to hold the cold finger at a specified temperature, and how precisely these heaters were cycled related to the temperature stability of the cold finger. The cold head incorporates a Lakeshore temperature controller (model 330) that can operate in autotune mode or in manual mode (see owner's manual). In manual mode there were three settings that are critical for fine temperature control: P (gain), I (reset), and D (rate). All the experimental data in this thesis were taken in manual mode using the following settings: P=15, I=90, and D=0. These setting all need to be altered if the pressure changes drastically in the cold head and

the "I" value will need to be altered if the temperature setting is changed. Read the manual for more details.

Polarization measurements required the matrix to be of high quality, transparent, and have no cracks. A cracked or cloudy matrix depolarizes the light. It should also be noted that annealing of a matrix utterly destroys its optical quality, which is needed for polarization measurements.

Furthermore, the concentration of the guest molecules in the matrix was important. If the matrix was too concentrated or too thick, it caused spectral aberrations, due to self -absorption. Self-absorption could be checked by examining the dispersed fluorescence spectrum; self absorption would lead to a reduction in the relative intensity of the origin compared with other lines. The sample concentration should also be kept low (molar ratio of matrix gas to guest molecule 10^{-4}) to reduce dimer formation, because most guest molecules have a greater affinity for themselves rather than the matrix.

It had been suggested that the best temperature to use should be approximately 0.3 the melting temperature of the matrix material[62]. The melting temperature of argon is 83.85^0K and nitrogen is 63.15^0K. The temperatures used in these experiments were found by trial and error, and the best temperature for argon was 20K and for nitrogen 30K (consistent with the above recipe).

Finally, O_2 will kill both the fluorescence and phosphorescence intensities. If air is in the system, then the matrix will appear cloudy with a slight

brown tint. This occurred because one or more of the gas inlet system fittings was leaking. To reduce these problems, the gas inlet system should be kept as simple as possible. If the gas line was ever opened up to the air, then it was reconnect and the line purged through the cold head with matrix gas for 20 minutes, before the experiment was started.

Supersonic Jet Instrument

The supersonic jet was built by Jungst Scientific located in Bozeman, MT to the specifications made by Callis and Sammeth, see Figure 11. The jet consisted of an aluminum box that was 25 cm on a side, with three axes (x, y, and z) running straight through the center of each face intersecting at the center of the box. Along the x-axis are two long cylindrical tubes extended from both ends of the jet. These tubes allowed the excitation laser beam to pass straight through the jet, with interior baffles to keep room light out of the jet. Two quartz windows (d=101.6 mm) were cemented to the end of the tubes to achieve the desired vacuum pressure. The nozzle, sample chamber, and solvent chamber were located on the z-axis (vertical). The nozzle is positioned 2.0 cm above the x-axis in one-photon experiments and 0.5 cm in two-photon experiments. The fluorescence was collected on the y-axis using a system of a mirror and lenses. The mirror, coated spherical mirror (d=60mm, f.l.=25mm), was placed opposite the PMT, while a fused quartz collecting lens (d=50.8mm, f.l.=50.8mm) and a focusing lens (d=50.8, f.l.=101.6mm) were placed in line with the PMT, thus all

three were used to focus the fluorescence onto a Hammamatsu R928 PMT cooled to -26^{0}C.

The low pressure (~10^{-6} torr) in the jet was maintained by a 6 inch Varian (VHS-6) diffusion pump backed by a Varian roughing pump. A gate valve was also connected to the jet chamber so the chamber could be isolated and opened to the atmosphere while the diffusion pump was operating. A cryogenic pump (kept at room temperature) was placed between the gate valve and the diffusion pump as a spacer to keep diffusion pump oil from entering the jet. The jet apparatus used three pressure gauges: 2 thermocouple gauges Varian (531) and accompanying controllers Varian (801), and for low pressure reading a Varian (524-EF) cold cathode ionization gauge with the accompanying Varian (860A) cathode gauge.

The laser and the nozzle were driven by a General Valve IOTA I controller operating at 20 Hz. The laser triggering pulse was delayed between the controller and the laser by 600 microseconds by the use of a Stanford research System (D6535) Digital Delay/Pulse Generator. The laser signal intensity was monitored at the end of the chamber on the x-axis by a Rhodamine B quantum counter built by Jones and Callis[63]. The sample chamber was heated to 60^0/70^0 C and the nozzle was heated to 100^{0}C using heat tape and Omega temperature controllers.

The carrier gas was ultra pure (99.99999%) helium and the sample chamber was pressurized to 4 atm. For complexation experiments, a desired

part of the helium was channeled through the solvent chamber and rerouted back to the sample chamber, and this flow was controlled by metering valves and toggle valves.

For one-photon experiments a 1 mm WG-320 filter (transmit 310-4200 nm) was used to block scattered exciting light and for two-photon experiments a 3mm UG-11 filter, saturated solution of $NiSO_4$, and a 0.5 cm aperture were used.

For complex experiments in the jet the metering valves had to be adjusted to suit the solvent. The valves had to be opened wide for water because of its low vapor pressure, and once water was in the system it was hard to get rid of. Deionized water was used entirely in this experiment. For the methanol experiments, the metering valves had to barely be open to achieve good complex signal, because of its higher vapor pressure, and care had to be taken not to get too much methanol in the system leading to cluster formation. This experiment used spectral grade methanol.

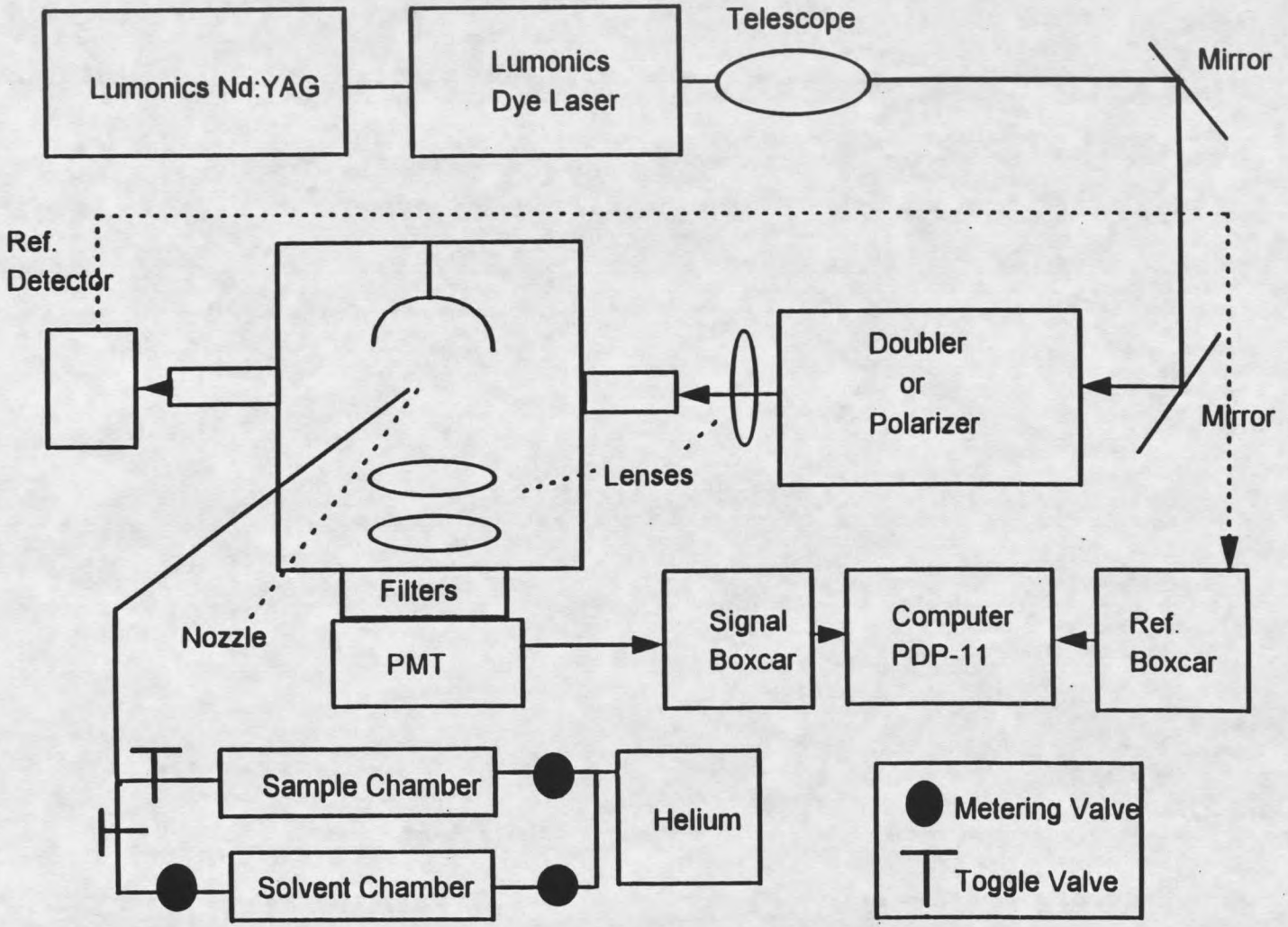

Figure 11. Jet experimental setup.

Chapter 4

RESULTS AND DISCUSSION

Indole In An Argon Matrix At 20K

The S_1 origin region of indole in an argon matrix was scanned for absorption, to get an idea of the site structure, the number of sites, and their locations. Figure 12 displays the transmittance spectrum of indole in argon at 20K. In the spectrum each site has a different absolute energy that corresponds to differences in the environment of each site. Indole entrained in argon at 20K under our experimental conditions resides mainly in five energy sites: site 1 at 285.85 nm (34,981 cm^{-1}), site 2 at 286.8 nm (34,858 cm^{-1}), site 3 at 286.4 nm (34,916 cm^{-1}), site 4 at 285.95 nm (34,971 cm^{-1}), and site 5 at 285.05 nm (35,081 cm^{-1}). These five sites each have a unique absorption strength that corresponds to the population of the site, and an intrinsic site width. Site 1 (34,981 cm^{-1}) was the main site used in the indole work because of its absorption strength and its narrow site width, 10 cm^{-1}. Site 2 (34,858 cm^{-1}) was the broadest site, with a site width of 30 cm^{-1}.

The indole lines are inhomogeneously broadened by the site, and variation in excitation frequency over the site produces subsequent shifts in the fluorescence. This is illustrated in Figure 13. This data is obtained by the laser

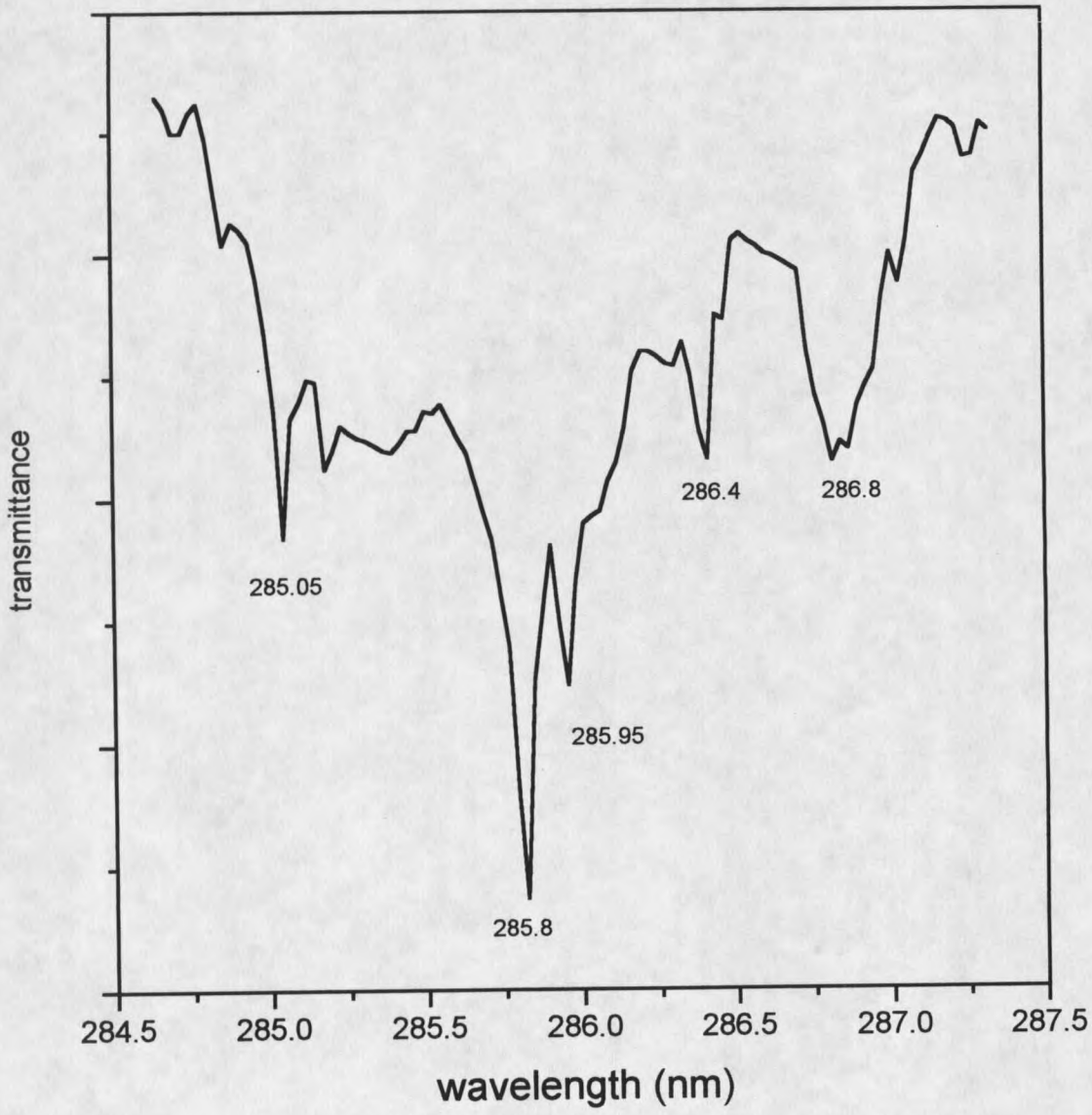

Figure 12. Transmittance spectrum of indole in argon at 20K, with a 0.2 cm^{-1} bandpass.

incrementally stepping across the S_1 origin, while at each increment the monochromator is scanned over the 26^0_1 line. It should be noted that, the fluorescence tracks the excitation frequency. The decrease in line intensity for redder excitation means that the laser is beginning to be scanned off the site.

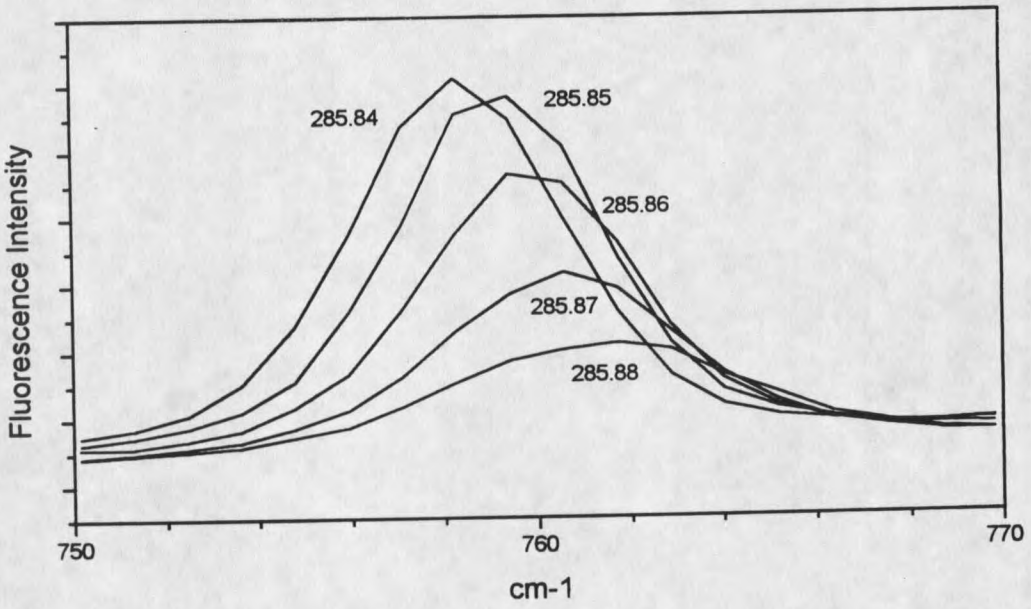

Figure 13. The 26^0_1 line excited at 285.84, 285.85, 285.86, 285.87, 285.88 nm, with a monochromator bandpass of 2 cm^{-1}.

The matrix environment affects the electronic energy of the molecule through stabilization without affecting the vibrational energy of the molecule, except for a few out-of-plane modes. This spectral alignment simplifies the comparison between the jet and argon spectra. Site 1, whose origin is 251 cm^{-1} red of the vacuum value, is used for the investigation of indole. The fluorescence excitation spectra were taken with the monochromator set at the

strongest fluorescence line (760 cm^{-1}), that being 26^0_1.

The fluorescence excitation spectrum of indole in argon at 20K is shown in Figure 14c, with the accompanying anisotropy in Figure 14d. For comparison, the jet fluorescence excitation spectrum is shown in Figure 14a and a simulated matrix spectrum from the jet data is shown in Figure 14b. All spectra are zeroed to the S_1 origin and have been aligned for comparison purposes in Figure 14. There are many similarities between the argon and the jet spectra, with many ^1L_b lines (Ω >1.3) have an accompanying line at the same relative position in the argon. The linewidths in the argon matrix are about 10 cm^{-1} and the phonon side band extends for 150 cm^{-1} to the blue.

The ^1L_b state is the S_1 state for indole, with high emission anisotropy. This anisotropy falls short of the theoretical maximum of r=+0.4 and theoretical minimum of r=-0.2, with an experimental high of r=0.1, indicative of a ^1L_b state, and an experimental low of r=-0.05, indicative of a ^1L_a state. These values are low in comparison to the theoretical values, but are at the proper ratio for perpendicular transition moments. This deviation from the theoretical values is due to depolarization of the light by matrix strained birefringence and simple light scattering. These reasons for the depolarization of light are not wavelength dependent, and do not hamper the experimental results. Therefore, the anisotropy is good for data analysis.

The jet spectrum in Figure 14a (with its 2-photon Ω values), the matrix spectrum and its emission anisotropy in Figures 14c and 14d display good

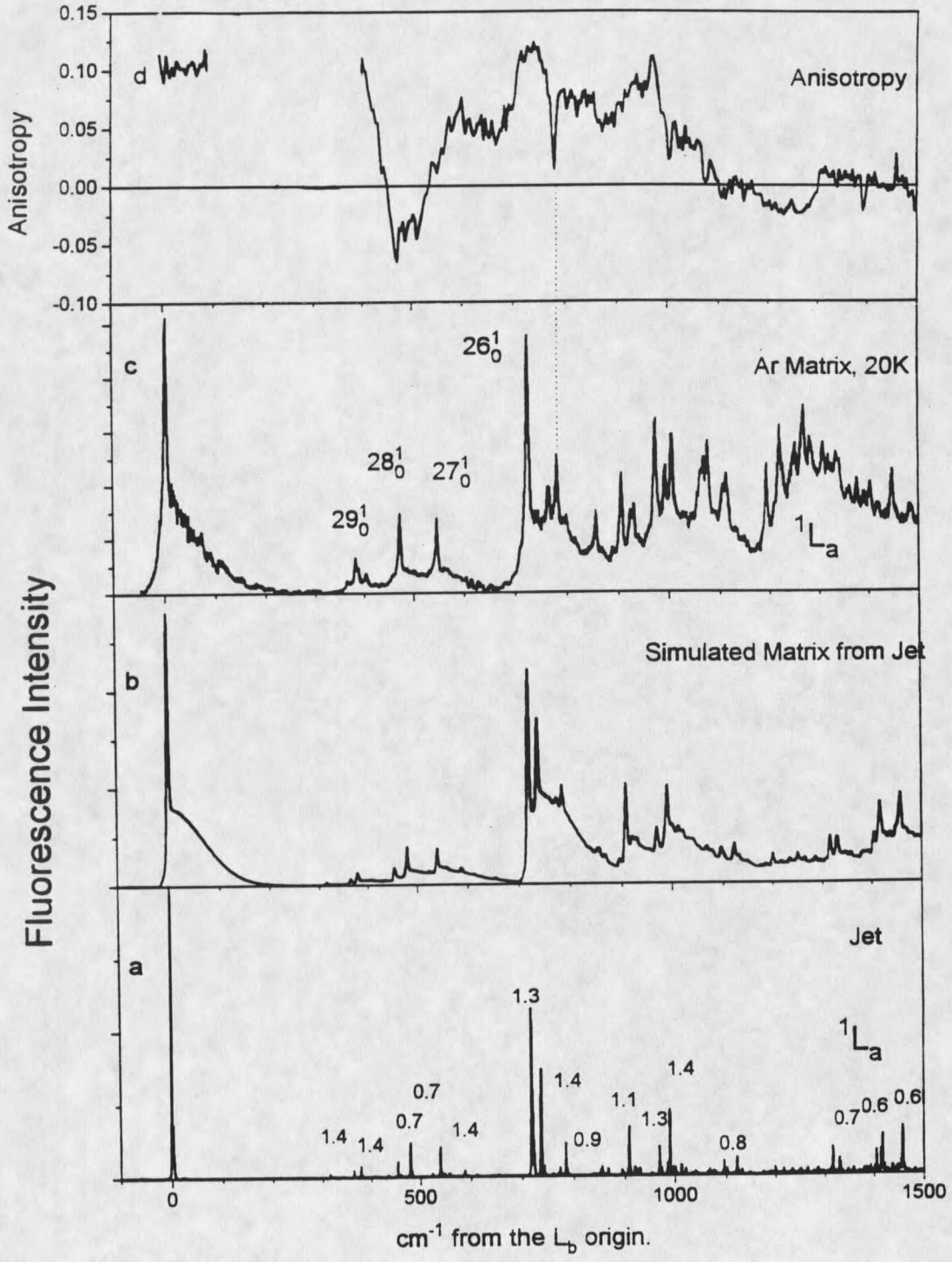

Figure 14. Supersonic jet fluorescence excitation spectrum of indole (with Ω values), (a), simulated matrix spectrum, (b), fluorescence excitation spectrum of indole in argon at 20K, (c), and the fluorescence anisotropy, (d).

correlation. Note that the 2-photon data is an absorption event and the anisotropy is an absorption + emission event. This provides a check of the experimental results with previous experimental data. Two good examples of this correlation are shown in both spectra, the 400-500 cm^{-1} region (Ω=0.7 and r=-0.05) and the line sitting at 780 cm^{-1} (Ω=0.9 and r=0.0), both displaying ^1L_a type character.

The final verification that the S_1 origin is indeed the ^1L_b came through 2-photon spectroscopy of indole in argon at 20K. The ^1L_b origin is found to have an Ω=1.3, the 26^1_0 line to have an Ω=1.3, and the 28^1_0 line to have an Ω=0.6 (the 2-photon spectra are shown in Figure15), also the 37^2_0 line has an Ω=1.2 and the vibronic active line around 780 cm^{-1} has an Ω=1.0. The line positions and the Ω values for the argon matrix and the jet are listed in Table 1. This data shows the compatibility between the argon matrix and the jet experiment.

Table 1. The two-photon Ω values of the argon matrix and the jet spectra.

Spectral shift[a] argon (jet)	Argon matrix[b] 20K	Jet[b]
0-0	1.3	1.4
471(454+480)	0.6	0.7
720(718.5)	1.3	1.3
763(737)	1.2	1.4
778(781.6)	1.0	0.9

a Values relative to the ^1L_b origin.
b The uncertainty is ±0.1.

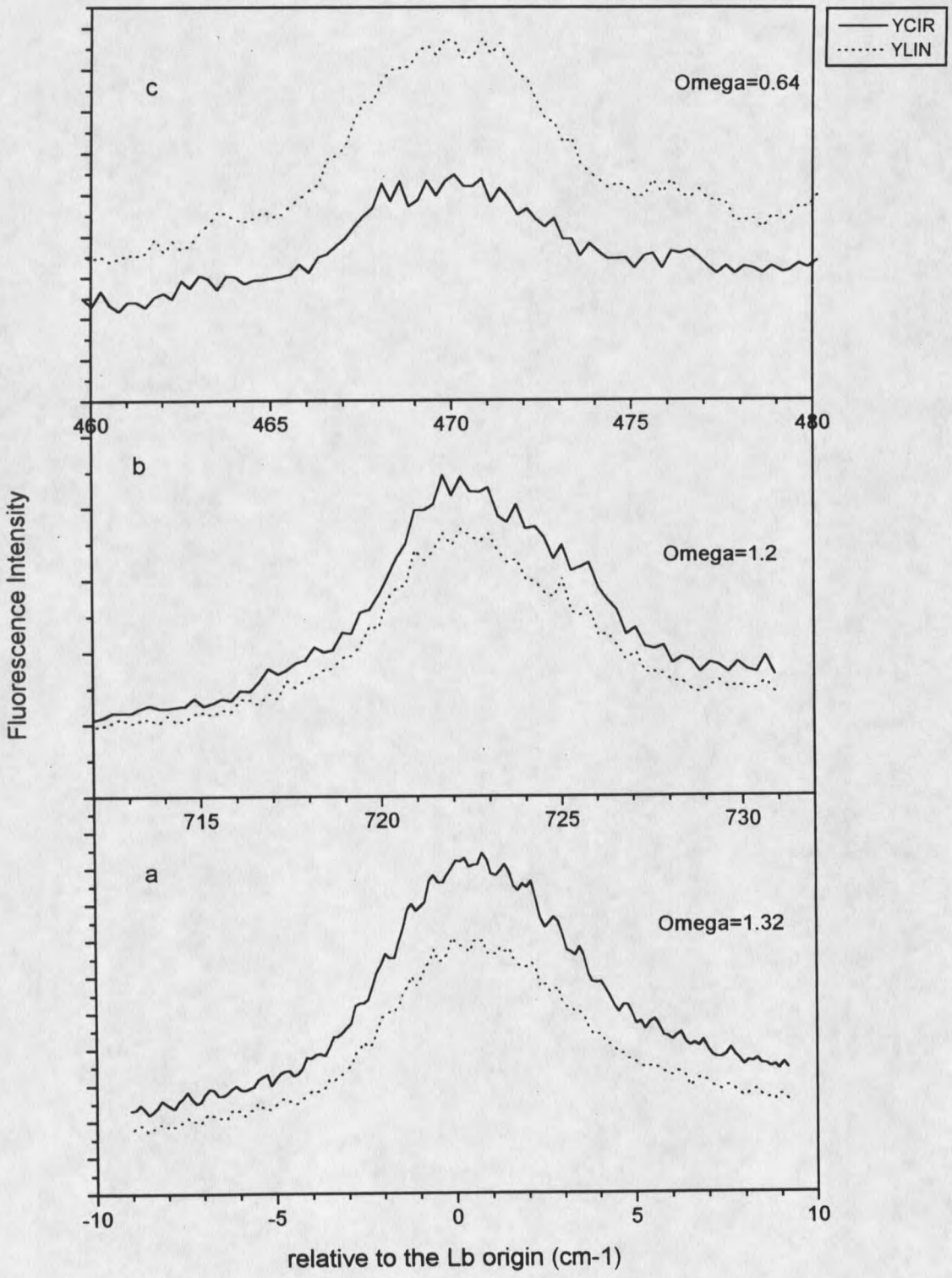

Figure 15. Two-photon spectrum of the ^1L_b origin, (a), 26^1_0, (b), and 28^1_0, (c), of indole in argon at 20K.

Fermi Resonance

The fluorescence excitation spectrum of indole in the jet gives lines at 455 and 480 cm^{-1}, which have an ^1L_a signature Ω=0.7 (see Figure 14a). In the same region in the argon matrix spectrum there is only one line at 471 cm^{-1}, r=-0.05. It has not yet been proven, but Fermi resonance has been proposed as a possible mechanism to explain these jet spectrum results. The 455 cm^{-1} line has been given the assignment $39^1_0 41^1_0$ [10] which is an out-of-plane combination vibration, and the 480 cm^{-1} line has been assigned 28^1_0, an in-plane vibration. The 455 cm^{-1} vibration is more intense than would be Franck-Condon allowed for an out-of-plane combination vibration of a planar molecule. This intensity can easily be explained if its intensity could be obtained by mixing with the strong neighboring 28^1_0 vibration.

The argon matrix spectrum, on the other hand, has broken the Fermi resonance and only one line appears at 471 cm^{-1}. The argon matrix increases the $39^1_0 41^1_0$ energy, removing the energy degeneracy and the weak $39^1_0 41^1_0$ line goes back down into the noise level of the spectrum. Since the Fermi resonance has been removed, then it would be expected that the 28^1_0 should be slightly red-shifted in energy. The 28^1_0 does red-shift by 9 cm^{-1} by the collapse of the Fermi resonance, which is nearly half the energy difference between the 480 and 455 cm^{-1} lines.

Yet another clear example of Fermi resonance can be seen in the out-of-plane 37^2_0 vibration, in which intensity is stolen from the in-plane 26^1_0 vibration.

The 37^2_0 line at 737 cm^{-1} in the jet and in the argon matrix the line blue-shifts 23 cm^{-1} to 760 cm^{-1} and loses much of its intensity. The intensity of the 37^2_0 line in the excited state is directly linked to its coupling to the 26^1_0 (718 cm^{-1}, jet) line, since the intensity of the 37^2_0 line in the fluorescence is relatively weak.

As listed below, additional evidence points to the 455cm^{-1} and 480 cm^{-1} lines being a Fermi doublet:

(1) When complexed with H_2O, D_2O, and methanol in the jet, or when placed in an argon matrix, the doublet intensity ratio varies or collapses into a single line[21].

(2) The aforementioned theoretical and empirical calculations predict the Franck-Condon factors for the $39^1_0 41^1_0$ combination to be small, and experimentally the $39^0_1 41^0_1$ is absent in the emission spectrum (660 cm^{-1} jet).

(3) Upon excitation of 28^1_0, some $28^0_1 39^0_1 41^0_1$ appears in the dispersed emission. Likewise, when $39^1_0 41^1_0$ is excited some $28^0_1 39^0_1 41^0_1$ also appears in the emission.

(4) There is evidence for the argon matrix shifting out-of-plane vibrations to higher energy. This is exemplified in the example of the 37^2_0 vibration mentioned above.

This and the evidence above confirm that the 455 cm^{-1} and the 480 cm^{-1} lines in the jet spectrum of indole are indeed a Fermi doublet.

From theory, the Fermi resonance coupling scheme can be deduced for these two lines. The intensity ratio of the 28^1_0 to the $39^1_0 41^1_0$ modes is 2 to 1,

and it can be assumed that all the intensity of the $39^1_0 41^1_0$ combination band came from the 28^1_0 line. Therefore, working backward and using the variation method, we can estimate the unperturbed energy separation and the coupling constant, β. The matrix that gives the proper coupling scheme is as follows:

$$\begin{bmatrix} 1 & 12 \\ 12 & 10 \end{bmatrix} \quad \begin{matrix} E_1 = -7.316 & c_1 = 0.822 & c_2 = 0.570 \\ E_2 = 18.316 & c_1 = -0.570 & c_2 = 0.822 \end{matrix} \qquad (18)$$

where E_1 and E_2 are α_1 and α_2, respectively, and c_1 (c^2_1=0.325) and c_2 (c^2_2=0.676) are the linear combination coefficients. The variation method places the unperturbed energy separation at (10-1 = 9 cm^{-1}) and the coupling constant (β) at 12 cm^{-1}.

Another case of Fermi resonance encompasses the out-of-plane combination band $41^1_0 42^1_0$ and the in-plane 29^1_0. The argon matrix apparently blue shifts the 41^2_0 and 42^2_0 lines from 315.7 and 364.9 to 364 and 403.2 cm^{-1}, respectively. The $41^1_0 42^1_0$ should have no Franck-Condon activity and it is not seen in the jet, yet it couples with the neighboring 29^1_0 line and its intensity is about the same as that of the 41^2_0 or the 42^2_0 line, see Figure 16. This increase in intensity is attributed to intensity borrowing via Fermi resonance.

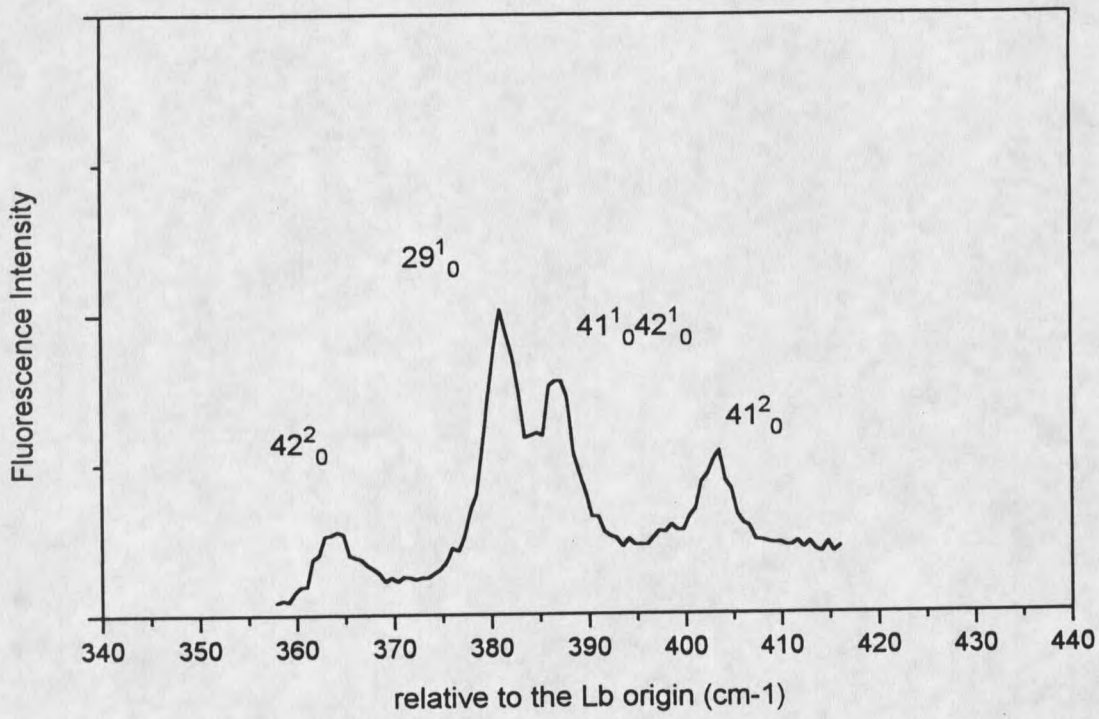

Figure 16. Fermi resonance of the 29^1_0 and the $41^1_0 42^1_0$ lines.

Herzberg-Teller Coupling

The 455 cm^{-1} and the 480 cm^{-1} lines in the jet spectrum of indole, which give ^1L_a signature, are really a Fermi doublet, as proven above. The line at 480 cm^{-1} is mostly the 28^1_0 vibration, which has red-shifted to 471 cm^{-1} in the matrix. The 28^1_0 still gives the ^1L_a signature in the argon matrix (low anisotropy), but the line shifts as an ^1L_b line. One explanation of this is Herzberg-Teller (HT) vibronic coupling by the 28^1_0 vibration between the ^1L_b and the ^1L_a manifold. If the 28^1_0 line displays vibronic coupling in the excited state, then it should be displayed in

the fluorescence. This requires polarization measurements both in the excited state and in the ground state. The excited state has already been examined, which leaves the ground state to be addressed, see Figure 17. Figure 17 shows three neighboring vibrational lines 28^0_1(545 cm^{-1}), 27^0_1(610 cm^{-1}), and 26^0_1(760 cm^{-1}); 26^0_1 and 27^0_1 are shown for contrast. The following anisotropy values for the 26^0_1, 27^0_1, and 28^0_1 lines are respectively: r=0.07, r=0.06, r=-0.02. Herzberg-Teller vibronic coupling can be proven by the following; first, the 28^1_0 and 28^0_1 lines are seen due to zero point motion (both in the ground state and the excited state) coupling intensity into the Franck-Condon integral in Equation 9. Second, the reason the lines are known to be coupled in because the vector that couples the intensity in Equation 9 is perpendicular the ^1L_b moment, giving low polarization both in the excited and the ground state of mode 28.

The ^1L_a Origin

The ^1L_a state of indole is expected to be differentially red-shifted relative to the ^1L_b state, due to their different permanent dipoles and their different dispersion interactions. The permanent dipole argument is the easier to grasp. The ^1L_a state is known experimentally and empirically to have a large permanent dipole (5-10 debye), which is much stronger than the dipole of the ^1L_b state (~2 debye)[64,65]. The relative shifts from vacuum to condensed phase medium caused by the permanent dipole difference can be estimated by the Onsager Mataga-Lippert type formula discussed in the theory section, with the refractive

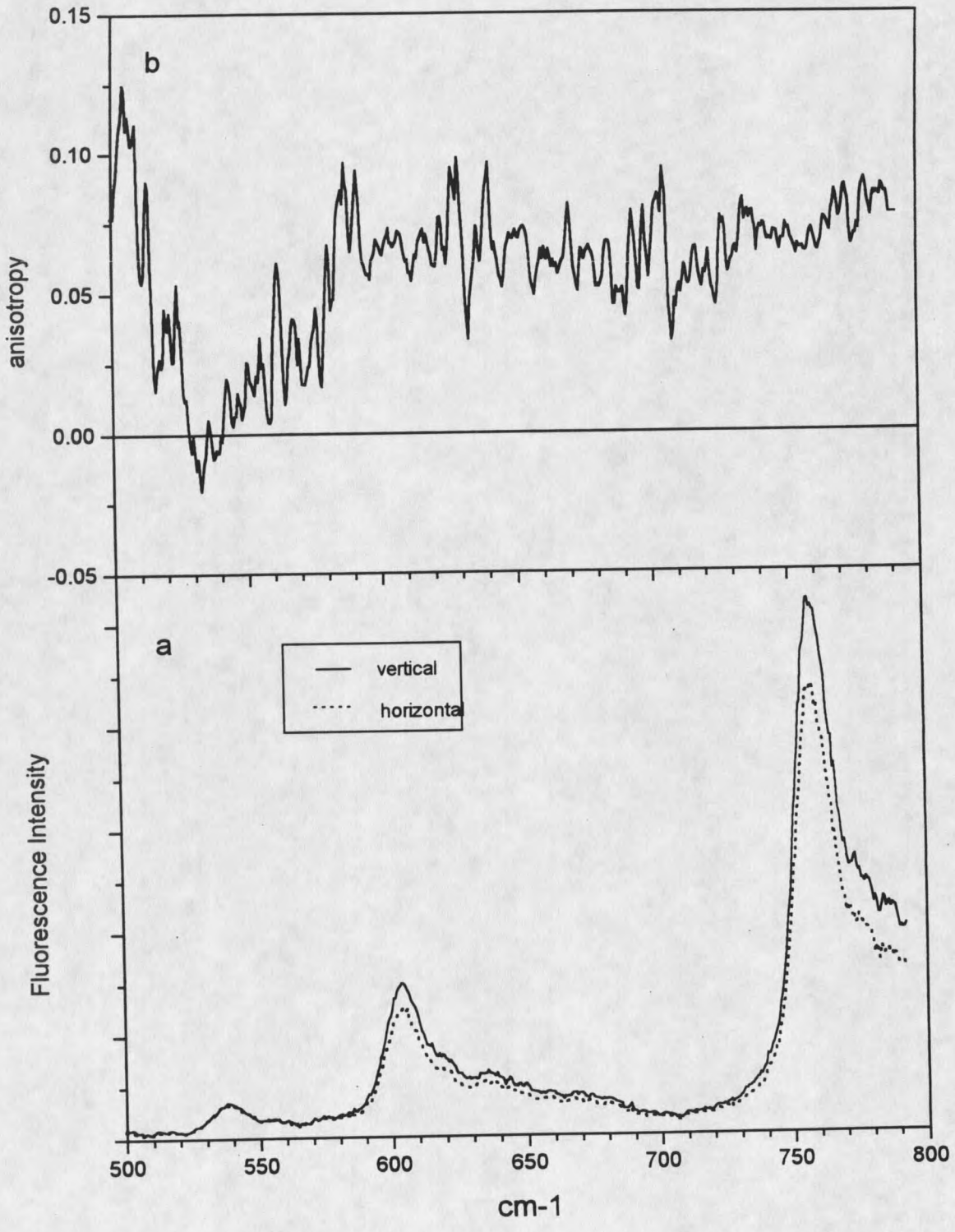

Figure 17. Fluorescence spectrum of indole in argon at 20K(500-850 cm^{-1}), (a), and fluorescence anisotropy, (b).

index of solid Ar (1.28)[77], cavity radius of 3.4 Å, ground dipole 2 debye, ^1L_a dipole 5 debye, and ^1L_b dipole 3 debye. The red-shift estimates are 400 cm^{-1} for the ^1L_a and 100 cm^{-1} for the ^1L_b. Following the method of Lami and Glasser[65], the estimates are 470 cm^{-1} for the ^1L_a and 120 cm^{-1} for the ^1L_b[66]. The ^1L_b red shift is known experimentally to be between 250 and 375 cm^{-1}, depending on the site. It would be feasible for the ^1L_a state to shift 100-200 cm^{-1} more than the ^1L_b state by this mechanism[66].

As mentioned in the theory section, a good portion of the observed shift comes from a dispersion mechanism, which is known to red-shift the ^1L_a state about 500 cm^{-1} more than the ^1L_b state in hydrocarbon solvent for naphthalene and anthracene[52]. The ^1L_a state of anthracene is known to red-shift 500-700 cm^{-1} in solid argon[51]. The process by which this shift occurs is not well understood.

Concerning the true location of the ^1L_a origin in published literature, there has been no definite conclusion found. However, there is a region (1100-1500 cm^{-1}) in the fluorescence excitation spectra of the argon matrix and the supersonic jet that does not correlate. It is this region that gives the true location of the ^1L_a origin. In the jet spectrum (Figure 14a) many ^1L_a lines appear between 1300-1500 cm^{-1} and no lines appear between 1100-1300 cm^{-1}. In contrast, in the matrix spectrum (Figure 14c) many ^1L_a lines appear between 1100-1300 cm^{-1}, but little ^1L_a intensity appears between 1300-1500 cm^{-1}. It can be concluded that the ^1L_a intensity has red-shifted approximately 200 cm^{-1} in the matrix when compared to the jet. Since the ^1L_a state differentially red-shifts

relative to the ^1L_b state in the matrix, a distinction can be made between actual ^1L_a lines and vibronically coupled ^1L_b lines (471 and 780 cm^{-1} lines). The ^1L_a origin is split into several lines in the argon matrix just as it is in the jet.

As observed in the ground state, the dispersed fluorescence spectrum of indole in an argon matrix at 20K is shown (Figure 18b) with excitation at the 26^1_0 (720 cm^{-1}) line and linewidths of 10 cm^{-1}. For comparison, the jet fluorescence spectrum is shown (Figure 18a, Kurt Short)[67], with the origins aligned. The line positions and intensities are very similar between the spectra, thus the matrix does not perturb ground state vibrational energy. The important regions of the spectrum are the strong 26^0_1 transition (760 cm^{-1}) and the region of strong intensity near 1250 cm^{-1} that suggest ^1L_b fluorescence. These differences will be discussed later in the thesis. Be it noted that the fluorescence spectrum also includes strong phonon wings extending to the blue 100 cm^{-1} from the zero-phonon line.

Site Structure

Indole incorporated in an argon matrix at 20 K fits into specific reproducible site classes within the argon matrix. Each separate site class has a distinctive solvent orientation and in turn, each site has a different induced field which indole causes and senses, due to its interaction with the surrounding argon. These fields are different enough in strength to cause the ^1L_b origin to vary by 223 cm^{-1} between the most blue and red-shifted sites. Since the ^1L_b

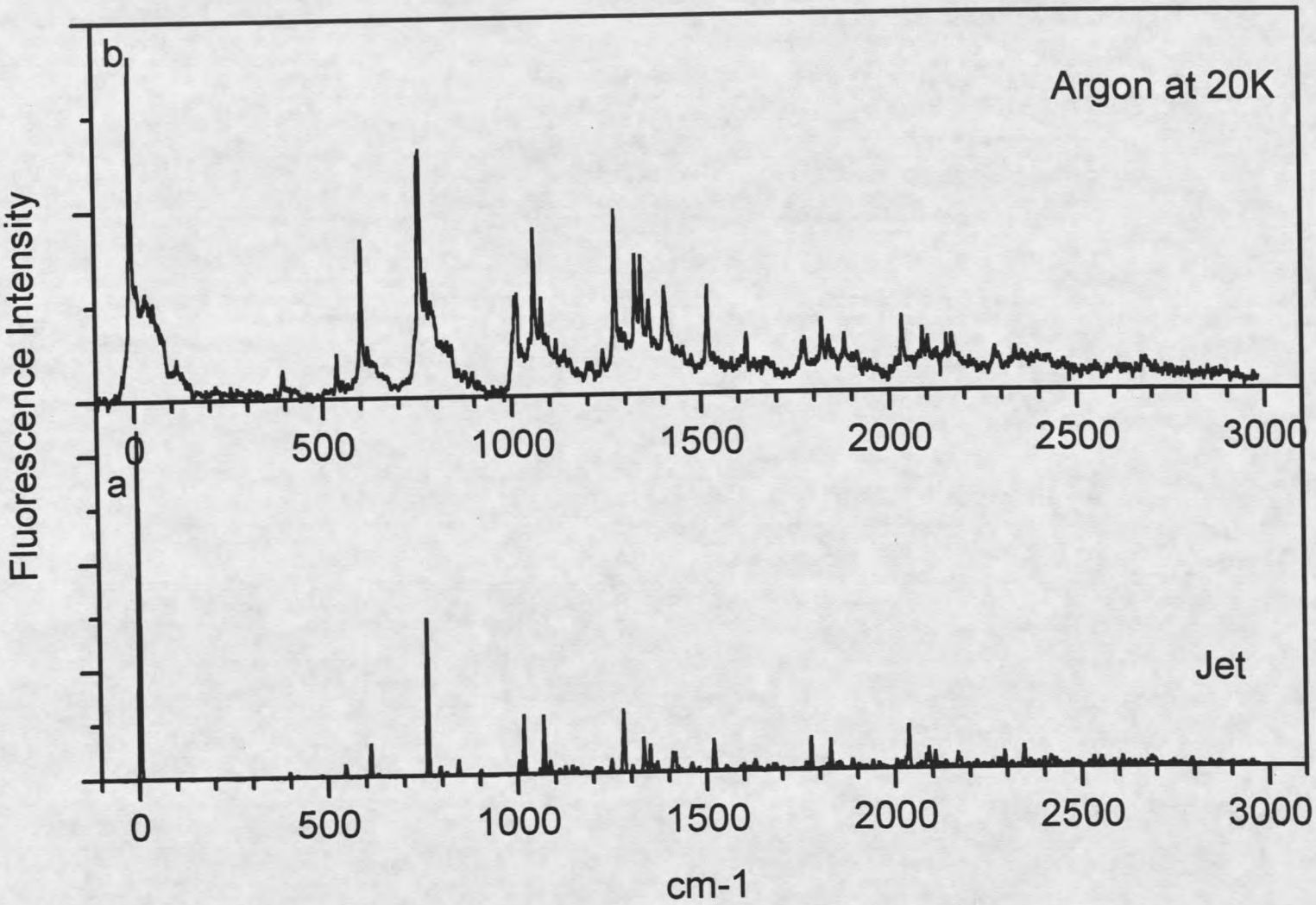

Figure 18. Fluorescence spectrum of indole in argon at 20K, (a), and the stick spectrum, (b).

origin shifts that much, it would be expected that the ^1L_a origin would shift as much or more, similar to anthracene shifts in solid argon[51]. Therefore, by inspecting the spectra of indole from different sites we can, in essence, track spectral differences caused by differences in ^1L_a -^1L_b energy gaps tuned by the site, see Figure 19. All spectra were taken while monitoring the 26^0_1 line in the emission.

The fluorescence excitation spectrum of indole in site 1 (the main site) is shown in Figure 19a. The ^1L_b origin of site 1 red-shifts 251 cm^{-1} from its vacuum value and the ^1L_a origin sits 1100-1300 cm^{-1} above the ^1L_b origin. The out-of-plane vibrations are blue-shifted by the argon matrix from their vacuum values; which are as follows, 37^2_0 shifts 27 cm^{-1} to 764 cm^{-1}, 42^2_0 shifts 48 cm^{-1} to 364 cm^{-1}, and 41^2_0 shifts 37 cm^{-1} to 403.2 cm^{-1}. The Fermi doublet made up of the 29^1_0 and the $41^1_0 42^1_0$ is at 381.2 and 386.7 cm^{-1} respectively. For simplicity, the rest of the sites will be compared with site 1.

The ^1L_b origin for site 5 is blue-shifted 100 cm^{-1} from site 1 (see Figure19c) and the ^1L_a grouping is in the 1200 to 1400 cm^{-1} region, further blue-shifted 70 cm^{-1} from site 1. This can be attributed to a larger ^1L_a-^1L_b energy gap. The larger energy gap has led to a reduction in the intensity of the 28^1_0 (vibronically active) line when compared with the 27^1_0 line. The out-of-plane vibrations all red-shift: 37^2_0 10 cm^{-1} to 755 cm^{-1}, 42^2_0 to 356 cm^{-1}, and 41^2_0 to 401.5 cm^{-1}. The Fermi doublet is also present at 375.3 cm^{-1} (29^1_0) and 380.7 cm^{-1} ($41^1_0 42^1_0$).

Site 2 displays the greatest red-shift of all the sites and gives the broadest lines (30 cm^{-1}). Also, the fluorescence excitation spectrum (see Figure 19b) has more unusual features than the other spectra. The unique feature of this is the broad line (60 cm^{-1}) at 638 cm^{-1} giving ^1L_a intensity. It is speculated that this is the vibronically active line that sits at 780 cm^{-1} in site 1, that red-shifts by 142 cm^{-1}, broadening to 60 cm^{-1}, and increasing in intensity, due to coupling to the nearby ^1L_a state. Furthermore, the vibronically active 28^1_0 line behaves similarly. This line red-shifts 27 cm^{-1} to 444 cm^{-1}, it also broadens, and increases in intensity to a point that it is nearly equal in intensity to the strong 26^1_0 line. It is the line at 776.4 cm^{-1} that is believed to be the out-of-plane 37^2_0 line that blue-shifts 12.2 cm^{-1} to this position, with its high anisotropy. Due to the broadness of this site, clarification of other points is difficult.

Lastly, site 3 is a weak site with high spectral background, therefore, making many comparisons to site 1 and 2 is difficult. This spectrum is very similar to the spectrum of site 1, with the out-of-plane 37^2_0 sitting at 760.5 cm^{-1}.

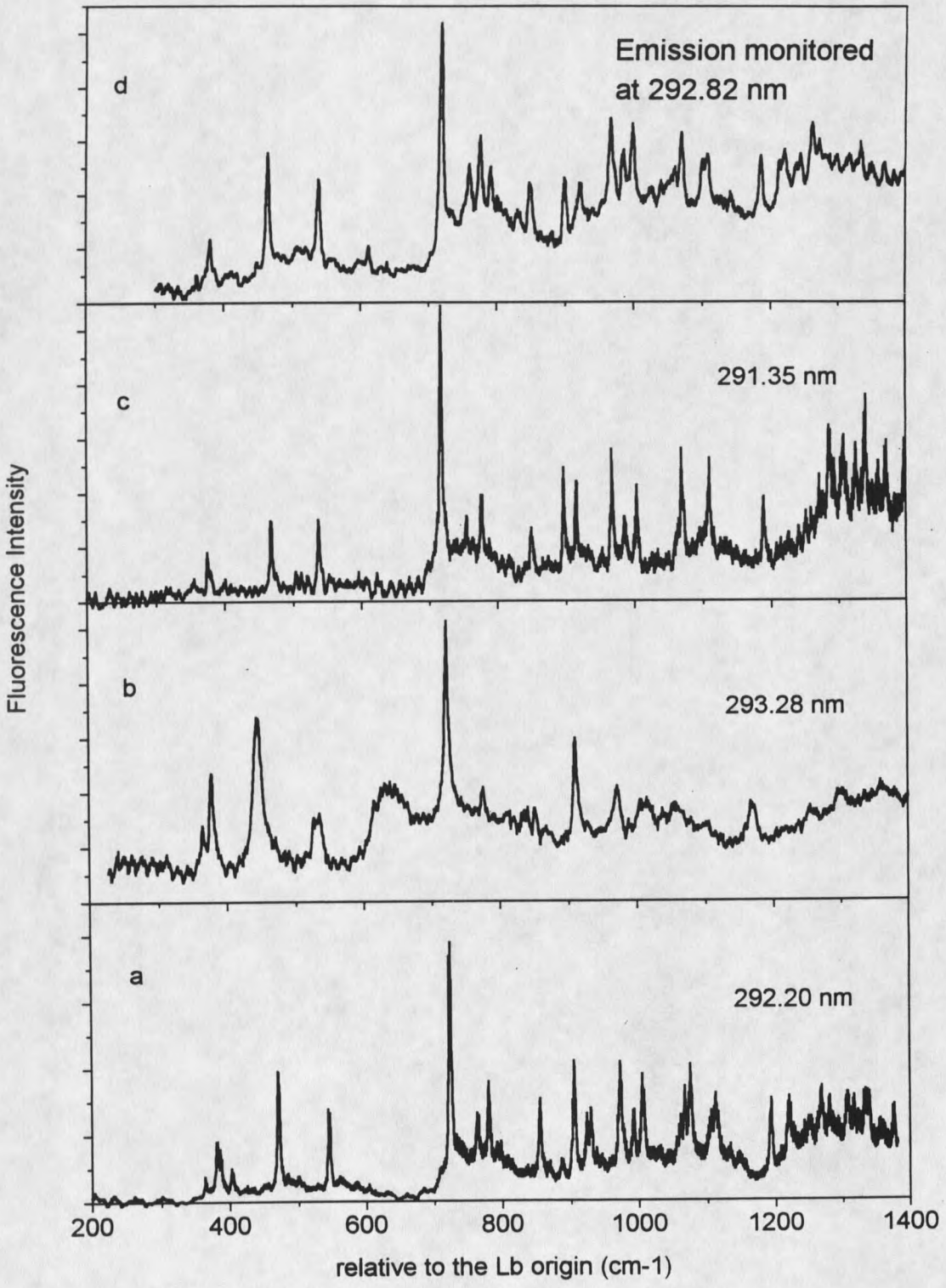

Figure 19. Fluorescence excitation spectra (200-1400 cm^{-1}) of indole in argon at 20K from site 1, (a), site 2, (b), site 5, (c), and site 3, (d).

Phosphorescence

The phosphorescence spectrum of indole in argon at 20K shows up in the blue region of the visible spectrum, with a triplet state lifetime of nearly 10 s. For the phosphorescence lifetime decay and the log plot, which is a single exponential, see Figure 20. The phosphorescence is also quite intense, about 1/3 the fluorescence intensity.

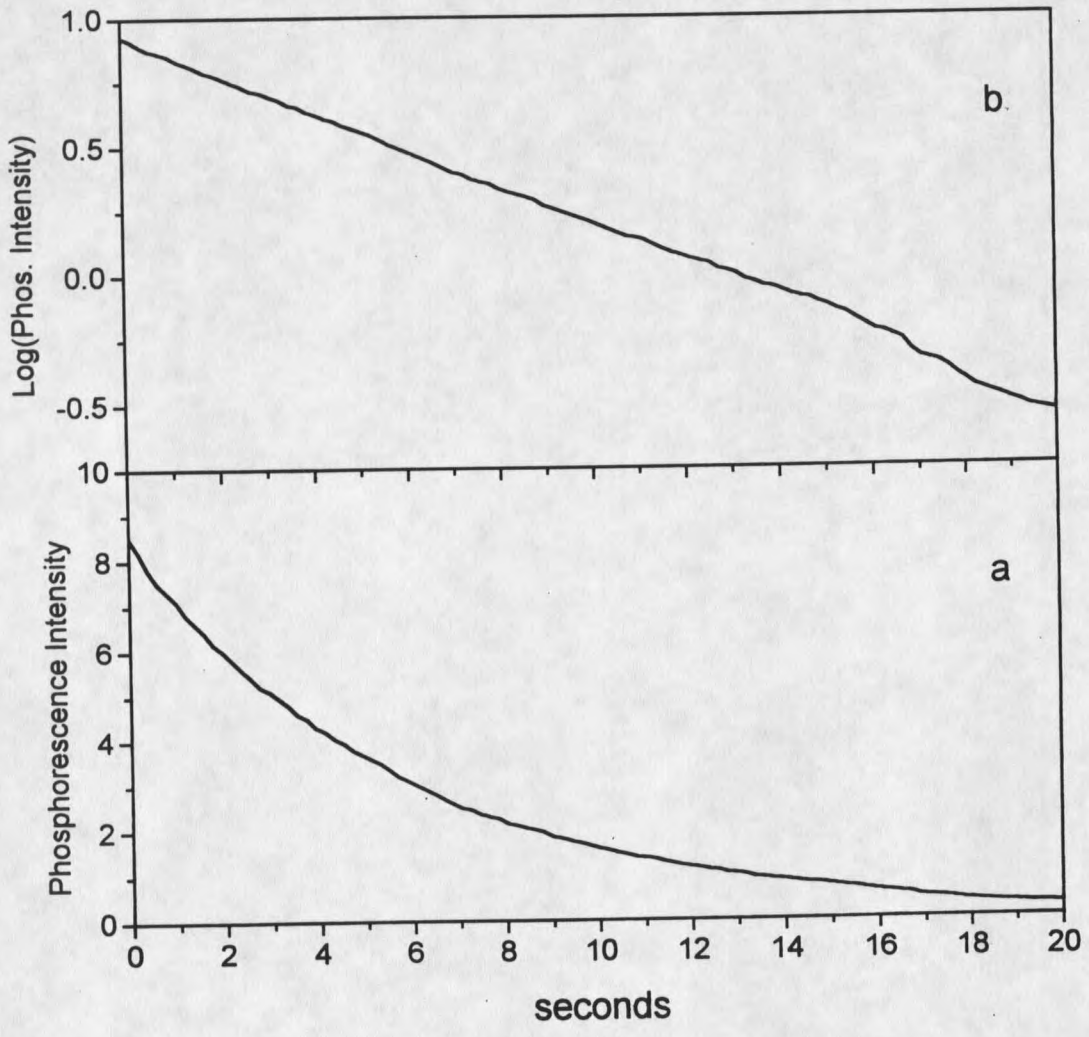

Figure 20. The phosphorescence intensity decay, (a), and the log plot, (b).

The accompanying phosphorescence spectra of indole in argon at 20K are shown in Figure 21 on an absolute wavelength scale. The three phosphorescence spectra shown are site selected from three different singlet energy sites. Figure 21a displays the phosphorescence from site 1 at 285.8 nm with the triplet origin ^3L_a at 403.4 nm (24, 789 cm^{-1}), Figure 21b displays the phosphorescence from site 5 (the most blue site) at 285.05 nm with the ^3L_a origin at 401.07 nm (24,933 cm^{-1}), and Figure 21c displays the phosphorescence from site 2 (the most red site) at 286.8 nm with the ^3L_a origin at 403.8 nm (24,764 cm^{-1}). All three spectra have the phosphorescence originating from the lowest triplet state, that is, the ^3L_a state.

The phosphorescence from both sites 1 and 2 has a linewidth of 100 cm^{-1}, which is quite broad when compared to the sharp fluorescence and the sharpness of the sites, which has been noted previously by Williamson and Kwiram[69]. The triplet state is known, from experiment, to have a smaller oscillator strength than the singlet state, and from theory, a smaller permanent dipole than the ground state[68]. If the broadness is solely due to the dipole, then phosphorescence would be expected to have sharper lines. Yet the phosphorescence is unexpectedly broad. An important point to remember is that the singlet sites are in resonance (tuned by the laser) and the triplet sites are not. The experiment results suggest that these molecules in this selected singlet site have differing triplet energies of about 200 cm^{-1}. This energy difference is similar to the energy difference between ^1L_b sites within the argon.

Experimentally, sharp singlet sites give broad phosphorescence and in one case, sharp phosphorescence. The phosphorescence spectrum from site 5 is shown (Figure 21b) and is made up of a sharp component (10 cm^{-1}) and a broad component (300 cm^{-1}) lying toward the red. The spectral data suggests that the phosphorescence from site 5 is really composed of two types of sites, one being highly ordered, giving sharp ^3L_a emission, and the others being more disordered, giving broad ^3L_a emission. The highly ordered component could be composed of indole in identically oriented argon cages, yielding a narrow energy distribution of triplet sites. The other component could be composed of indole all having identical S_1 energies, but in different oriented argon cages giving a broader energy distribution of triplet energy. This theory is speculative, and the real reason may include differences in lifetime and spin-orbit coupling.

The phosphorescence spectrum from site 5 is shown in Figure 22a and the accompanying stick spectrum is shown Figure 22b. Both spectra are zeroed to the ^3L_a origin and are aligned for convenience of comparison. The stick spectrum is made from the phosphorescence spectrum by taking the peak heights of all the lines and subtracting the background, giving sharp L_a emission. The line frequencies, intensities, and assignments are listed in Table 2. This emission has the ^1L_a fingerprint and can be distinguished easily from its ^1L_b counterpart. It has nearly equal intensity in the 27^0_1 at 599 cm^{-1} and the 26^0_1 at 750 cm^{-1} lines and has strong intensity in the 10^0_1 line at 1502 cm^{-1}, the 9^0_1 line at 1570 cm^{-1}, and the 8^0_1 line at 1608 cm^{-1}, which are absent in ^1L_b.

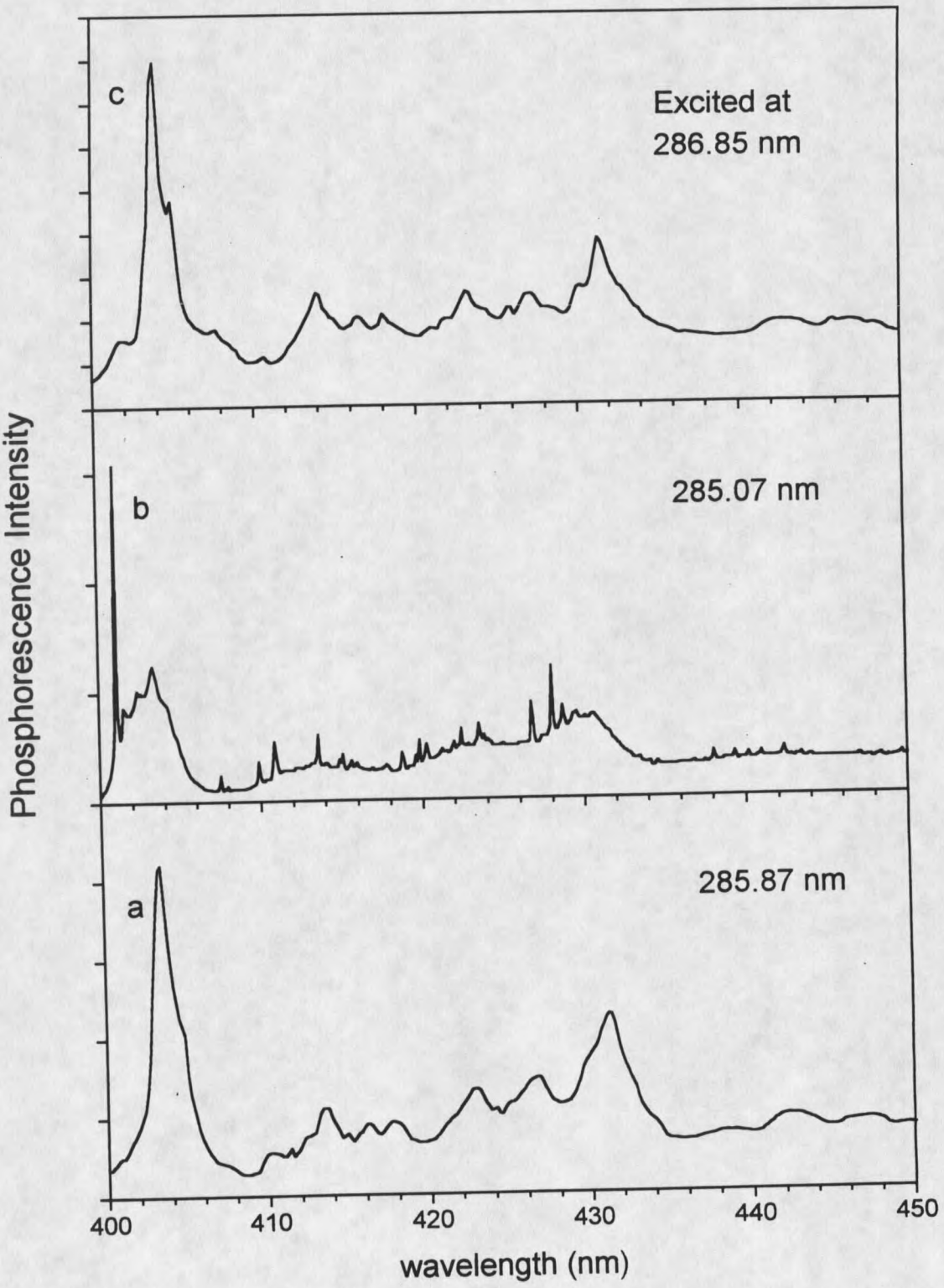

Figure 21. The phosphorescence spectra of indole in argon at 20K from site 1, (a), site 5, (b), and site2, (c).

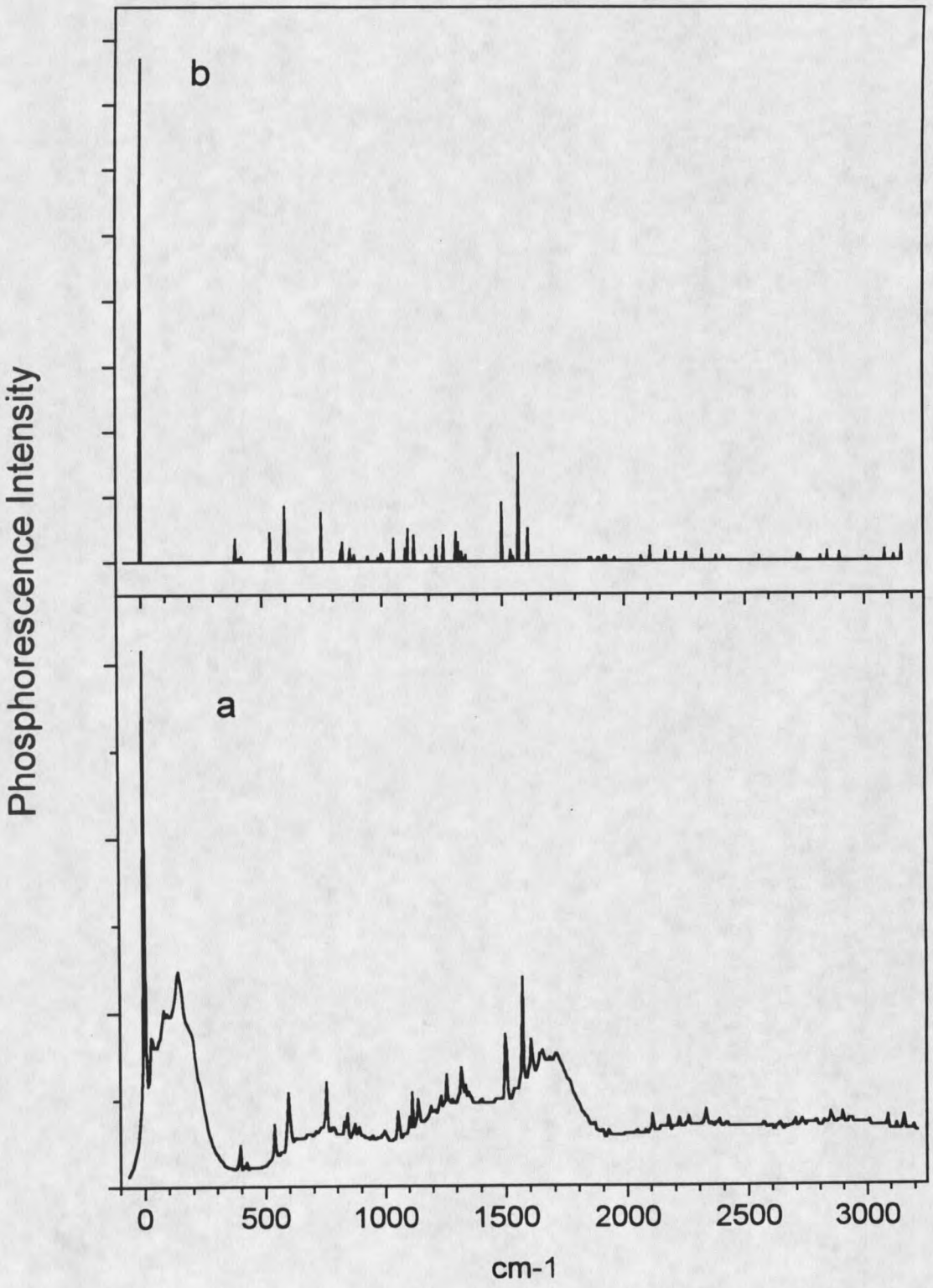

Figure 22. The phosphorescence spectrum of indole in argon at 20K from site 5, (a), and the stick spectrum, (b).

Table 2. Indole Phosphorescence

Spectral[a] shift (cm^{-1})	Intensity[b]	Assignment	Spectral[a] shift (cm^{-1})	Intensity[b]	Assignment
0.0	1.00		1354.6	0.01	
392.5	0.05	29^0_1	1502.0	0.12	10^0_1
408.7	0.01		1537.4	0.02	
418.4	0.01	42^0_2(?)	1546.3	0.01	
537.7	0.06	28^0_1	1569.8	0.21	9^0_1
598.5	0.11	27^0_1	1608.0	0.06	8^0_1
750.7	0.10	26^0_1	1857.5	0.01	
832.4	0.02		1866.1	0.01	
838.6	0.04	39^0_1(?)	1894.8	0.01	
869.9	0.03	25^0_1	1900.5	0.01	
888.6	0.01	24^0_1	1920.5	0.01	
944.6	0.01		1926.2	0.01	
987.9	0.01		1963.2	0.01	
1000.3	0.02		2073.6	0.01	
1006.4	0.01	23^0_1	2110.2	0.03	
1052.6	0.05	22^0_1	2174.5	0.02	
1101.7	0.03	21^0_1(?)	2213.6	0.02	
1112.4	0.07	20^0_1	2258.0	0.02	
1138.4	0.05	19^0_1	2324.3	0.02	
1190.1	0.01		2382.0	0.01	
1232.6	0.03	16^0_1	2412.1	0.01	
1262.8	0.05	15^0_1	2561.5	0.01	
1315.6	0.06	14^0_1(split)	2692.9	0.01	
1323.1	0.04	14^0_1	2720.8	0.01	
1338.1	0.02				

Table 2. Continued

Spectral[a] Shift (cm^{-1})	Intensity[b]	Assignment	Spectral[a] Shift (cm^{-1})	Intensity[b]	Assigment
2732.8	0.01		3010.9	0.01	
2817.5	0.01		3088.3	0.02	
2846.4	0.02		3126.8	0.01	
2897.6	0.02		3157.5	0.03	

a Frequencies ± 10 cm^{-1}.
b Intensity relative to the ^3L_a origin.

3-Methylindole

3-methylindole (3MI) is an important molecule to study because it bridges the gap between indole and tryptophan. It is the 3-position at which indole links to form tryptophan, therefore, the perturbation made by the methyl group to the energy levels would be similar to indole found in tryptophan. This aids the understanding of the photophysics of indole in proteins. It is also known from previous spectroscopic studies that methyl substitution in the 3-position reduces the ^1L_a-^1L_b separation[8] and the methyl rotor is not active upon excitation[9,22].

The S_1 origin region of 3MI, incorporated into solid argon at 20K is shown in the transmittance spectrum in Figure 23. The spectrum displays the ^1L_b origin at 288.8 nm and the ^1L_a origin 260 cm^{-1} higher in energy at 286.6 nm. Neither origin region shows any intrinsic narrow site structure, only a broad site of 200 cm^{-1} that is most likely composed of many closely spaced narrow sites.

Figure 24b displays the fluorescence excitation spectrum of 3MI in solid argon at 20K, with the emission monitored at the 760 cm^{-1} line, 26^0_1, and Figure

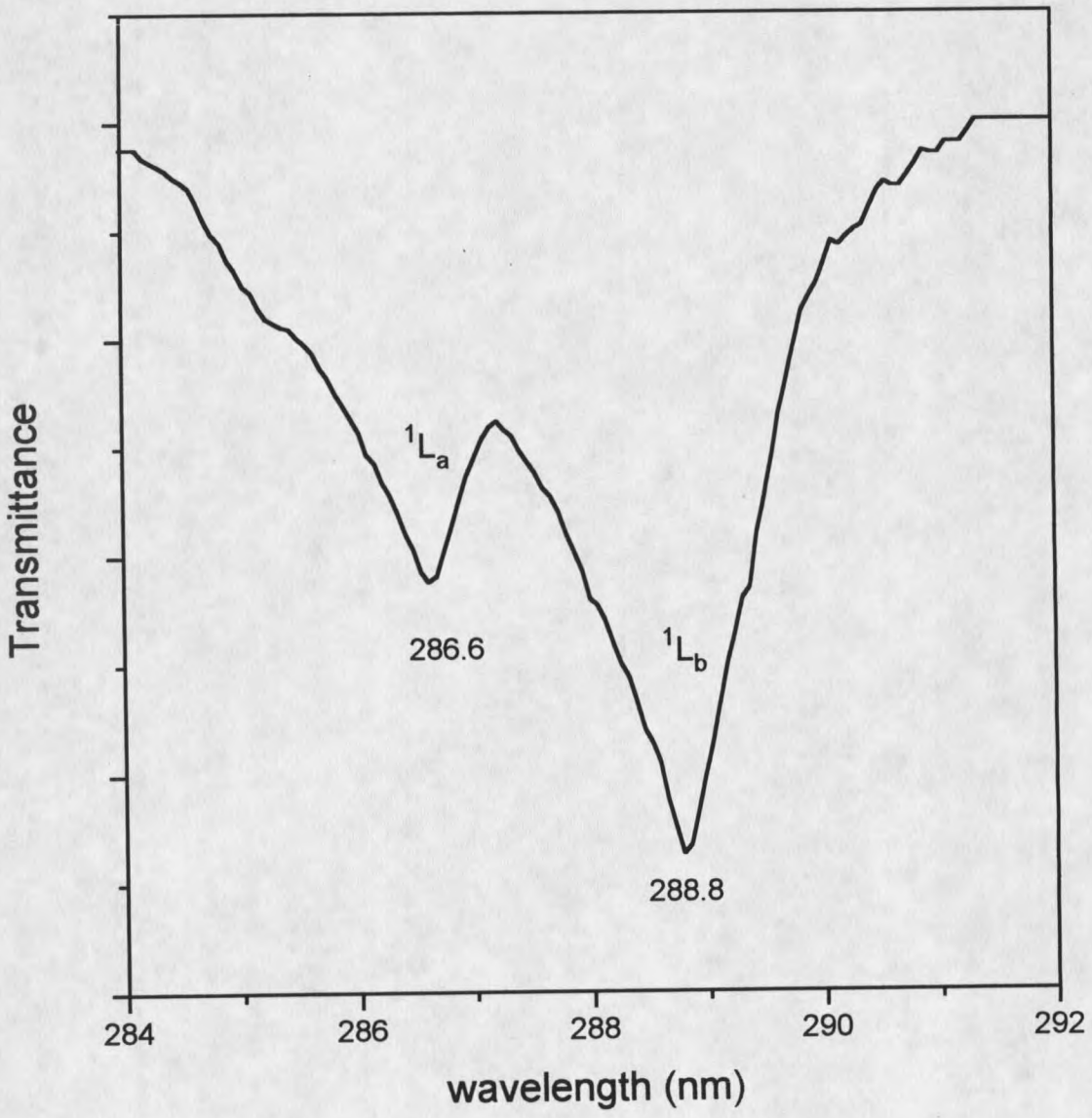

Figure 23. Transmittance spectrum of 3MI in argon at 20K, with a 0.2 cm^{-1} bandpass.

24c displays the fluorescence anisotropy. For comparison, Figure 24a displays the fluorescence excitation spectrum of 3MI in the jet (with Ω values indicated). All spectra are zeroed to the ^1L_b origin. The argon matrix stabilizes the ^1L_b origin 254 cm^{-1} from its vacuum value, and is located at 288.78 nm (34,628 cm^{-1}).

By examining Figure 24b, the first thing to note is that 3MI has broader lines (70 cm^{-1}) than the sharp lines intrinsic to indole (12 cm^{-1}) in an argon matrix at 20^{0}K. However, this difference is expected upon examination of the site structure (see Figure 23). The lineshape of 3MI is quite different from indole. 3MI has a sharp zero-phonon component (but, not has sharp as indole's) with a phonon sideband that extends further up the zero-phonon band, giving an apparent broadness of 70 cm^{-1} at half width.

The site width comes from either the intrinsic site that 3MI holds within the argon matrix under these conditions, or the energy separations of these sites. It would be reasonable to suppose that indole and 3MI occupy different sites and 3MI only occupies a site with greater inhomogeneous broadening, possibly a more loose fitting site. Structurally 3MI and indole are very different. The alternative is that this broad site is composed of many overlapping sharp sites that are close in energy, and cannot be site selected. 1MI clarifies this issue. 1MI is nearly geometrically equivalent to 3MI and expecting both 3MI and 1MI to sit in a similar site would be reasonable. 1MI fits into at least one sharp site within the argon (see Figure 38); therefore, it is also conceivable that 3MI also fits into sharp sites. This evidence suggests that the broadness comes from

tightly packed overlapping sites.

The anisotropy in Figure 24c is low in comparison to the theoretical values (maximum anisotropy=+0.08 and minimum=-0.04). However, they are at the proper ratio for perpendicular transition moments, and the anisotropy is useful for analyzing data.

In Figure 24a and 24b there exist many differences between the two spectra. The jet spectrum in Figure 24a contains many ^1L_a lines (Ω~0.5) between 300 cm^{-1} and 800 cm^{-1} that are absent in the matrix spectrum in Figure 24b. The major line contributors being the 356, 409, 420, 467(?), 609, 617, and 739-749 cm^{-1} lines. The sum of these lines is close to the intensity of the ^1L_b origin, supporting the notion of a split origin. The 467.5 cm^{-1} line will not be counted as an ^1L_a line and is believed to be the vibronically active 28^1_0 ^1L_b line, because the 2-photon spectral contour using linear polarized light shows no a_1, e splitting seen for all other ^1L_a lines[22]. The intensity of the 28^1_0 line is also greater than its indole counterpart, which can be explained by the closer proximity of the ^1L_a state, thus enhancing the coupling.

The matrix fluorescence excitation spectrum in Figure 24b displays a distinct, intact ^1L_a origin (r=-0.04) 260 cm^{-1} to the blue of the ^1L_b origin. By 3MI being placed in the argon matrix, the ^1L_a origin has been red-shifted 100 to 200 cm^{-1} more than the ^1L_b origin, which is similar to that found in indole. The integrated intensities of the two origins are nearly equivalent, as predicted by theory[38,70]. The ^1L_a origin is not split in this case. The reason the ^1L_a origin is

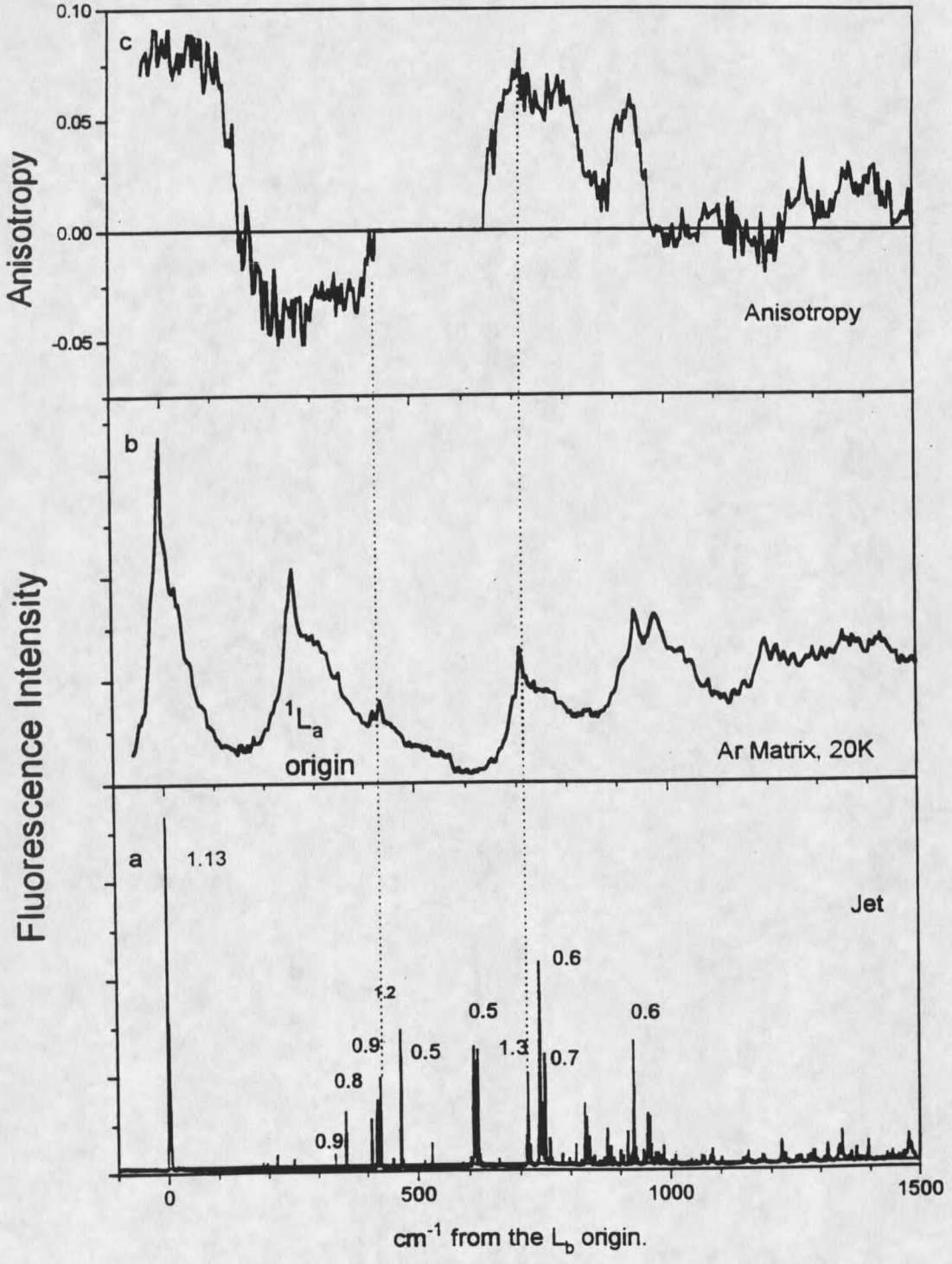

Figure 24. Supersonic jet fluorescence excitation spectrum of 3MI (with Ω values), (a), fluorescence excitation spectrum of 3MI in argon at 20K, (b), and fluorescence anisotropy, (c).

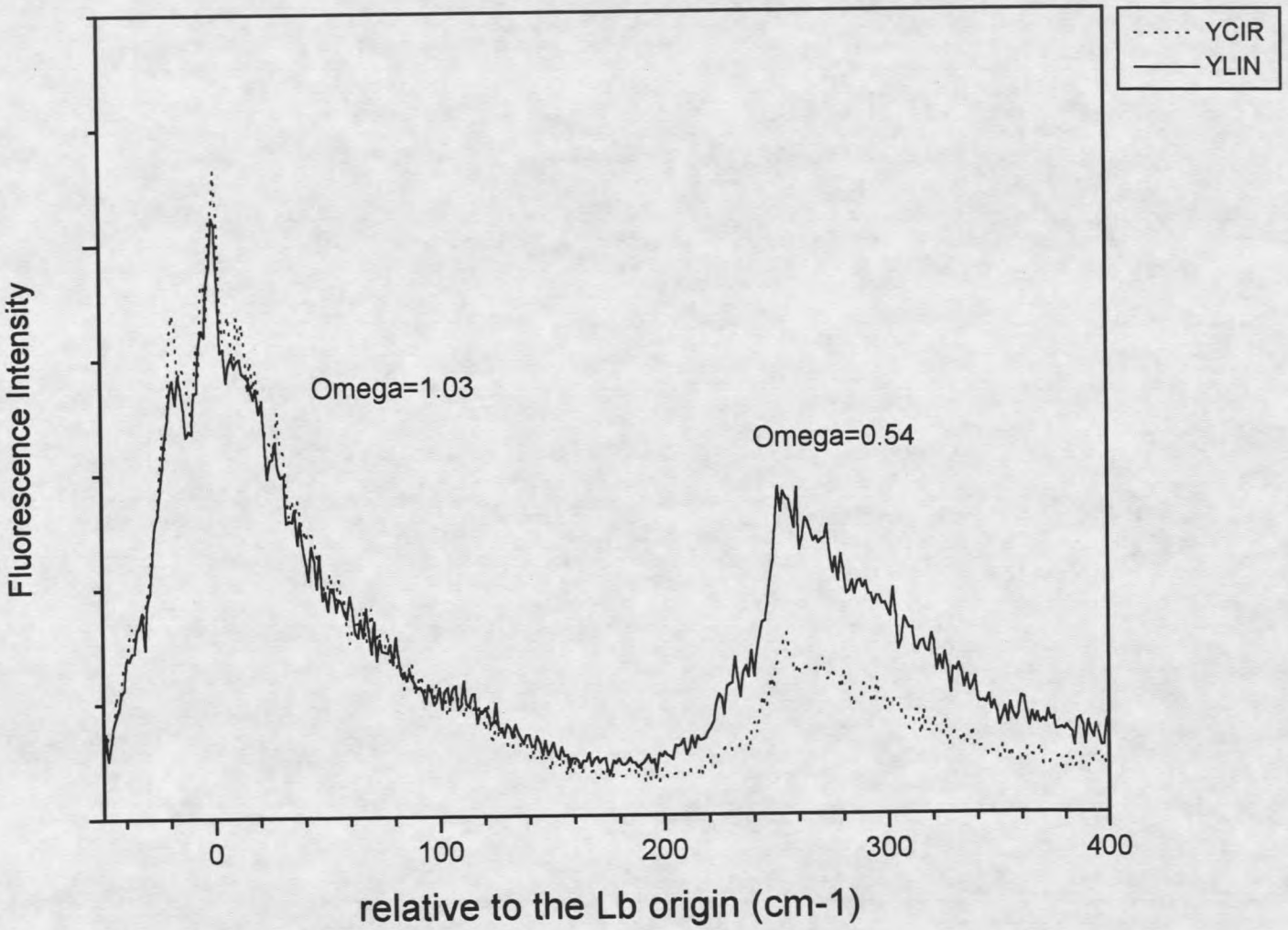

Figure 25. Two-photon spectrum of the ^1L_a and ^1L_b origin region (-50-400 cm^{-1}) of 3MI in argon at 20K.

intact may lie in its new position 260 cm^{-1} above the ^1L_b origin, where many vibrational states do not exist, or perhaps the vibrational states (out-of-plane) that are in the vicinity cannot couple. Working backwards from the argon into the jet, the uncoupled ^1L_a origin in the jet should lie 450 cm^{-1} above the ^1L_b origin under jet conditions. The ^1L_a and ^1L_b origins are verified by 2-photon data taken of 3MI in argon at 20K, see Figure 25. The S_1 has Ω=1.03 and the S_2 has Ω=0.54. The two photon spectrum displays at least two sites on the ^1L_b origin, due to the large slit width (40 cm^{-1} bandpass) used in collecting the 2-photon data.

In the jet fluorescence excitation spectrum, two prominent lines have ^1L_b character: 27^1_0 at 427 cm^{-1} and 26^1_0 at 715 cm^{-1} . These two lines also appear in the matrix spectrum at the same relative positions and can be identified by their high anisotropy. The 27^1_0 line at 427 cm^{-1} is the small line in the phonon shoulder of the ^1L_a origin. The anisotropy jumps from -0.04 to 0.0 over this line, clearly displaying ^1L_b character. The other line is the strong 26^1_0 line at 715 cm^{-1} and it is clearly ^1L_b, r=+0.06. The matrix spectrum also has a strong ^1L_b line centered at 930 cm^{-1}, r=+0.06, and in the jet spectrum there lie many lines in this region, yielding great intensity.

The ^1L_a manifolds are difficult to compare due to the splitting in the jet, but in the argon matrix spectrum there is a strong ^1L_a line centered at 980 cm^{-1} with an anisotropy dip from r=+0.075 to r=0.0. This ^1L_a line lies 720 cm^{-1} above the ^1L_a origin and identifies it possibly as the 26^1_0 line of the ^1L_a manifold. The

anisotropy above 1000 cm^{-1} pivots around zero due to overlapping of low ^1L_a and ^1L_b intensity.

The fluorescence spectrum of 3MI in argon at 20K is shown in Figure 26. The fluorescence spectrum lines are as broad as the fluorescence excitation spectrum lines (70 cm^{-1}) and are composed of two narrow lines. There are three strong lines in this spectrum, with the strongest Franck-Condon line being the 26^0_1 vibration at 760 cm^{-1} and the other lines occur at 1230 and 1350 cm^{-1}. The strength of the 26^0_1 line and the weakness of the 27^0_1 (500 -600 cm^{-1} region) is characteristic of ^1L_b emission. The emission has a similar appearance to that of indole and has been assigned ^1L_b. There is also the appearance of site structure, with at least two sites visible, reaffirming the conviction that the broadness is due to overlapping sharp sites.

The phosphorescence spectrum of 3MI in solid argon at 20K is shown in Figure 27 with excitation from the ^1L_b origin at 288.78 nm. The ^3L_a origin of the triplet state is at 416.5 nm (24,009 cm^{-1}), which is 900 cm^{-1} lower in energy than that of indole under similar conditions. It also gives the characteristic L_a emission with no features in the 760 cm^{-1} region and strong intensity in the 1500 cm^{-1} region.

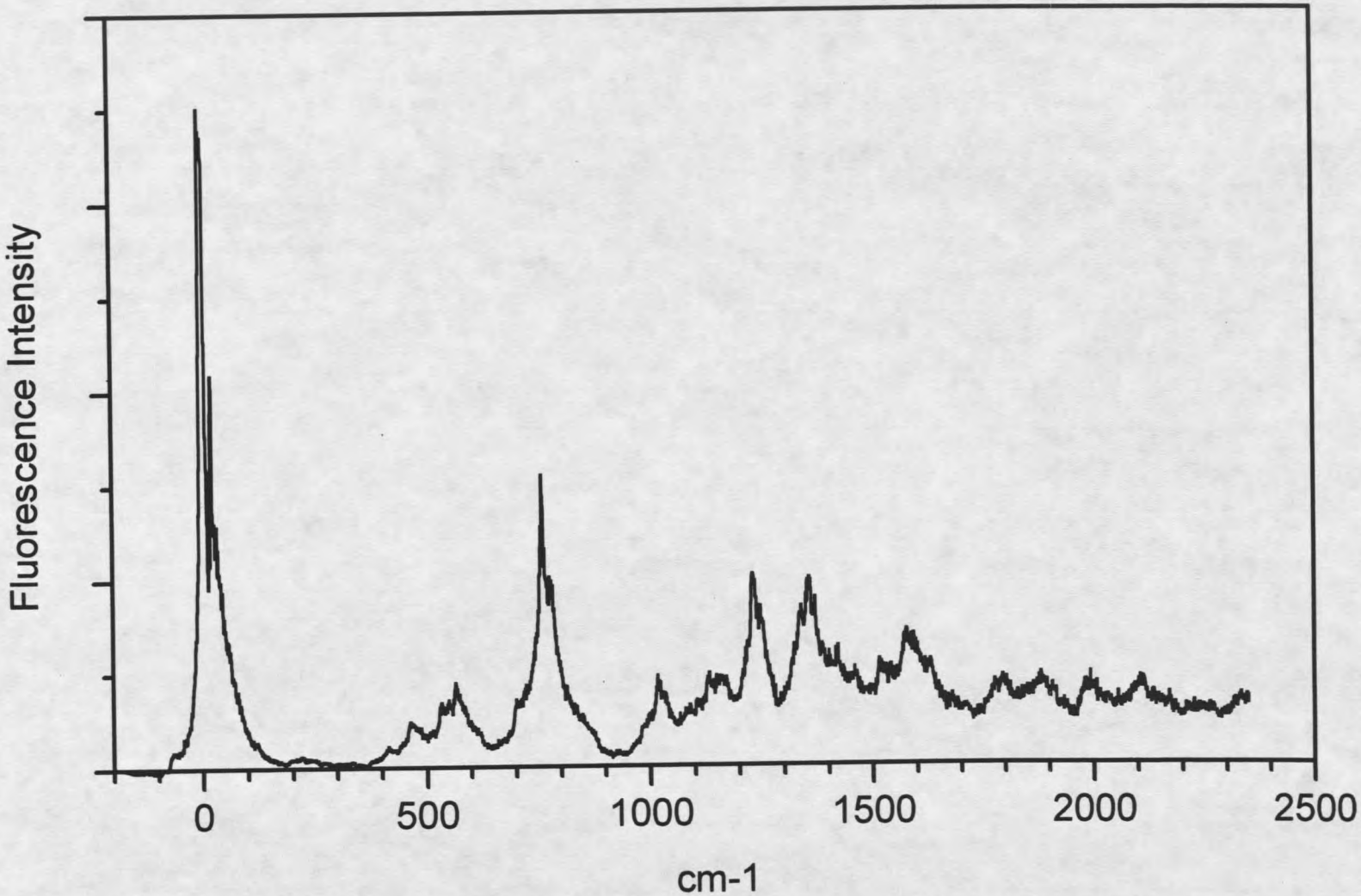

Figure 26. Dispersed fluorescence spectrum of 3MI in argon at 20K.

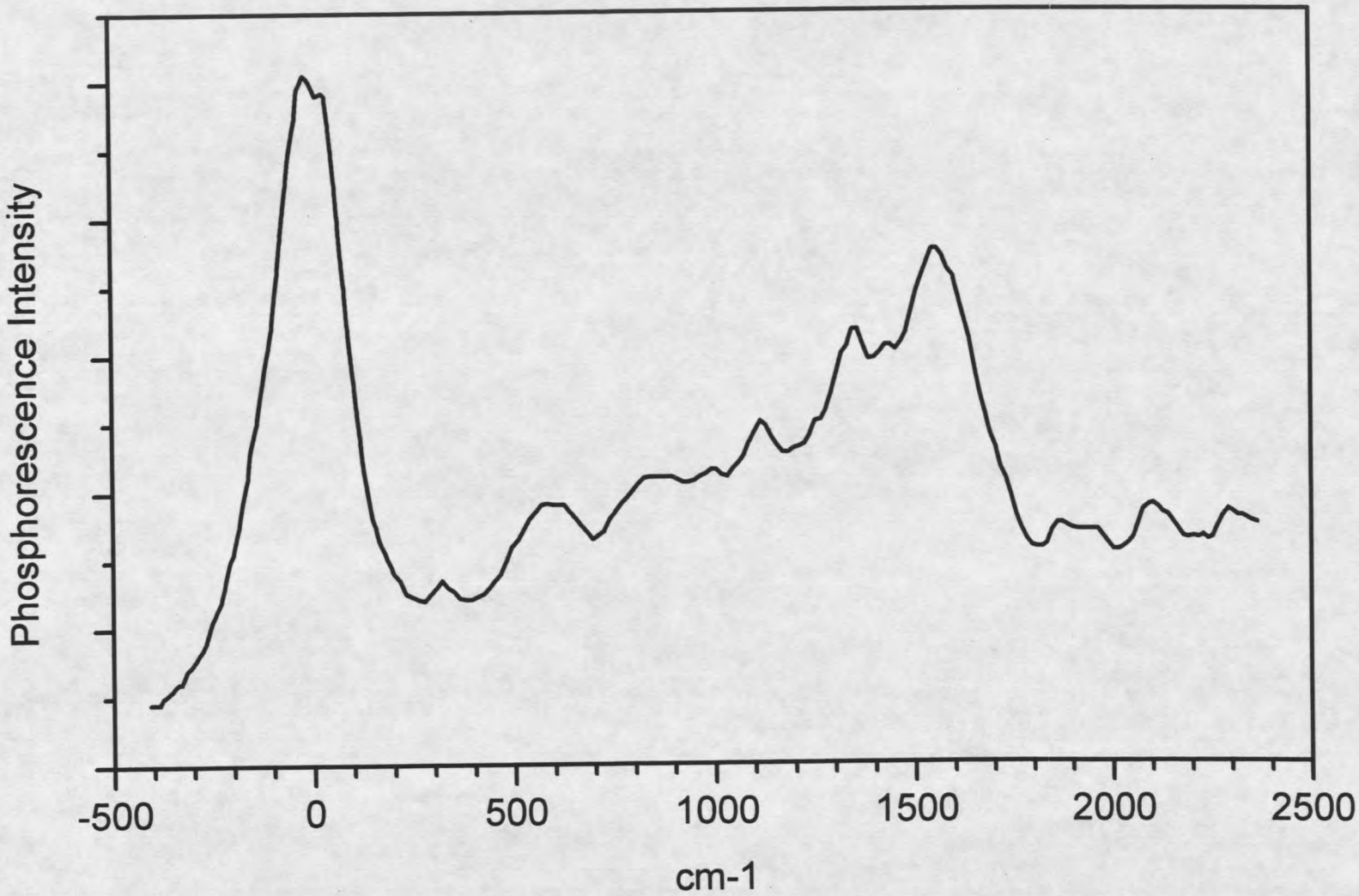

Figure 27. Dispersed phosphorescence spectrum of 3MI in argon at 20k, with ^1L_b origin excitation at 288.78 nm.

5-Methylindole

From previous spectroscopic studies of 5MI, it is known that methylation in the 5-position increases the ^1L_a-^1L_b energy separation with ^1L_b being the lowest state[70,71,8,82]. 5MI is also known to have the methyl rotor potential surface displaced 60^0 upon excitation, giving strong Franck-Condon activity in the methyl rotor normal mode[22,15]. In Figure 28a, the methyl rotor progression is quite extensive and is built off the origin and all other skeletal modes of the molecule. The individual line intensities are low because the intensity is distributed over the entire methyl progression of five major lines spanning 200 cm^{-1} rather than a single line.

Figure 28b displays the fluorescence excitation spectrum of 5MI in solid argon at 20K when the fluorescence is monitored at the 760 cm^{-1} line. The matrix spectrum in Figure 28b, extends to 2750 cm^{-1} above the ^1L_b origin and displays 200 cm^{-1} linewidths. This broadness is believed to be caused by the underlying methyl rotor structure. The matrix broadens all methyl rotor lines, causing them to collapse and fuse into broad lines. The argon matrix spectrum matches the jet spectrum for the first 1000 cm^{-1}. After this, the matrix spectrum has features that lie between 1000-1500 cm^{-1}, which are not present on first inspection of the jet spectrum. However, in the jet spectrum there exists great integrated intensity, due to the high density of lines between 1000-1500 cm^{-1}. Figure 28c displays the fluorescence anisotropy and Figure 28a displays the jet

fluorescence excitation spectrum (with Ω values). The spectra are all zeroed at the ^1L_b origin and are aligned for convenience of comparison. The ^1L_b origin of 5MI is stabilized by 80 cm^{-1} from its vacuum value by the argon matrix and sits at 291.75 nm (34,276 cm^{-1}).

The anisotropy values for 5MI are low (maximum value of r=0.075 and a minimum value of r=-0.03), but are nearly in the proper ratio for the perpendicular transition moments, thus, the anisotropy is useful for data analysis. The ^1L_b features of the spectrum are the ^1L_b origin at 0 cm^{-1} (r =0.075), the 26^1_0 line at 720 cm^{-1}(r=0.06), the ^1L_b intensity between 800-1000 cm^{-1} (r=0.075), and the strong ^1L_b transition at 1450 cm^{-1} (r=0.06).

The low anisotropy (r=0.0) region between 400-600 cm^{-1}, r=0.0, corresponds to the vibronically active 28^1_0. There are also several anisotropy dips between 700 and 1500 cm^{-1} that can also be explained by this mechanism.

The emission anisotropy remains high, for the most part, until 1800 cm^{-1} above the ^1L_b origin where the ^1L_a intensity manifests itself at this point where the anisotropy drops to r=-0.03 and remains at this level throughout the rest of the spectrum. There are three strong transitions at 2100, 2350, and 2600 cm^{-1}, all giving identical anisotropy, r=-0.03, and with a separation of 250 cm^{-1}. These lines are assigned to the split ^1L_a origin and the linewidths are 200 cm^{-1}, which are equivalent to the ^1L_b linewidths.

Figure 29 is the fluorescence spectrum of 5MI, with excitation at the 26^1_0 line at 285.9 nm. The spectrum positively exhibits ^1L_b fluorescence because the

^1L_a origin is 2000 cm^{-1} above the ^1L_b origin. Although, the spectrum is broad (200 cm^{-1}), attributed to the methyl rotor structure, it still has the pronounced ^1L_b features at the 760 cm^{-1} (26^0_1) and the 1200-1300 cm^{-1} regions.

The phosphorescence spectrum of 5MI in solid argon at 20K is shown in Figure 30 with excitation from the ^1L_b origin at 291.75 nm and linewidths of 200 cm^{-1}. The origin of the triplet state is located at 406.0 nm (24,630 cm^{-1}), 400 cm^{-1} lower in energy than indole under similar conditions. This emission exhibits the characteristic L_a emission profile, with near equal intensity of the $28^0_1 + 27^0_1$ modes in the 400-600 cm^{-1} region and the 26^0_1 mode centered at 760 cm^{-1}, and the large intensity centered at 1550 cm^{-1} composed of the 8^0_1, 9^0_1, and 10^0_1 modes.

2,3-Dimethylindole

2,3-Dimethylindole (2,3DMI), in many respects, has been a difficult molecule to understand in the jet. The jet fluorescence excitation spectrum is unusual in that it has no resemblance to the other indoles. It has a strong S_1 origin, but all the vibrational lines are extremely weak due to a non-radiative process, and there is no correlation with indole's normal mode frequencies. Even the strong 26^1_0 line is absent. It is known through this research that methylation in the 3-position brings the origins to within 260 cm^{-1} in the argon matrix and methylation in the 2-position is known to stabilize the excited states further.

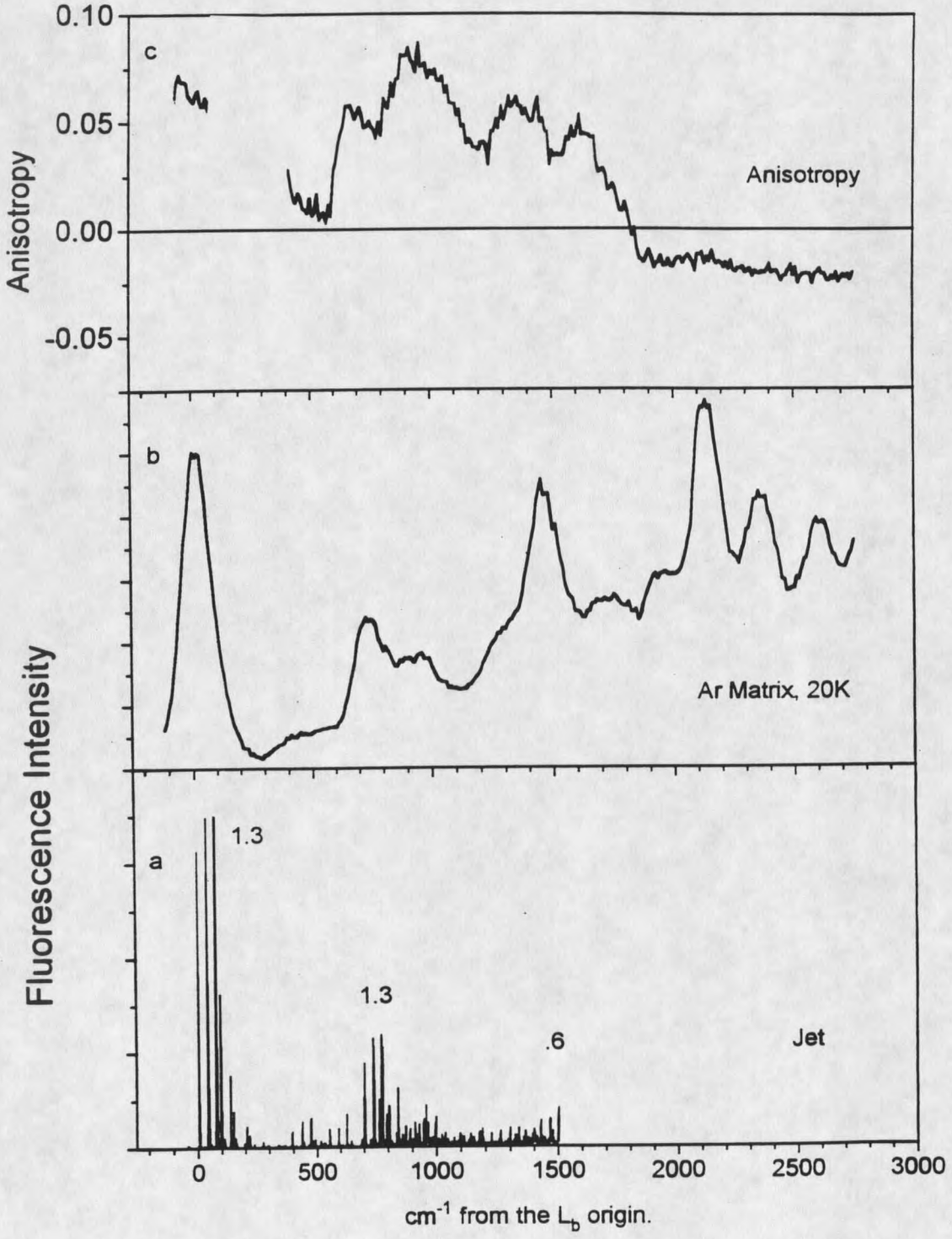

Figure 28. Supersonic jet fluorescence excitation spectrum of 5MI (with Ω values), (a), fluorescence excitation spectrum of 5MI in argon at 20K, (b), and fluorescence anisotropy, (c).

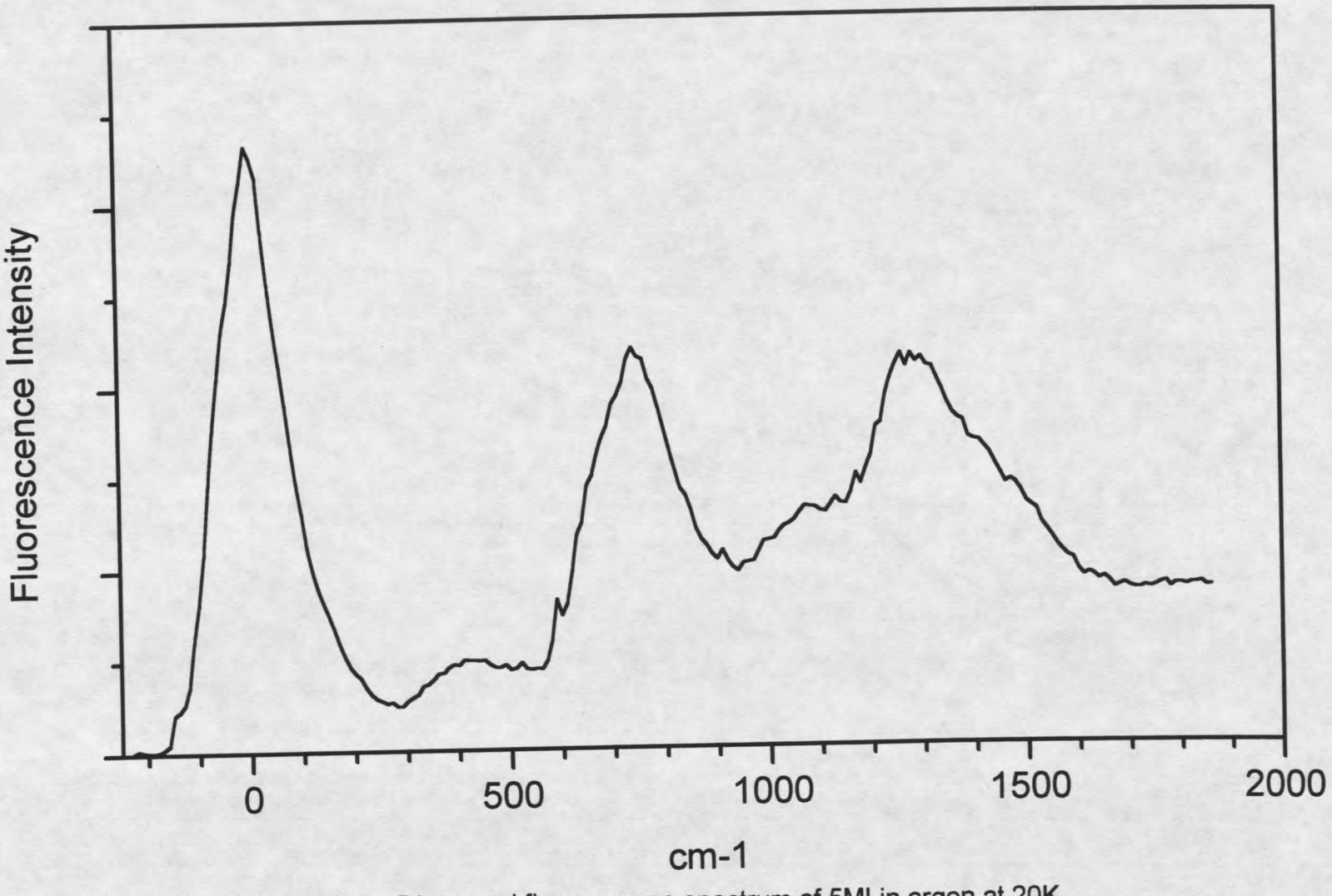

Figure 29. Dispersed fluorescence spectrum of 5MI in argon at 20K.

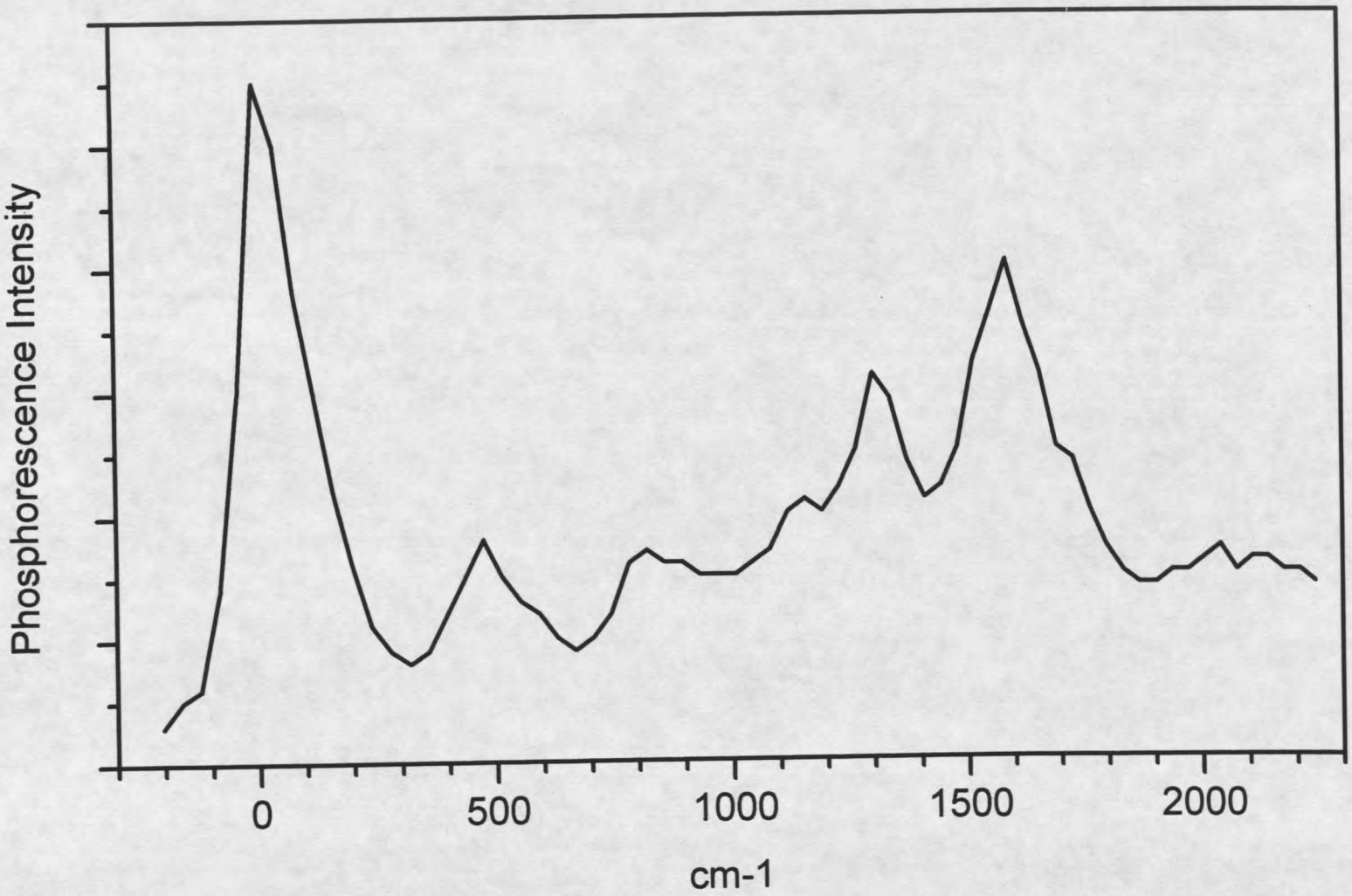

Figure 30. Dispersed phosphorescence spectrum of 5MI in argon at 20k, with ^1L_b origin excitation at 291.75 nm.

The fluorescence excitation spectrum and the emission anisotropy of 2,3-DMI in argon at 20K are shown in Figure 31a and 31b respectively, and are zeroed to the S_1 origin at 288.6 nm (34,642 cm^{-1}). The anisotropy is also at the proper ratio (2:-1), for perpendicular transition moments making it useful for data analysis. One striking detail is the broadness of the fluorescence excitation spectrum, which is even broader than the 5-MI case. This broadness is most likely due to the intrinsic site structure that 2,3-DMI holds within solid argon, possibly by overlapping of closely packed sites. Displayed here are two origins separated by 190 cm^{-1} and the anisotropy drops from r=+0.08 to r=-0.05 across the pair. This raises the question of which origin is the ^1L_a and which is the ^1L_b. The anisotropy does answer this question. The fluorescence spectrum and the 2-photon data must be taken into account to identify the S_1 and S_2 origins positively.

The fluorescence spectrum of 2,3DMI in argon at 20K is shown in Figure 32. There are two major differences between the emission of 2,3DMI and known ^1L_b emitters indole, 3MI, and 5MI in argon. First, the linewidths are much wider, on the order of 300 cm^{-1}. Second, the fluorescence spectrum does not have the same general structure as ^1L_b fluorescence with two profound differences: there is less intensity in the 750 cm^{-1} region and intensity has shifted from the 1350 cm^{-1} region to the 1600 cm^{-1} region of the spectrum as compared to the ^1L_b fluorescence.

An aid to understanding the emission result comes from theoretical

treatment of indole, phosphorescence data, and 2-photon data. Along these lines, Callis *et al.*[38] have shown through theoretical results that there are stark differences between the Franck-Condon factors of the ^1L_a and ^1L_b states due to the distinct nature of the excited state potential wells. ^1L_b emission is expressed through dominant modes 26 (760 cm^{-1} region), 23 (1000 cm^{-1} region), 14 (1350-1450 cm^{-1} region) with the absence of modes 25,19,18,10-8, and a strong origin. This explains the fundamental expression of ^1L_b emission intensity in the 750 cm^{-1} and the 1200-1400 cm^{-1} regions, as expressed in 5MI fluorescence. On the other hand, ^1L_a emission has a reduction of mode 26 (760 cm^{-1} region) and an increase in mode 27 (610 cm^{-1} region) to the extent that they are nearly identical in intensity. Also, there is an increase in the CC stretches with modes 8, 9, and 10 active and predicted to lie near 1600 cm^{-1}. Theory explains the exact differences noted between 2,3DMI fluorescence and other known ^1L_b emitters.

In further support of this theory, the comparison of 2,3DMI fluorescence to indole phosphorescence (known to emit from the ^3L_a state[1]) is made (see indole phosphorescence spectra in Figures 21 and 22). There are many similarities in these spectra, especially in the dominant intensity region between 1500-1700 cm^{-1}. 2-photon data (S_1 Ω=0.6 and S_2 Ω=0.9) verifies that the S_1 state is indeed ^1L_a.

In conclusion, theory, phosphorescence data, and 2-photon data (not shown) proves that for 2,3DMI the S_1 state is the ^1L_a state and the fluorescence is ^1L_a and this fluorescence can be distinguished from its ^1L_b counterpart by

distinct Franck-Condon differences. Furthermore, this is the sharpest ^1L_a fluorescence seen and is much sharper than Rnase fluorescence[72].

The question of which origin is lower is answered; the ^1L_a origin of 2,3DMI is 190 cm^{-1} below the ^1L_b origin in argon at 20K. The combined perturbation of the two methyl groups has caused the ^1L_a state to be pushed to lower energy. If the energy difference between the two states is 190 cm^{-1} in argon, and the argon matrix is known to stabilize the ^1L_a state approximately 200 cm^{-1} more than the ^1L_b, then it would be reasonable to expect the ^1L_a and ^1L_b states to be nearly equivalent in energy in the jet. The convergence of the two states in the jet may be the reason behind the non-radiative process that plagues the jet fluorescence excitation spectrum.

The phosphorescence spectrum of 2,3DMI in solid argon at 20K is shown in Figure 33 with excitation from the ^1L_a origin at 288.66 nm and linewidths of 200 cm^{-1}. The ^3L_a origin of the triplet state is located at 411.2 nm (24,319 cm^{-1}), 600 cm^{-1} red-shifted in comparison to indole under similar conditions. The emission is characterized as ^3L_a with similar features to the fluorescence spectrum with a broad line centered at 500 cm^{-1} made up of the 28^0_1 and 27^0_1 modes, lower intensity over the 26^0_1 region, and strong intensity centered at 1550 cm^{-1} (the 8^0_1 ,9^0_1 , and 10^0_1 modes).

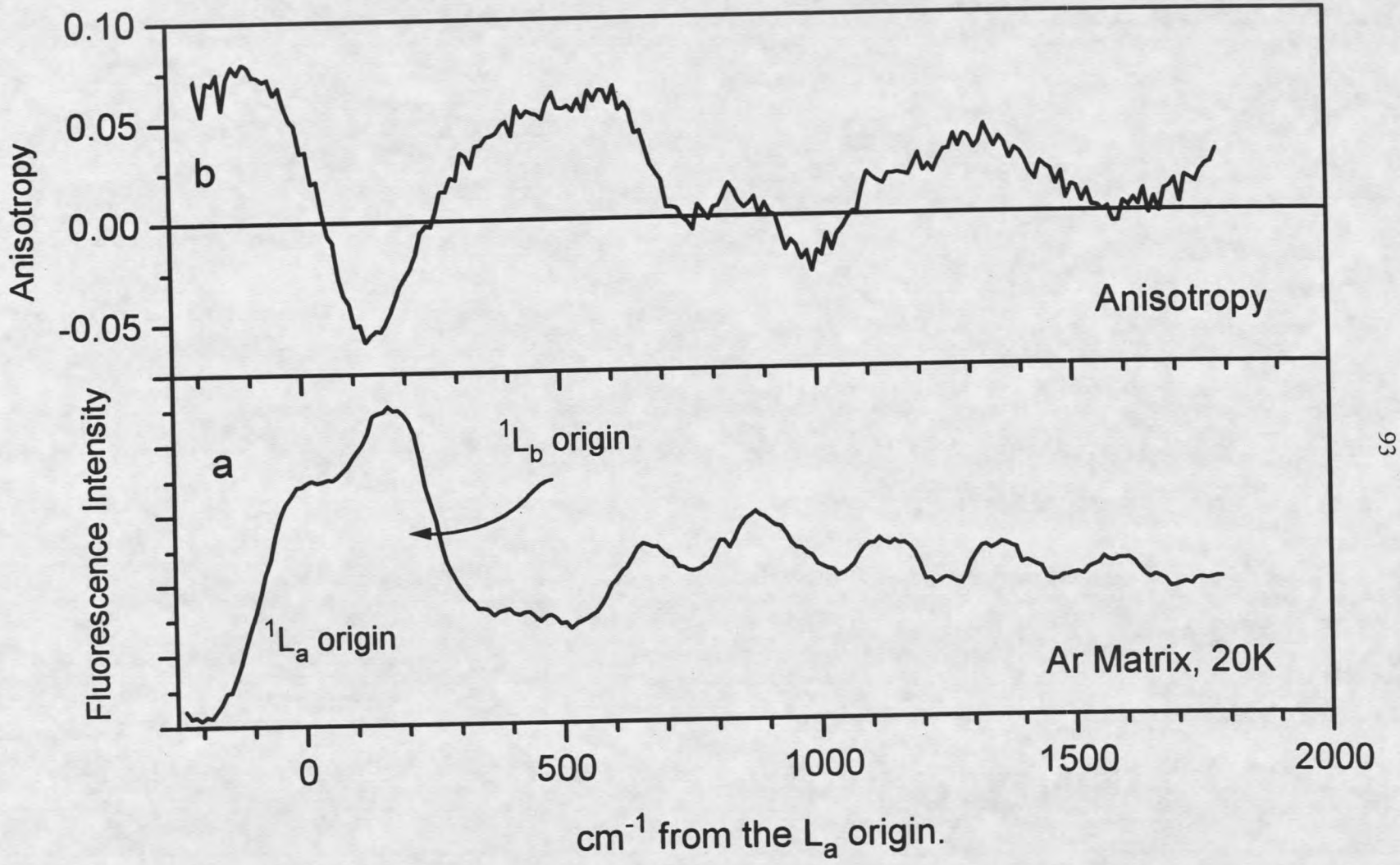

Figure 31. Fluorescence excitation spectrum of 2,3DMI in argon at 20K, (a), and the fluorescence anisotropy, (b).

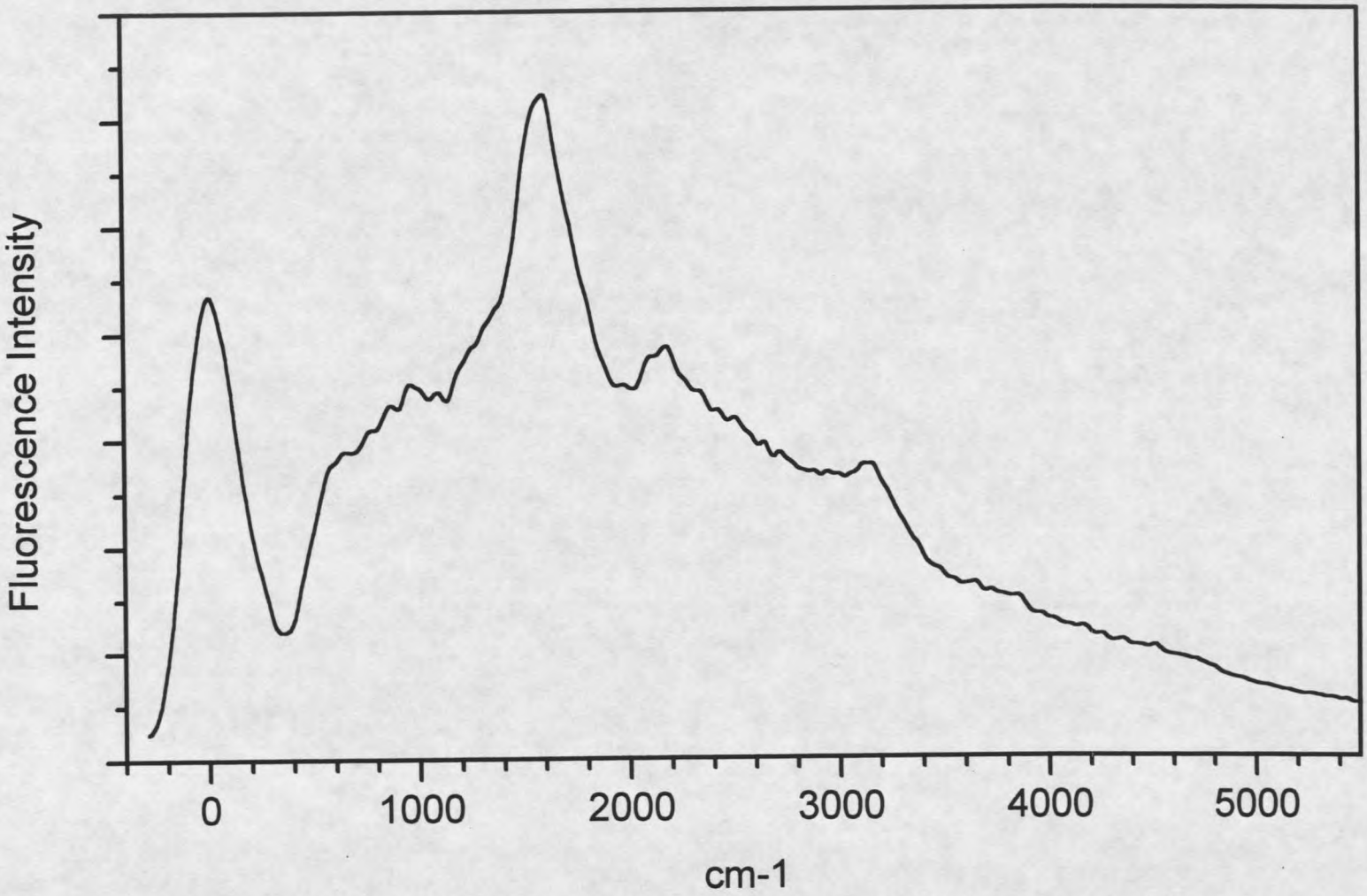

Figure 32. Dispersed fluorescence spectrum of 2,3DMI in argon at 20K.

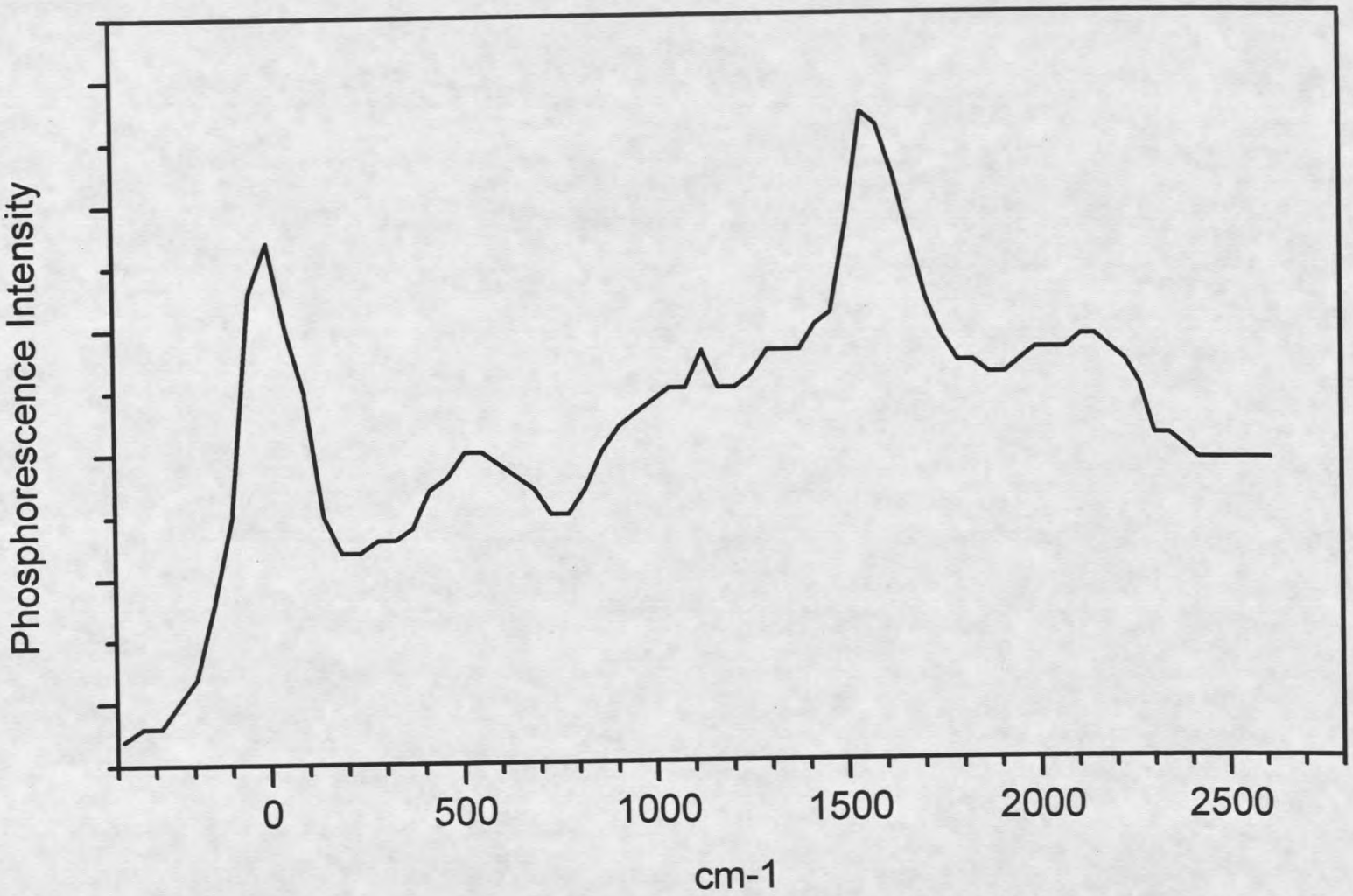

Figure 33. Dispersed phosphorescence spectrum of 2,3DMI in argon at 20k, with ^1L_a origin excitation at 288.66 nm.

2-Methylindole

In 2MI, the methyl group is attached to the main axis of indole, affecting certain normal mode frequencies. 2MI is not methyl rotor active on excitation, and the fluorescence excitation manifold in a jet is weak due to a nonradiative process, similar to 2,3DMI[17].

The incorporation of 2MI into argon at 20K produces an array of closely spaced sites, see the transmittance spectrum in Figure 34. There are five main sites, four within a 55 cm^{-1} region (site 1 at 285.6, site 2 at 285.72, site 3 at 285.91, and site 4 at 286.07 nm and site 5 at 286.32 nm), each site having an intrinsic site width of 10 cm^{-1}. This evidence proves that methylated indoles can sit in sharp sites within argon and may shed light on the 3MI case.

To eliminate site contamination due to the closely spaced sites, all spectra were taken from site 4 (unless specifically noted) at 286.07 nm (34, 956 cm^{-1}), which is 214 cm^{-1} to the red of its vacuum value. Figure 35a displays the fluorescence excitation spectrum of 2MI in argon at 20K taken while monitoring the 26^0_1 line in the emission and Figure 35b displays the fluorescence anisotropy. Both spectra are zeroed to the ^1L_b origin and have spectral linewidths of 10 cm^{-1}.

The ^1L_a origin lies between 400-600 cm^{-1} with 2 main lines at 418.1 and 488.2 cm^{-1} and two small lines at 529 and 574 cm^{-1} (low anisotropy). These lines are not in a jet spectrum[17] and have red shifted by incorporation into argon,

giving supporting evidence for their ^1L_a assignment. The ^1L_a intensity in this region is reasonable from our data on indole, 3MI, and 2,3DMI in argon at 20K.

The strong 26^1_0 normal mode is believed to be split into two lines at 611.9 and 647.6 cm^{-1}, both lines have high anisotropy, r=+0.12. Another possibility is that indole's 26^1_0 is a linear combination of 26^1_0 and 25^1_0 in 2MI. These lines are The positions of these lines agree with MOPAC, which predicts a 100 cm^{-1} red-shift 26^0_1 mode (ground state), due to the large amplitude motion of the 2-position in mode 26. Lastly, there is a small line at 251.1 cm^{-1} that is common for substituted indoles.

The emission spectrum of 2MI in argon at 20K is shown in Figure 36 with excitation at the 611.9 cm^{-1} line in the excited state. This emission does not have the exact appearance of indole fluorescence, but it is definitely ^1L_b fluorescence. The most intense line is the 26^0_1 line at 659.7 cm^{-1} (50% of the origin), which is red-shifted by 110 cm^{-1}. This, as mentioned earlier, was predicted by MOPAC. The second quantum 26^0_2 line is also present at 1316 cm^{-1}.

The two small lines lying to the red of the 26^0_1 line are identified as the 27^0_1 line at 612.2 cm^{-1} and the 28^0_1 line at 493.2 cm^{-1}. The 28^0_1 line lies 43 cm^{-1} to the red of indole's, which is the exact difference predicted by MOPAC. There are also three lines from site contamination built off the 26^0_1 line at 537.1, 577.4, and the red shoulder of the 611.9 cm^{-1} line. Care must be taken not to confuse site contamination with normal mode lines. These lines can also be seen built

off the S_1 origin.

The phosphorescence spectrum for 2MI in solid argon is shown in Figure 37 with excitation from the ^1L_b origin of site 4 at 286.07 nm. The ^3L_a triplet origin is at 398.5 nm (25,095 cm^{-1}), which is 160 cm^{-1} higher in energy than indole. This spectrum is composed of a sharp component (13 cm^{-1}), suggesting a component from an ordered site, and a broad component that adds to the high background. The phosphorescence and the fluorescence frequencies for the 28^0_1 (493 cm^{-1}), 27^0_1 (612 cm^{-1}), and 26^0_1 (660 cm^{-1}) are in agreement, affirming the assignment of the 26^0_1 vibrational mode. The phosphorescence displays the L_a characteristics with the low frequency 28^0_1 and 27^0_1 modes having greater intensity than the accompanying 26^0_1 mode. Moreover, the large intensity in the 9^0_1 (1584 cm^{-1}) and the 8^0_1 (1616 cm^{-1}) modes. The 10^0_1 mode does not appear to stand out in the spectrum, perhaps it is seen in the red-shoulder of the 9^0_1 line or it has drastically red-shifted at least 300 cm^{-1} to a region where it is indistinguishable from other lines.

1-Methylindole

1-Methylindole (1MI) is not only the near geometric equivalent to 3MI, but it is also the only methylated indole in this study that is not in crystalline form at room temperature. The methyl rotor is known to be inactive upon excitation[17].

The transmittance spectrum of the S_1 origin region is shown in Figure 38. The spectrum displays a broad site from 290.6 to 291.4 nm, with one strong

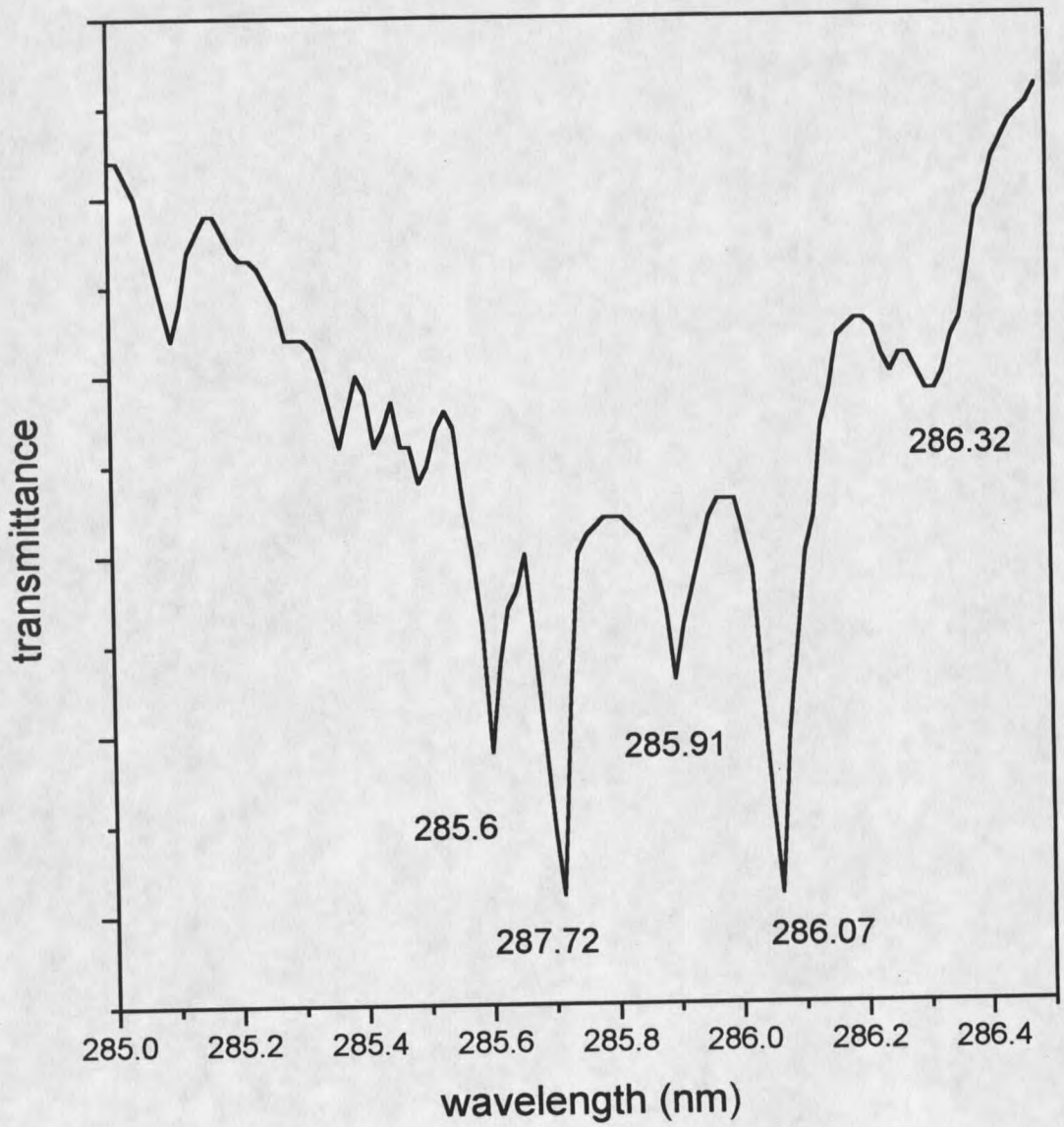

Figure 34. Transmittance spectrum of 2MI in argon at 20K, with a 0.2 cm^{-1} bandpass.

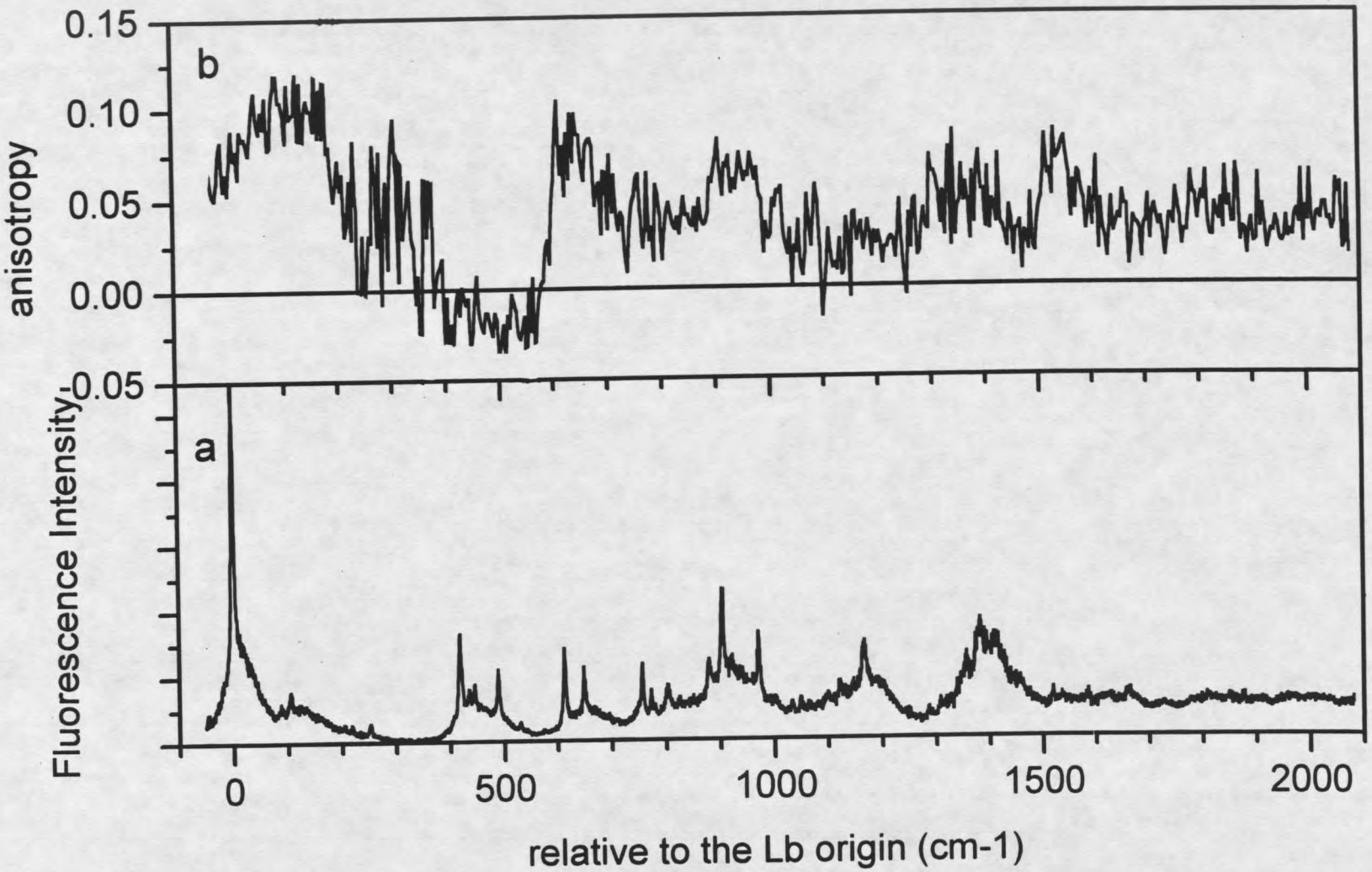

Figure 35. Fluorescence excitation spectrum of 2MI in argon at 20K, (a), and the fluorescence anisotropy, (b).

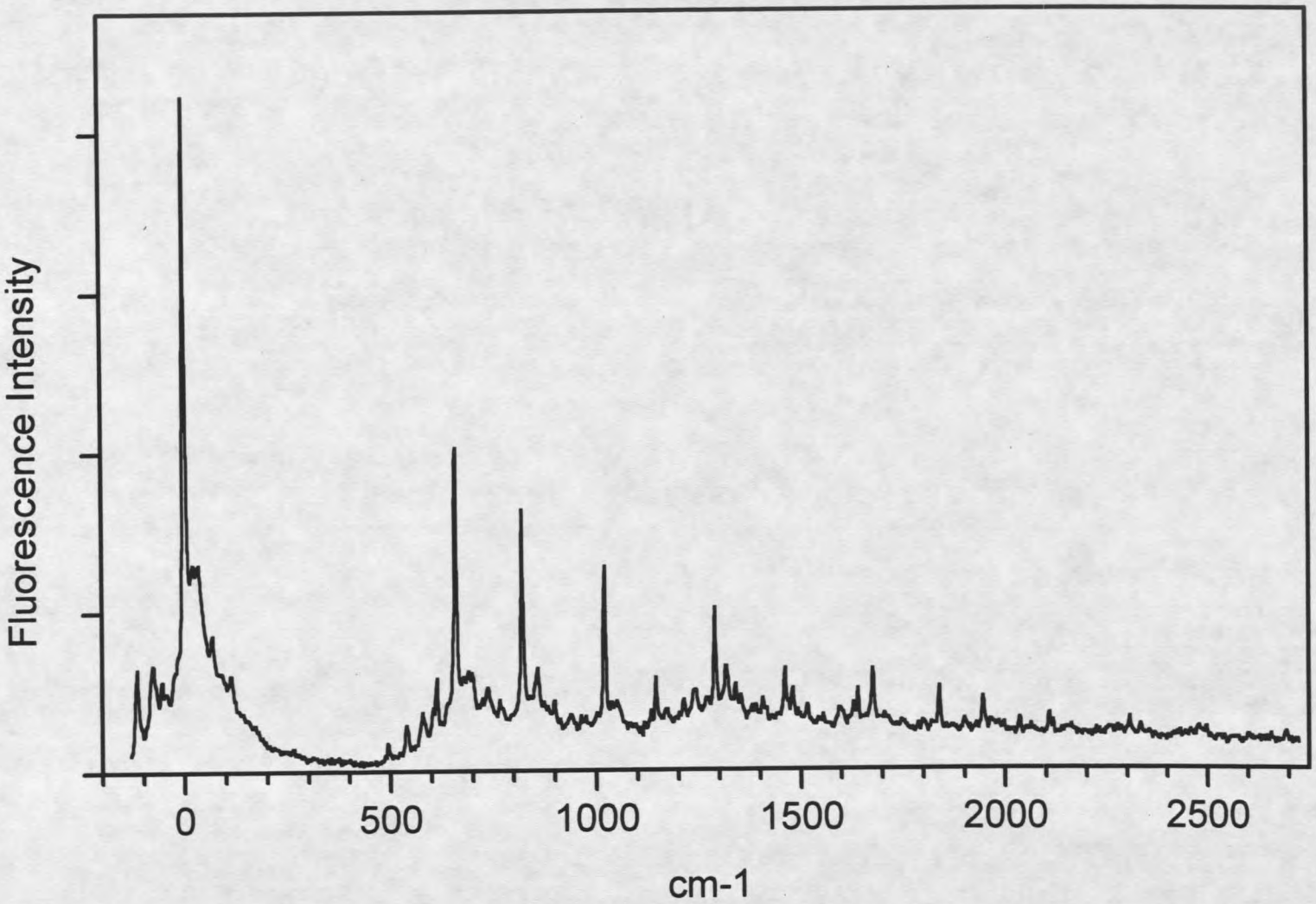

Figure 36. Dispersed fluorescence spectrum of 2MI in argon at 20K.

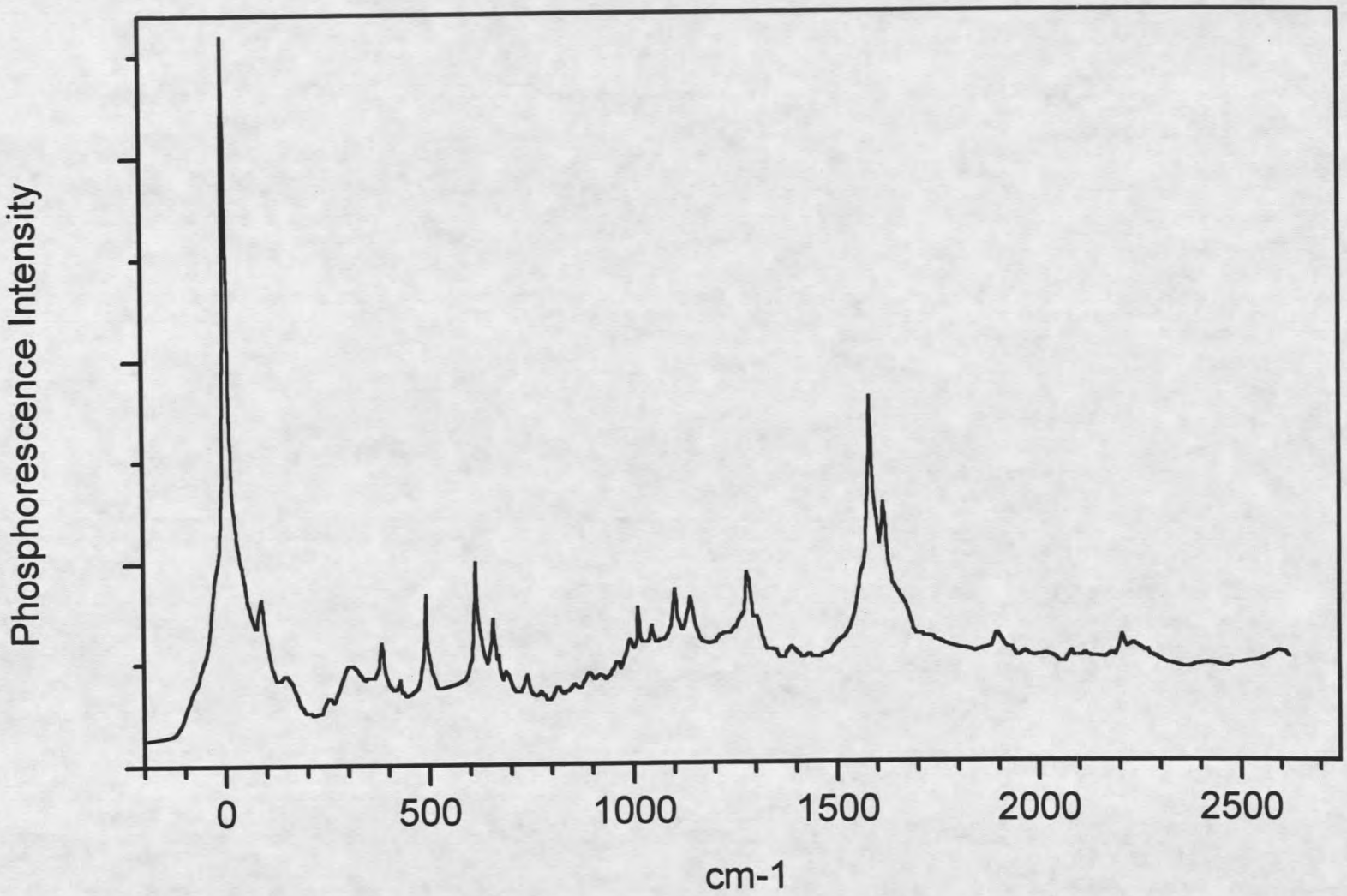

Figure 37. Dispersed phosphorescence spectrum of 2MI in argon at 20k, with ^1L_b origin excitation at 286.07 nm.

narrow site (site 1) at 291.55 nm (34,300 cm^{-1}). Site 1 has an intrinsic site width of 10 cm^{-1}, from which all the data is collected, and the electronic energy is red-shifted 246 cm^{-1} from its vacuum value. The fluorescence excitation spectrum and the accompanying anisotropy of 1MI in solid argon at 20K are shown in Figure 39a and 39b respectively, and are zeroed to the S_1 origin. The fluorescence excitation spectrum was taken by monitoring the 26^0_1 line in the emission. The emission spectrum is shown in Figure 40 and was taken by exciting the 713.3 cm^{-1} line in the excited state.

The S_1 origin of the fluorescence excitation spectrum in Figure 39a is the ^1L_b origin, because the emission has been identified as ^1L_b. It should be noted that for 1MI, the anisotropy is not at the proper ratio with maximum anisotropy (r=0.3) and a minimum anisotropy (r=-0.075). This deviation could be caused by, ^1L_b intensity in this region, an experimental artifact of polarizer alignment, or an angle less than 90^0 between the absorption and emission moments. Lastly, the spectral linewidths are 15 cm^{-1}.

Two key ^1L_b lines may be identified by their high anisotropy. The 27^1_0 line can be identified at 528.0 cm^{-1} (r=0.15). The anisotropy is lower than the origin because of ^1L_a intensity in the vicinity. The 27^1_0 mode is also 12 cm^{-1} lower in frequency than indole's. Secondly, the 26^1_0 line can be identified at 713.3 cm^{-1} (r=0.2), which is only slightly frequency shifted. Lastly, there is an ^1L_b line present at 253 cm^{-1} which is common for certain substituted indoles.

Also observed is the ^1L_a origin 430-700 cm^{-1} above the ^1L_b origin (low

anisotropy), and is split into three strong lines at 445.1, 472.9, and 555.9 cm^{-1}. The spectrum also displays low anisotropy between 1150-1300 cm^{-1}, corresponding to the 26^1_0 line of the ^1L_a state which is 720 cm^{-1} higher in energy.

The fluorescence spectrum of 1MI in argon at 20K in Figure 40 displays ^1L_b emission. The four characteristic lines are as follows: 29^0_1 (470.0 cm^{-1}), 28^0_1 (540 cm^{-1}-red shoulder of the 27^0_1), 27^0_1 (576 cm^{-1}), and 26^0_1 (765 cm^{-1}). Compared to indole, mode 27^0_1 is also 28 cm^{-1} lower in frequency, while modes 28^0_1 and 26^0_1 remain at their usual frequency in the ground state. The low frequency line at 256 cm^{-1} is also observed. There are also three unusual lines in the 1MI fluorescence spectrum at 1528.8, 1588.4, and 1620 cm^{-1}, identified as the 26^0_2 (partially 10^0_1), identified as a combination of 27^0_1 (575.6 cm^{-1}) and the 1010.6 cm^{-1} line (partially 9^0_1), and 8^0_1 modes, respectively, using phosphorescence data. These lines are usually ^1L_a active only. The lines at 1918, 2106, and 2348 cm^{-1} are combination bands as follows respectively: 1340 cm^{-1} line and 27^0_1 line, 1340 cm^{-1} line and 26^0_1 line, and, 1340 and 1010.6 cm^{-1} lines.

Phosphorescence

The phosphorescence spectrum of 1MI in argon at 20K is shown in Figure 41a with excitation from the ^1L_b origin at 291.55 nm. The stick spectrum shown in Figure 41b was produced by subtracting the background from the line heights. The ^3L_a state is located at 407.4 nm (24,546 cm^{-1}) and is 387 cm^{-1} to the red of

indole.

The emission is definitely L_a, with near equal intensity of the 28^0_1 line (534 cm^{-1}) and the 26^0_1 line (762 cm^{-1}), intensity in the 27^0_1 line (592 cm^{-1}), and strong intensity in the 10^0_1 line (1522 cm^{-1}), the 9^0_1 line (1580 cm^{-1}), and the 8^0_1 line (1622 cm^{-1}) . There is a slight frequency discrepancy of 16 cm^{-1} for the 27^0_1 between the phosphorescence and the fluorescence data, which is within experimental error. The phosphorescence data also displays strong lines at 717, 836, 1008, 1157, 1206, and 1330 cm^{-1}. The corresponding line frequencies, intensities, and assignments are found in Table 3.

Table 3. 1-Methylindole phosphorescence

Spectral[a] shift (cm^{-1})	Intensity[b]	Assignment	Spectral[a] shift (cm^{-1})	Intensity[b]	Assignment
0.0	9.0		717	0.35	
118	0.1		762	1.0	
284	0.3		836	0.5	
349	0.15		852	0.1	
413	0.1		885	0.25	
534	1.0		919	0.15	
545	0.15		947	0.1	
569	0.07		1008	0.4	
586	0.5		1080	0.3	
632	0.18		1135	0.5	

Table 3. Continued

Spectral[a] shift (cm^{-1})	Intensity[b]	Assignment	Spectral[a] shift (cm^{-1})	Intensity[b]	Assignment
1146	0.1		1522	1.6	
1157	0.9		1527	0.35	
1206	0.8		1548	0.15	
1298	0.2		1580	1.2	
1330	0.9		1622	1.0	
1368	0.15		1690	0.2	
1384	0.1		1726	0.15	
1400	0.15		1840	0.15	
1421	0.2		1871	0.2	

a Uncertainty of ± 16 cm^{-1}.
b Absolute intensity.

4-Fluoroindole

4-Fluoroindole (4FI) was examined because of its connection to the tryptophan analogue 4-fluorotryptophan (4FT) used recently as an *antiprobe* in proteins since it is the only fluorinated analogue found not to fluoresce[23]. Upon spectroscopic investigation of 4FI, carried out at room temperature, with 0.75 absorbance solutions (1 cm path), and a nonpolar solvent (methylcyclohexane), 4FI fluoresced strongly whereas 4FI in a polar solvent (H_20) was 10 times weaker.

Encouraged by these results, the investigation was expanded. 4FI was incorporated into solid argon at 20K and measurements were taken. The transmittance spectrum of the S_1 region of 4FI is shown in Figure 42. The

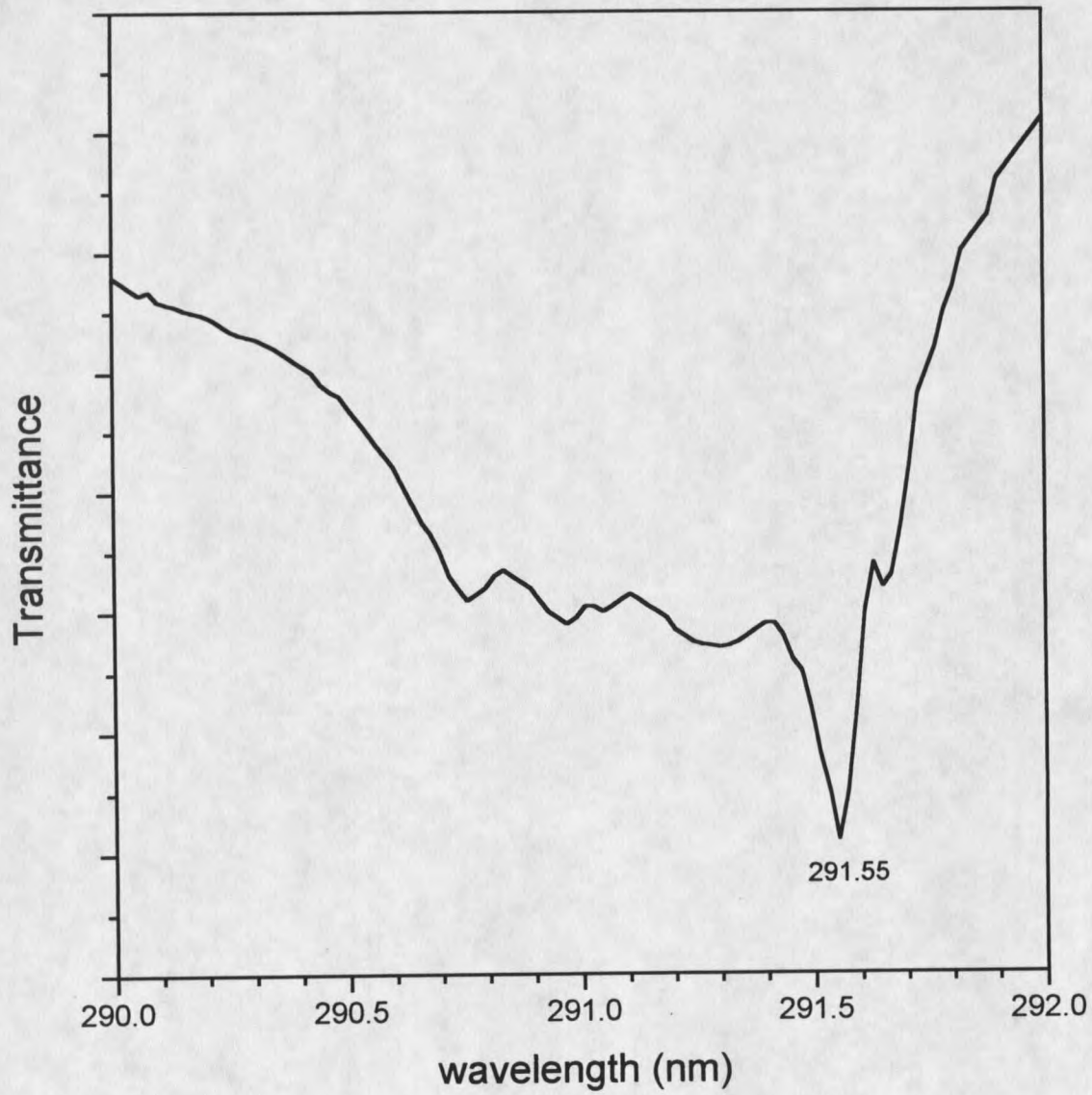

Figure 38. Transmittance spectrum of 1MI in argon at 20K, with a 0.2 cm^{-1} bandpass.

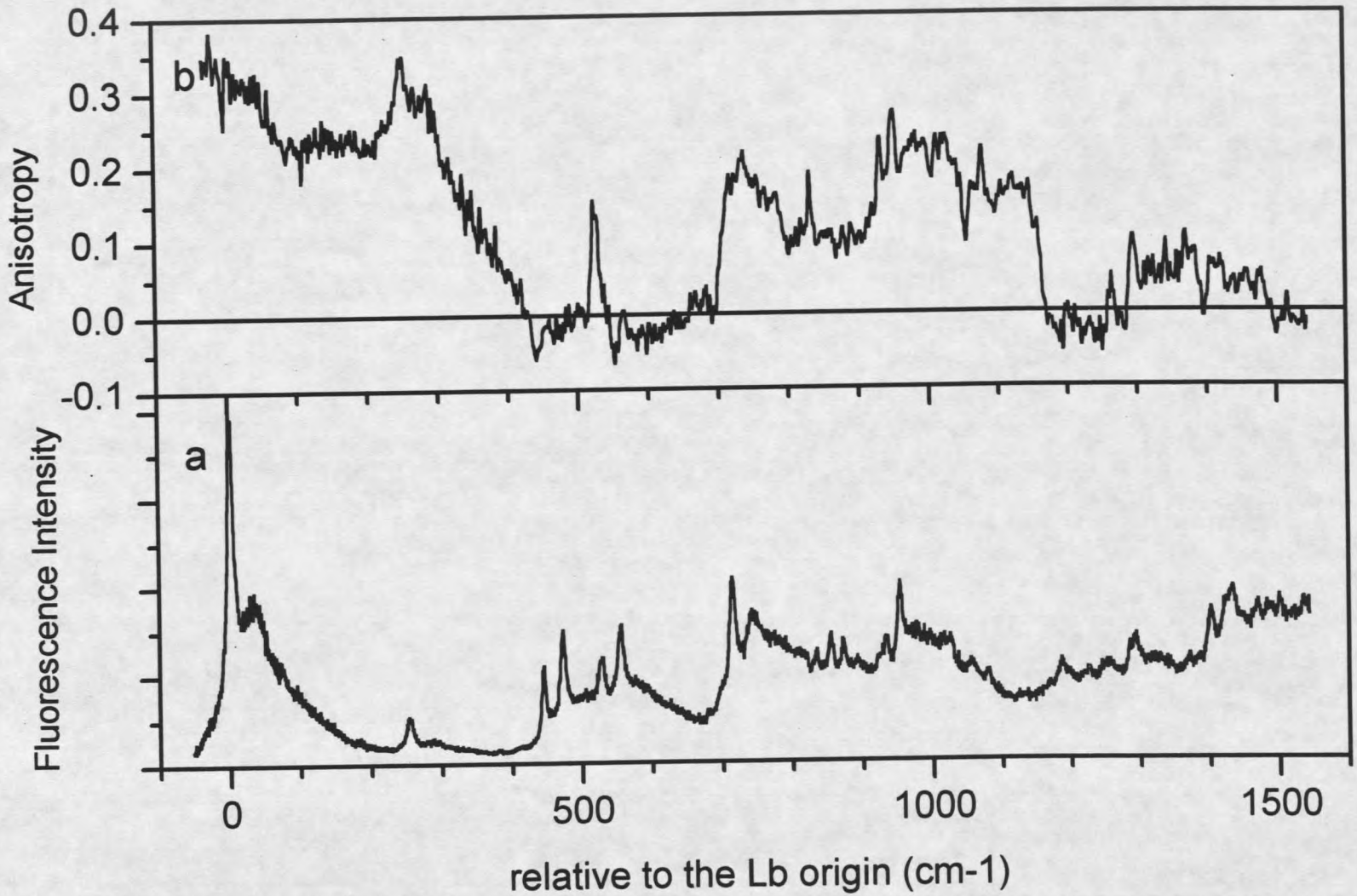

Figure 39. Fluorescence excitation spectrum of 1MI in argon at 20K, (a), and the fluorescence anisotropy, (b).

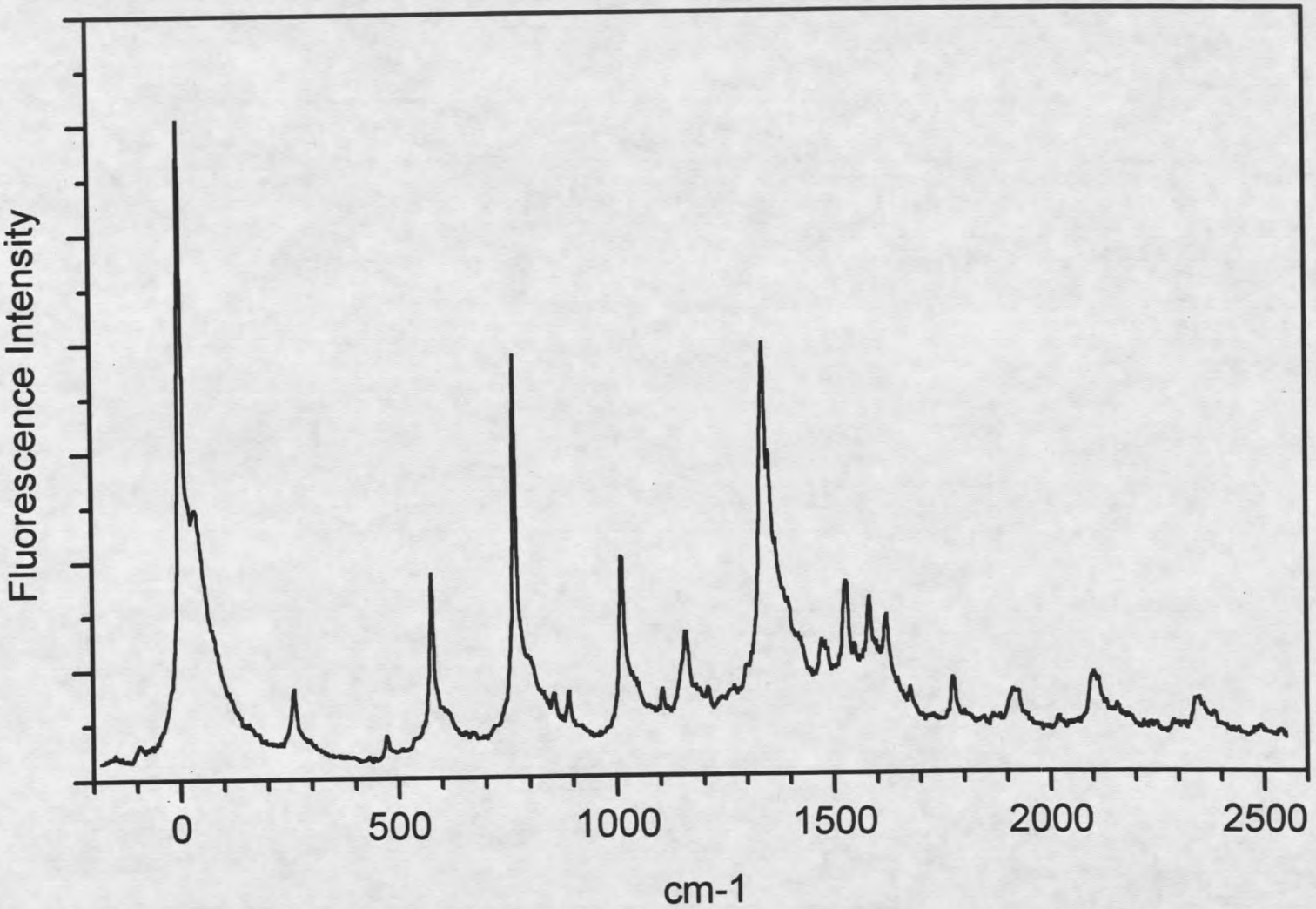

Figure 40. Dispersed fluorescence spectrum of 1MI in argon at 20K.

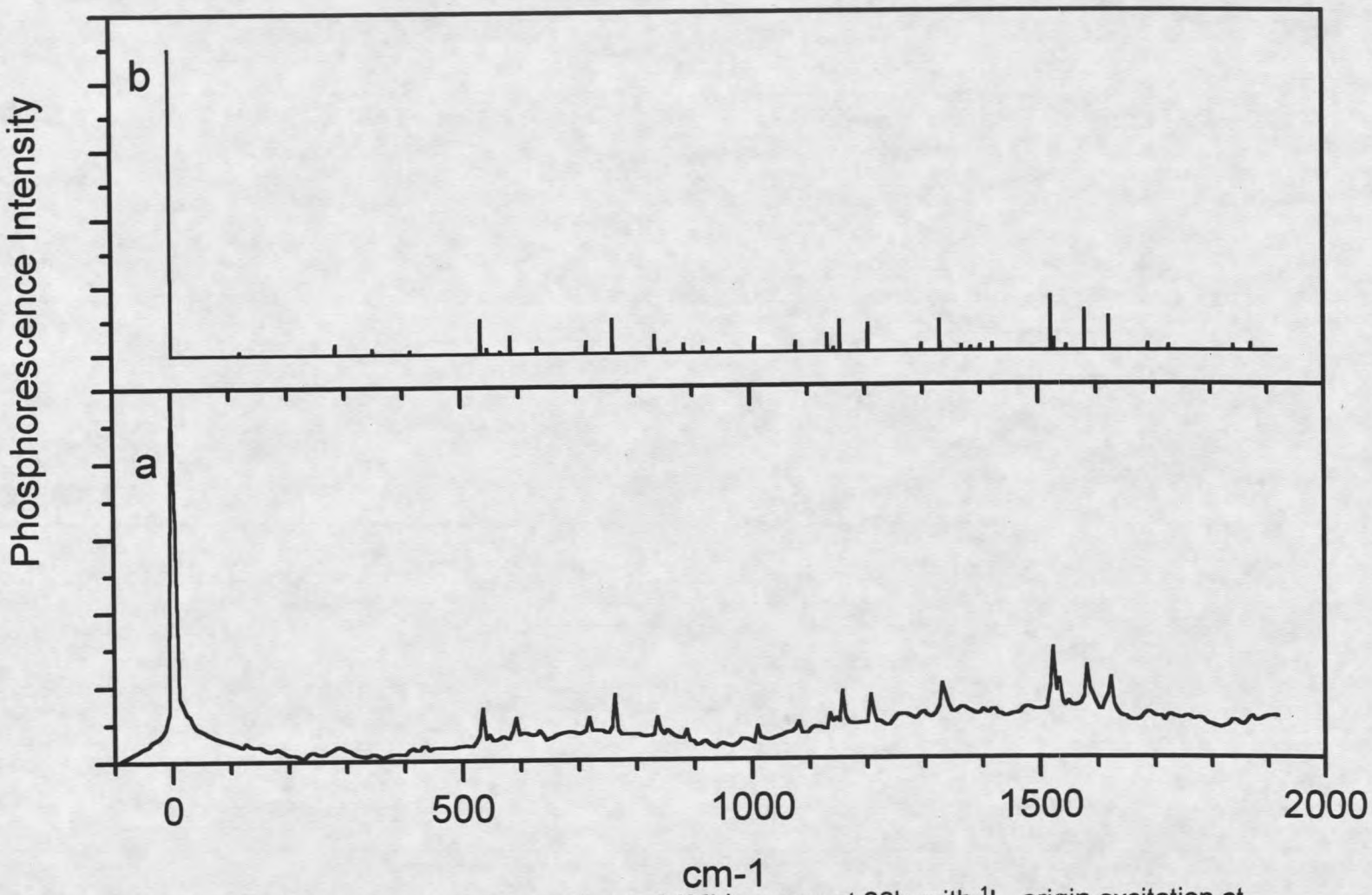

Figure 41. Dispersed phosphorescence spectrum of 1MI in argon at 20k, with ^1L_b origin excitation at 291.55 nm, (a), and the stick spectrum, (b).

spectrum displays six energy sites that 4FI populates in the argon under these conditions. Site 1 is located at 281.9, site 2 at 282, site 3 at 282.1, site 4 at 282.4, site 5 at 282.6, and site 6 at 282.8 nm. These site widths range from 5 to 20 cm^{-1}. All the data was taken from site 1 at 281.9 nm (35,476 cm^{-1}). The argon matrix has red-shifted the S_1 origin of site 1 167 cm^{-1} from its vacuum value, and the intrinsic site width is 5 cm^{-1}.

The fluorescence excitation spectrum of 4FI is shown in Figure 43a with the accompanying emission anisotropy in Figure 43b. The spectra are zeroed to the S_1 origin, which is believed to be the ^1L_b origin at 281.875 nm. Due to the number of sites lying in close proximity, site contamination was unavoidable, and is evident at -72, 30, and 70 cm^{-1}. These contamination lines were built off all molecular normal modes and should not be confused with the 4FI normal mode lines. The anisotropy values, however, are closer to the theoretical values and have approximately the proper ratio for perpendicular transition moments, with a maximum anisotropy r=0.26 and a minimum anisotropy r=-0.15. This anisotropy is higher than other indoles in argon, which is possibly produced by a more oriented sample caused differences in the argon matrix (moving towards a single crystal lattice).

In the literature, there is a slight normal mode numbering difference between indole and 4FI. The excited state normal modes of 4FI are one number lower than the corresponding normal modes for indole, but in the ground state they are identical. For convenience of comparison and clarity all excited

state normal modes of 4FI will have the corresponding normal mode of indole in parentheses. The strong ^1L_b line 25^1_0 (26^1_0) line is located at 646 cm^{-1} and is 75cm^{-1} lower in frequency than indole's. This red-shift is verified in the jet spectra[83] and predicted in theory. Callis *et al.*,[38] through a theoretical model, predicts a large amplitude motion of the 4-position in the 25^1_0(26^1_0) mode. The added mass of the fluorine in the 4-position causes a frequency reduction of the mode. Also, MOPAC predicts the 25^1_0 mode to be 65 cm^{-1} lower in energy than indole's 26^0_1 (ground state). This spectrum also displays a strong second quantum 25^2_0 (26^2_0) at 1290.9 cm^{-1}, signifying a large displacement of this mode upon excitation. This large displacement of this mode will become more evident when examining the fluorescence. The line at 718 cm^{-1}, sitting 72 cm^{-1} to the blue of the 25^2_0 (26^2_0) line, is believed to be site contamination, although its intensity is rather large. There are two reasons for making this prediction: 1) the line sits at the proper relative position to the 25^2_0 (26^2_0) line for site contamination and 2) there is no line that intense in that location in a comparable jet spectrum[73].

Many lines in the spectrum display low polarization. The 27^1_0 (28^1_0) line at 430 cm^{-1} gives an ^1L_a signature (r=-0.12) from Herzberg-Teller vibronically coupling. This mode has red-shifted 41 cm^{-1} relative to indole which MOPAC predicts. The low anisotropy region centered at 430 cm^{-1} extends between 350-500 cm^{-1}, which is due to site contamination. In addition to, many other lines also give an ^1L_a signature seen at 1392.3, 1304, 1206, 1075, 912, and 900 cm^{-1}.

Most of these lines receive their ^1L_a intensity through a similar mechanism.

The ^1L_a origin of 4FI is assigned at 1520.5 cm^{-1} above the ^1L_b origin and can be seen by its low anisotropy, r=-0.15. The ^1L_a origin is strong and is comparable to the ^1L_b origin in intensity. No splitting of the ^1L_a origin has occurred, apparently because of less coupling between the two states. With the addition of the fluorine in the 4-position, the ^1L_a energy has increased by 900 cm^{-1} and the ^1L_b energy by 500 cm^{-1}.

The fluorescence spectrum of 4FI is shown in Figure 44 with excitation at the 26^1_0 line. Self-absorption posed a problem for 4FI, possibly due to a higher vapor pressure, and to combat this, thinner matrices were used. The fluorescence spectrum of 4FI is different from other indole analogs studied, in that, it is dominated by a long Franck-Condon progression (4 quanta) of the 26^0_1 vibration at 673, 1352, 2025, and 2699 cm^{-1}. This progression consumes most of the fluorescence intensity. Because of this, the fluorescence spectrum does not mirror the fluorescence excitation spectrum. Therefore, since all of the Franck-Condon intensity is found in the 26^1_0 mode, there must be a large molecular displacement along the coordinates of this mode upon excitation. Secondly, the resulting progression does not follow the proper Franck-Condon intensity distribution. None of the other indoles behave in this manner and it is not understood, at this point, why a fluorine in the 4-position would cause these dramatic spectral changes.

Lastly, the frequency of the 26^0_1 mode is 673 cm^{-1} and is 87 cm^{-1} lower in

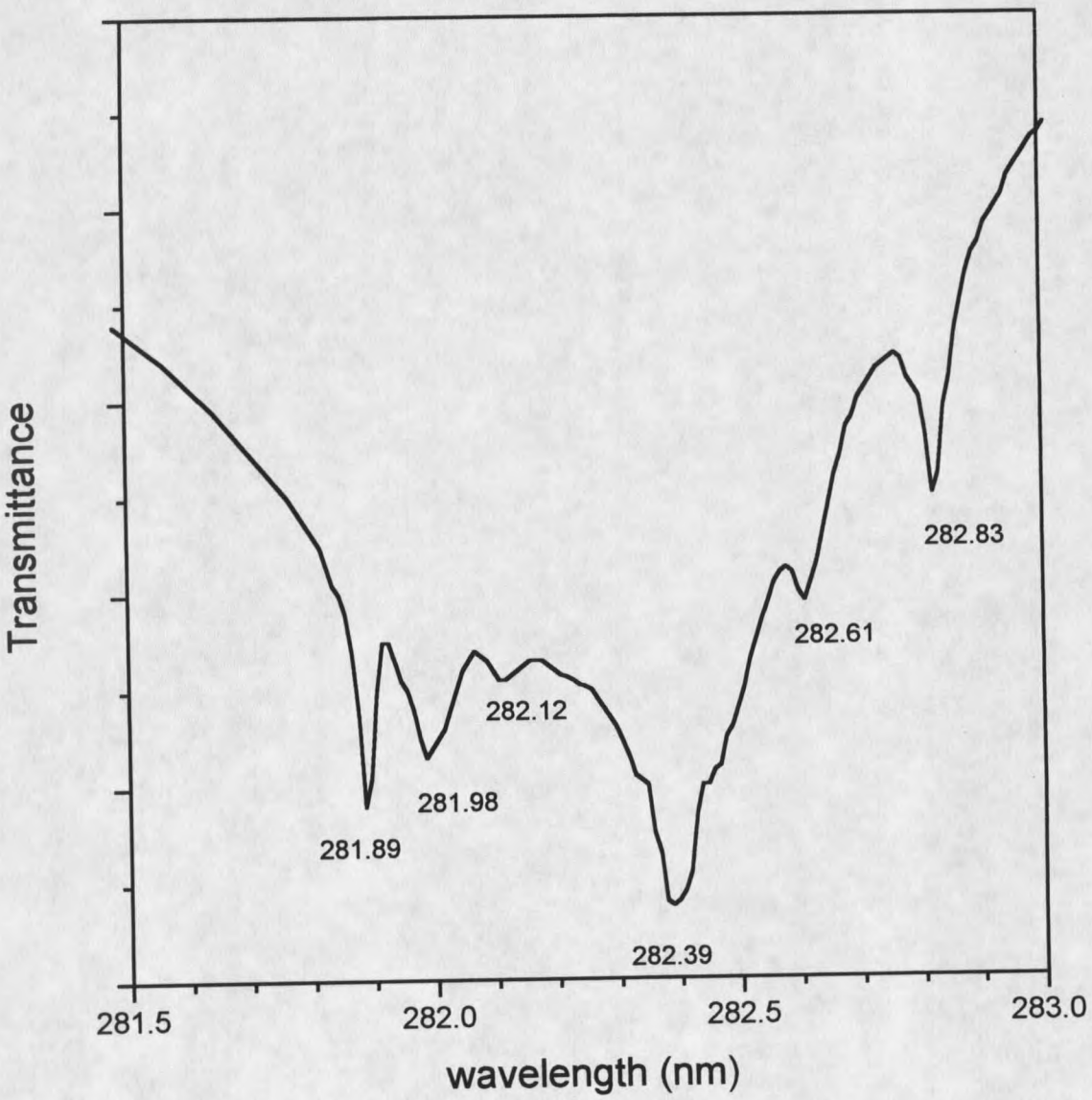

Figure 42. Transmittance spectrum of 4FI in argon at 20K, with a 0.2 cm^{-1} bandpass.

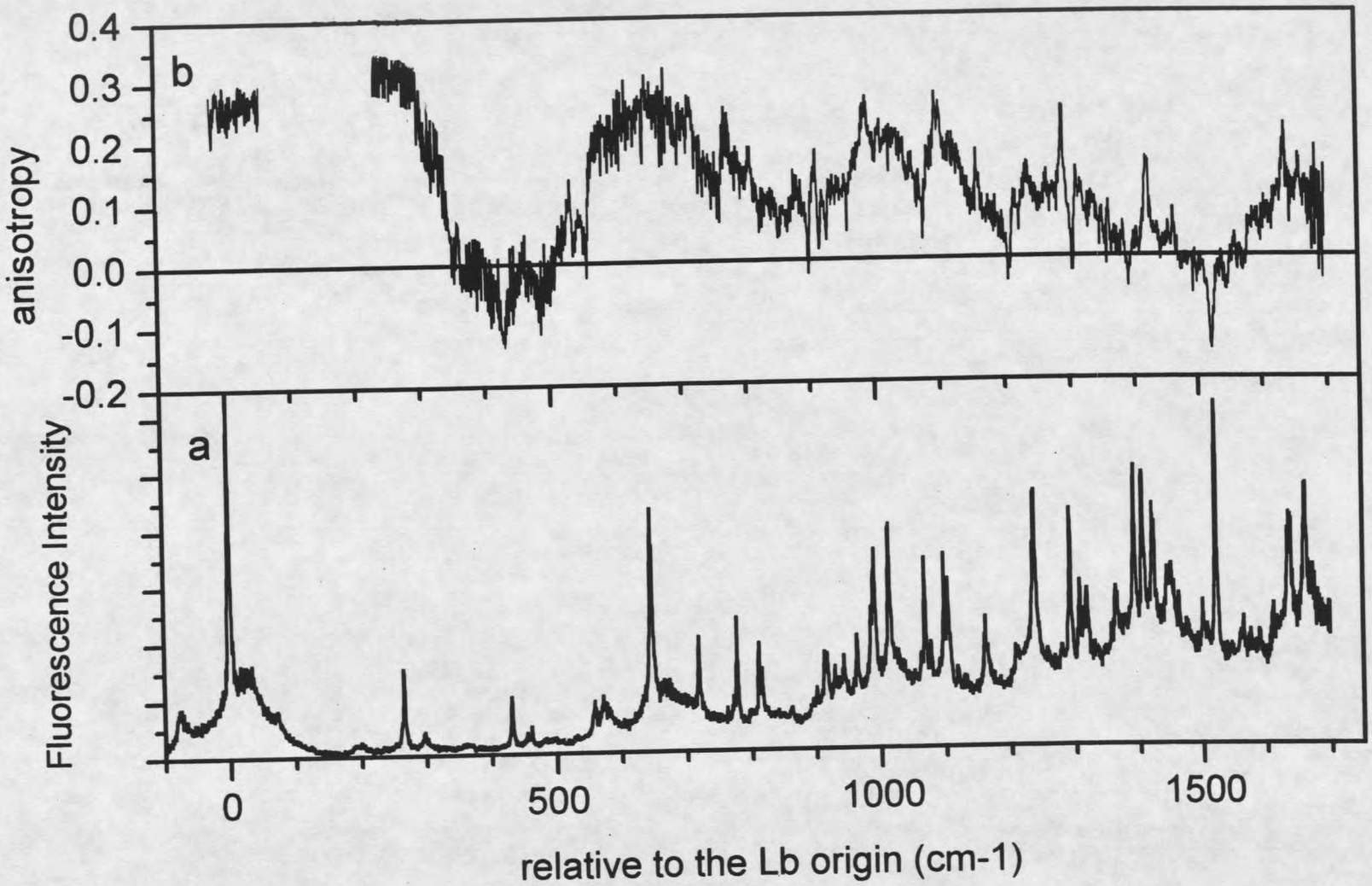

Figure 43. Fluorescence excitation spectrum of 4FI in argon at 20K, (a), and the fluorescence anisotropy, (b).

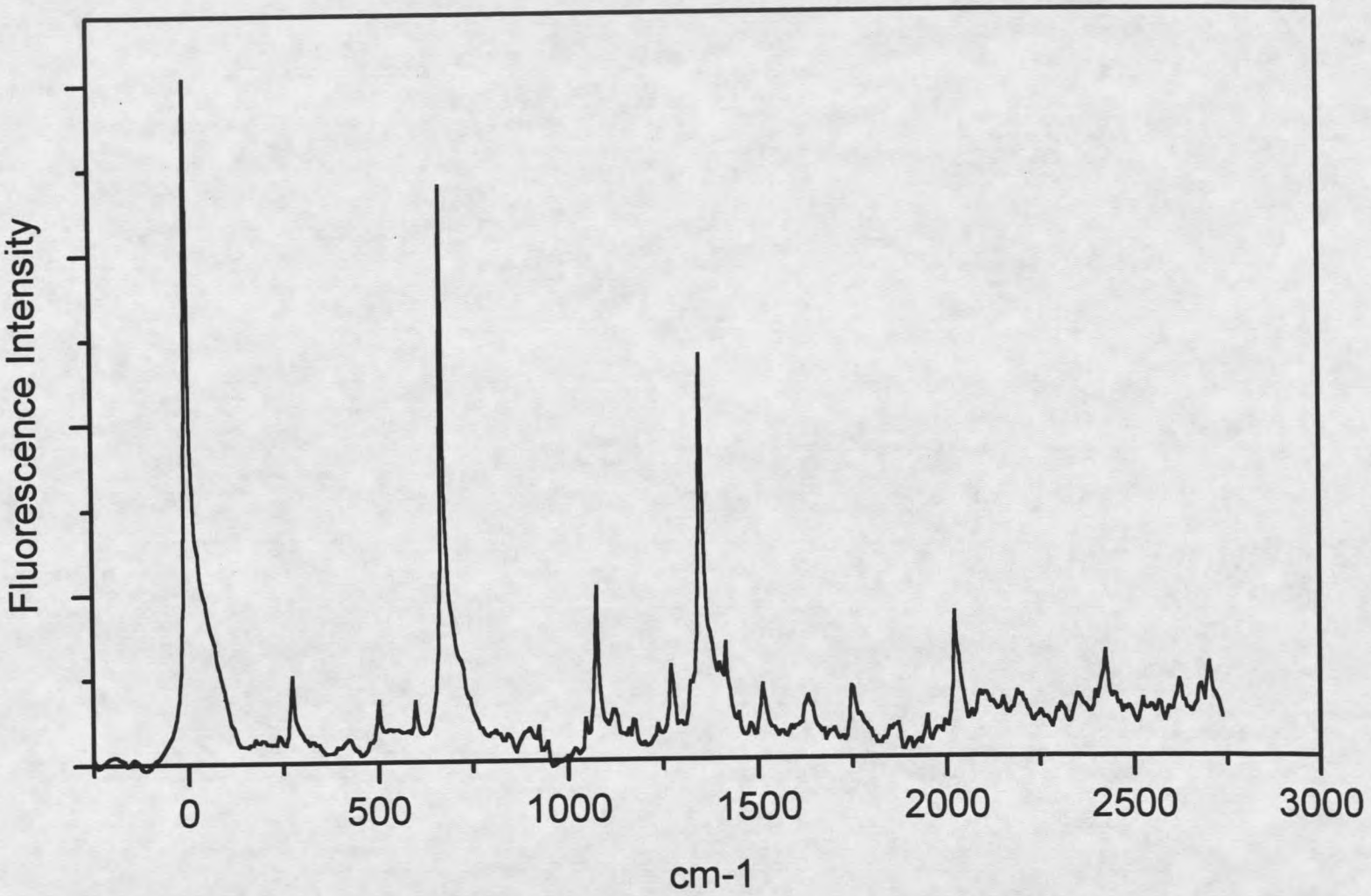

Figure 44. Dispersed fluorescence spectrum of 4FI in argon at 20K.

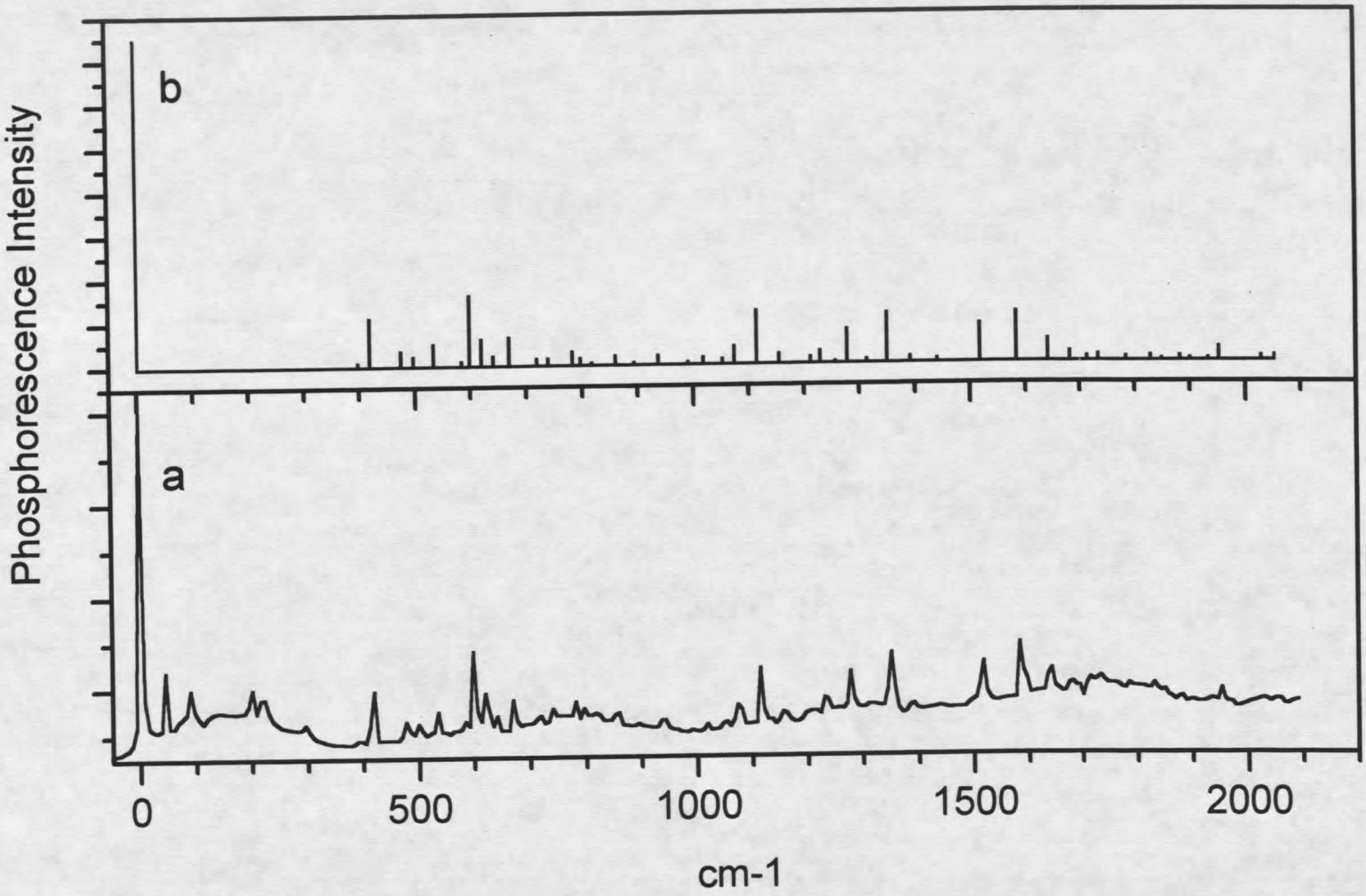

Figure 45. Dispersed phosphorescence spectrum of 4FI in argon at 20k, with ^1L_b origin excitation at 281.89 nm, (a) and the stick spectrum, (b).

energy, also predicted by MOPAC, which estimates a red-shift of 65 cm^{-1}. Also, the other medium strength vibration is the 21^0_1 at 1076 cm^{-1}.

Phosphorescence

The phosphorescence spectrum of 4FI in argon at 20K is shown in Figure 45a with excitation at 281.89 nm, the ^1L_b origin of site 1. The stick spectrum (shown in Figure 45b) was again produced by subtracting the background from the individual line heights. The intensity lying in the first 300 cm^{-1} is considered to be site contamination and subsequently, is not included in the stick spectrum or in the following discussion. The sharp component of the phosphorescence spectrum has linewidths of 10 cm^{-1}, coming from what is believed to be a more ordered site, while the broad background comes from what is believed to be one or more disordered sites.

A triplet ^3L_a origin is found at 395.5 nm (25,284 cm^{-1}) in solid argon which is 350 cm^{-1} higher in energy than that of indole under similar conditions. Line identifications were made by comparing the fluorescence and the phosphorescence spectra. The phosphorescence spectrum has the distinct L_a appearance with stronger intensity in the 27^0_1 line (the strongest line in the spectrum) at 598 cm^{-1} rather than the 26^0_1 line at 669 cm^{-1}, and high intensity in the 28^0_1 line at 498 cm^{-1}. In the higher energy region of the spectrum, the 10^1_0 line (1517 cm^{-1}), the 9^1_0 line (1583 cm^{-1}), and the 8^1_0 line (1641 cm^{-1}) also display high intensity. There are also several other strong lines found at 533, 619,

1114, 1277, and 1350 cm^{-1}. The corresponding line frequencies, intensities, and assignments are found in Table 4.

Table 4. 4-Fluoroindole phosphorescence

Spectral[a] shift (cm^{-1})	Intensity[b]	Assignment	Spectral[a] shift (cm^{-1})	Intensity[b]	Assignment
0.0	7.5		1018	0.15	
397	0.09		1052	0.11	
418	1.1		1073	0.4	
476	0.35		1114	1.2	
498	0.22		1155	0.22	
533	0.5		1212	0.14	
583	0.1		1229	0.27	
598	1.6		1256	0.03	
619	0.6		1277	0.76	
640	0.22		1313	0.07	
669	0.65		1350	1.12	
718	0.15		1391	0.13	
739	0.15		1440	0.07	
782	0.3		1517	0.87	
796	0.15		1583	1.12	
817	0.05		1641	0.5	
859	0.2		1681	0.22	
893	0.05		1713	0.1	
936	0.2		1733	0.14	
990	0.05		1784	0.08	

Table 4. Contiuned

Spectral[a] shift (cm^{-1})	Intensity[b]	Assignment	Spectral[a] shift (cm^{-1})	Intensity[b]	Assignment
1829	0.11		1932	0.05	
1849	0.03		1951	0.3	
1881	0.1		2027	0.1	
1900	0.04		2052	0.11	

a Uncertainty ± 10 cm^{-1}.
b Absolute intensity.

Comparisons Of Properties

There are several tables that summarize much of the data from the above results and discussion section on argon. Table 5 displays the energy difference (Δ value) between the ^1L_a and the ^1L_b states in substituted indoles. Table 7 displays the absolute energies of the ^1L_a, ^1L_b, and ^3L_a states of the seven indoles. Table 6 lists the ground state vibrational energy of modes 28, 27, and 26 for indole, 3MI, 1MI, 2MI, and 4FI. The absolute energies of the ^1L_a and ^1L_b states for the substituted indoles are shown pictorially in Figure 46.

Table 5. The energy differences for the ^1L_a and ^1L_b states of substituted indoles relative to indole.

Molecule	$\Delta\ ^1L_b\ (cm^{-1})^{a,b}$	$\Delta\ ^1L_a\ (cm^{-1})^{a,b}$
Indole	0.0	0.0
3MI	-353	-1194
5MI	-705	-5.0
23DMI	-189	-1439
2MI	-25	-725
1MI	-681	-1331
4FI	+495	-915

a All values are obtained by subtracting indoles values
b Positive value is energy increase and negative values are energy decrease

Table 6. The frequencies of modes 28, 27, and 26.

Molecule	$\nu_{28}\ (cm^{-1})$	$\nu_{27}\ (cm^{-1})$	$\nu_{26}\ (cm^{-1})$
Indole	536.0	601.0	760.0
3MI	471.0	568.0	758.0
2MI	493.2	612.2	659.7
1MI	470.0	573.0	765.0
4FI	470.0	575.6	767.0

Table 7. Site energies for the S_1, S_2, and T_1 states of indoles in argon at 20K.

Molecule	Vacuum (cm^{-1})	Site	S_1 nm(cm^{-1})[a]	S_2 nm (cm^{-1})[b]	T_1 nm (cm^{-1})[c]
Indole	35,294[d]	1	285.5(34,981)	277.2(36,081)	403.4(24,789)
		2	286.6(34,858)		403.8(24,764)
		3	286.4(34,916)		
		4	285.95(34,971)		
		5	285.05(35,081)		401.1(24,933)
3MI	34,882[d]	1	288.78(34,628)	286.6(34,888)	416.5(24,009)
5MI	34,353[d]	1	291.75(34,276)	277.2(36,076)	406.0(24,630)
23DMI	34,843[d]	1	288.6(34,642) ^1L_a	287.4(34,792) ^1L_b	411.2(24,319)
2MI	35,170[d]	1	285.6(35,014)		
		2	285.72(34,999)		
		3	285.91(34,976)		
		4	286.07(34,956)	282.3(35,356)	398.5(25,095)
		5	286.32(34,925)		
1MI	34,546[d]	1	291.55(34,300)	287.7(34,750)	407.4(24,546)
4FI	35,644[e]	1	281.9(35,476)	270.3(36,996)	395.5(25,285)
		2	282.0(35,461)		
		3	282.1(35,448)		
		4	282.4(35,411)		
		5	282.6(35,386)		

a S_1 is the ^1L_b origin unless marked otherwise.
b S_2 is the ^1L_a origin unless marked otherwise.
c T_1 is the ^3L_a origin.
d Hager *et al.*[13].
e Bartis *et al.*[73].

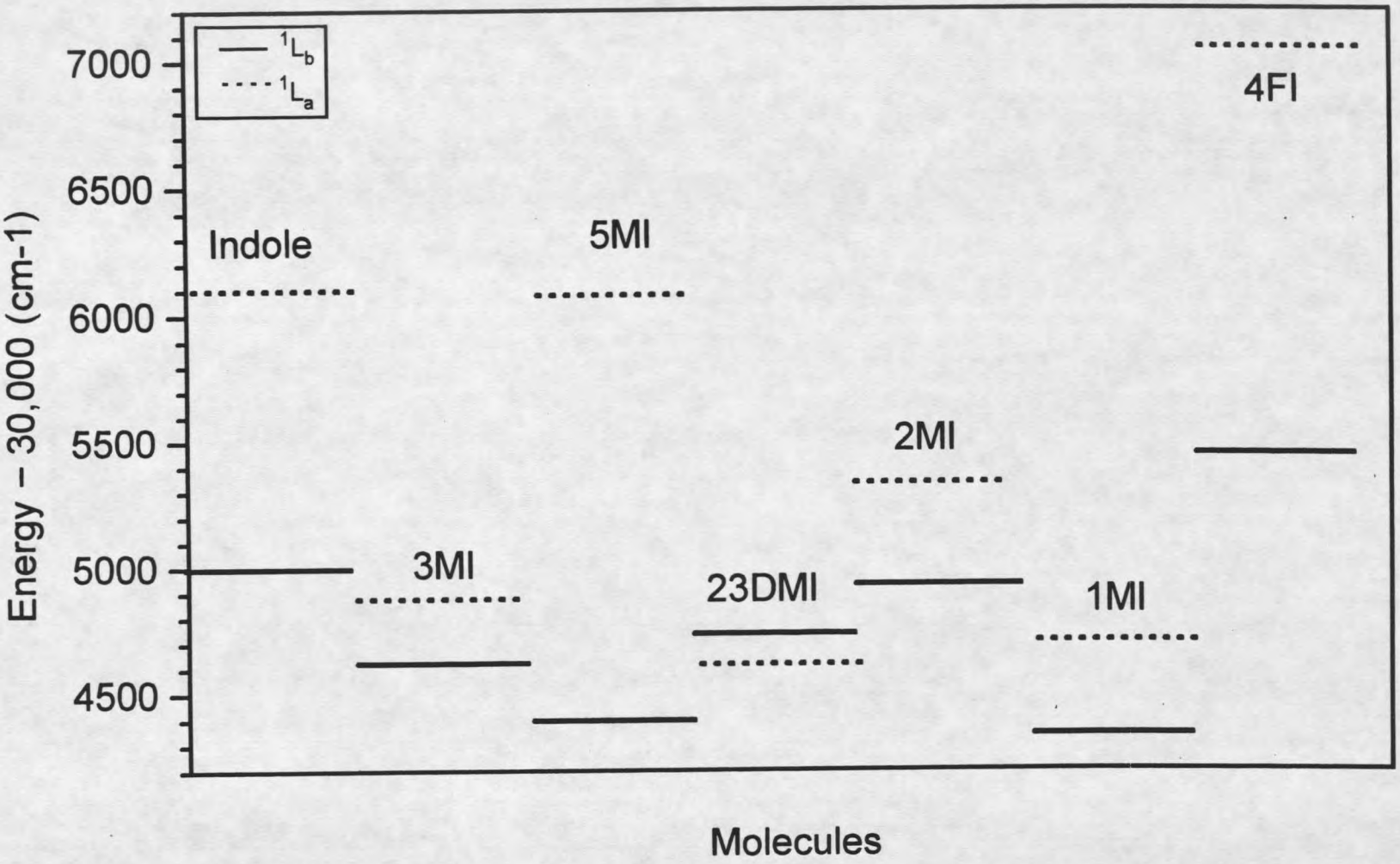

Figure 46. Energies of the ^1L_a and ^1L_b states.

Nitrogen

Nitrogen (N_2) is noted to be another good matrix material[62]. It was found by trial and error that 30K is the best operational temperature for N_2, giving the highest quality matrices needed for polarization measurements. The bulk polarizability of N_2 is ($1.74 * 10^{24}$ cm^3)[74], which is 1.06 times greater than argon. Ab initio calculations, however, predict an anisotropic distribution of polarizability for N_2, with nearly twice the polarizability along the bond axis compared with the other axes of the molecule[76]. This result could greatly affect the local environment indole senses inside the rigid matrix. At temperatures below 35 K, N_2 assumes a cubic close-packing structure, which is isotropic, and above that temperature N_2 assumes a hexagonal structure[75].

Indole in N_2 at 30K

The fluorescence excitation spectrum of indole in N_2 at 30K and the accompanying anisotropy is shown in Figure 47. The spectrum is taken with the monochromator set at 294 nm and, is zeroed to the ^1L_b origin 287nm (34,843 cm^{-1}), and has linewidths of 200 cm^{-1}. The N_2 matrix has stabilized the ^1L_b origin by 150 cm^{-1} and the ^1L_a origin by 700 cm^{-1} over argon, with the ^1L_a origin centered at 400 cm^{-1} above the ^1L_b origin (r=-0.075). This intensity is the ^1L_a origin rather than the vibronically active 28^1_0 line (470 cm^{-1}) because it sits too far to the red and the anisotropy remains low after this point, reflecting the

overlap of the excited states. There is also a discrepancy in the anisotropy ratio, which possibly stems from an experimental artifact of polarizer alignment.

The 26^1_0 line is centered at 720 cm^{-1} with the anisotropy rising from r= -0.075 to r=0.0 over the peak. Little can be determined from this spectrum due to its broadness.

The emission spectra are shown in Figures 48a and 48b with excitation at 280 nm. The emission spectrum in Figure 48a is taken of indole and N_2 layered at 30K with the temperature kept constant during the experiment. The emission spectrum in Figure 48b is taken of indole and N_2 layered at 30K and allowed to cool to 15K before data collection. Both spectra are ^1L_b fluorescence with peaks centered at 760 and 1330 cm^{-1} and linewidths of 200 cm^{-1}. The spectrum in Figure 48b has structure built off the line shape and reveals that at 15K the line shape is made up of closely spaced lines. This difference could come from two sources: the difference in kT or a phase change in the N_2. The latter is a more likely source because N_2 does go through a phase change at 35K at 30K both structures may be present[75]. The phosphorescence spectrum of indole in N_2 at 30K is shown in Figure 49 with excitation at the ^1L_b origin, 287.5 nm. The origin of the ^3L_a triplet state is 403.2 nm (24,801 cm^{-1}), and the spectrum has a linewidth of 200 cm^{-1}. The phosphorescence has the usual L_a appearance.

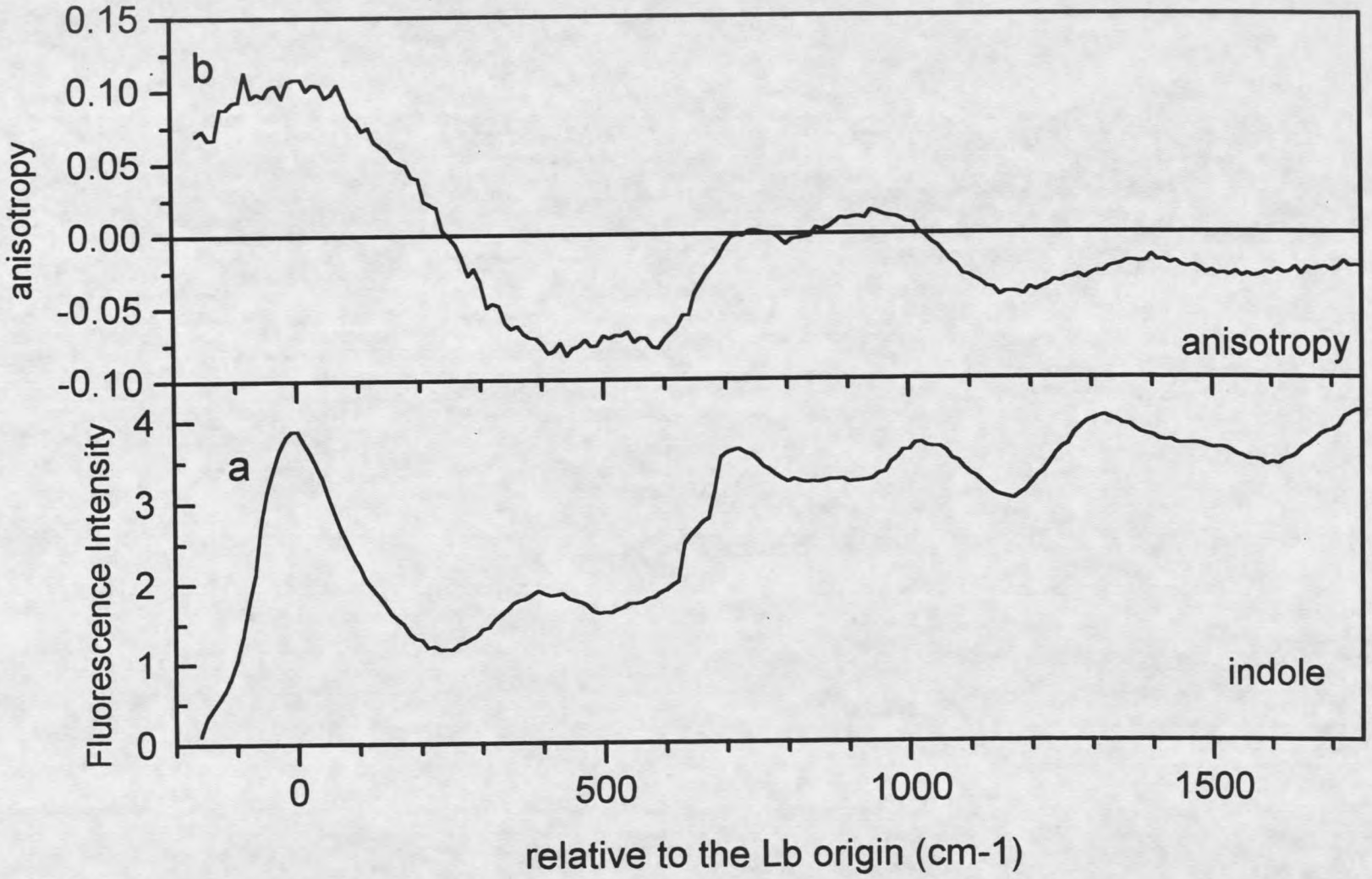

Figure 47. The fluorescence excitation spectrum of indole in N_2 at 30K, (a), and the fluorescence anisotropy, (b).

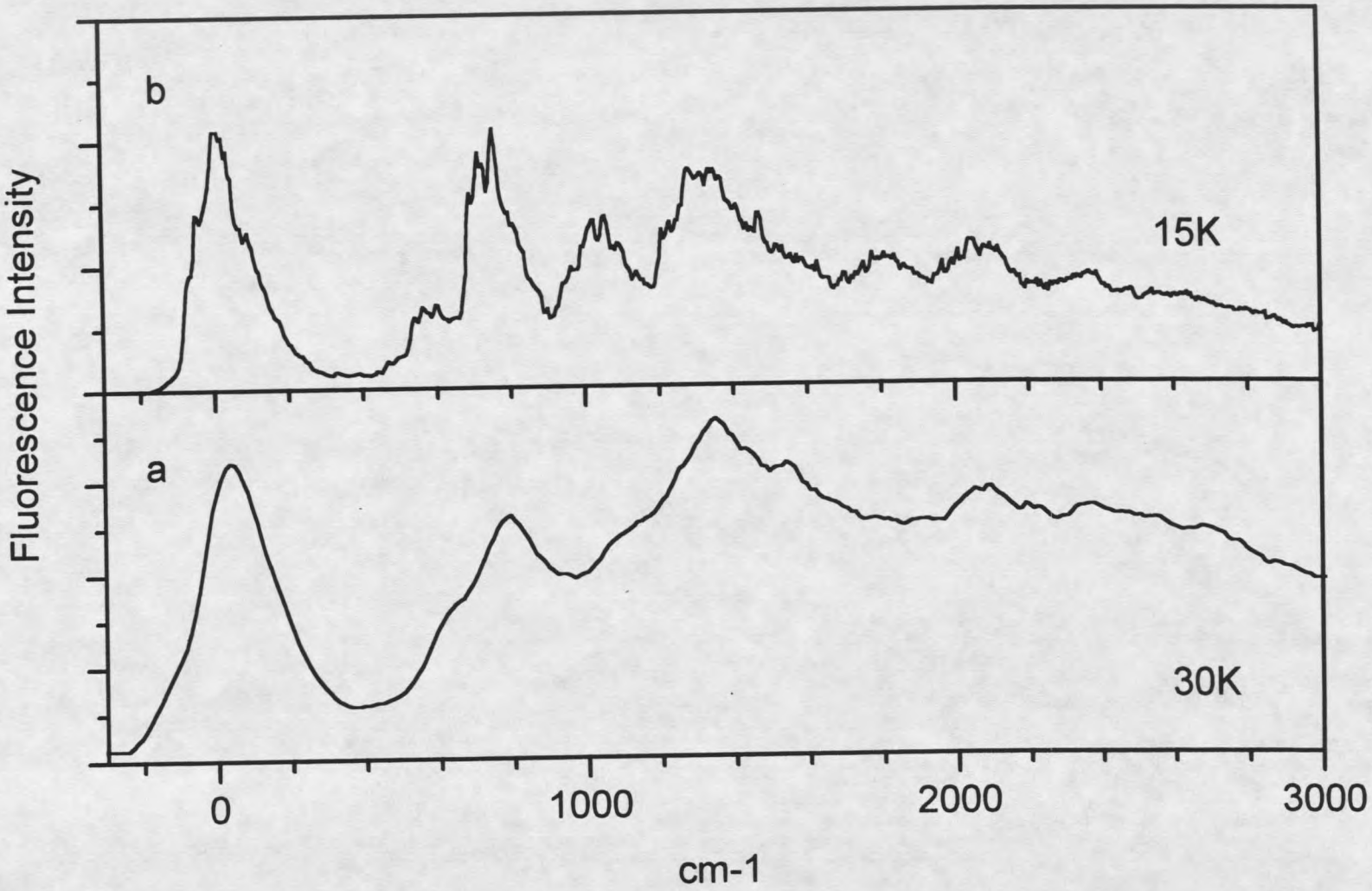

Figure 48 Fluorescence spectra of indole in N_2 at 30K, (a), and N_2 at 15K, (b).

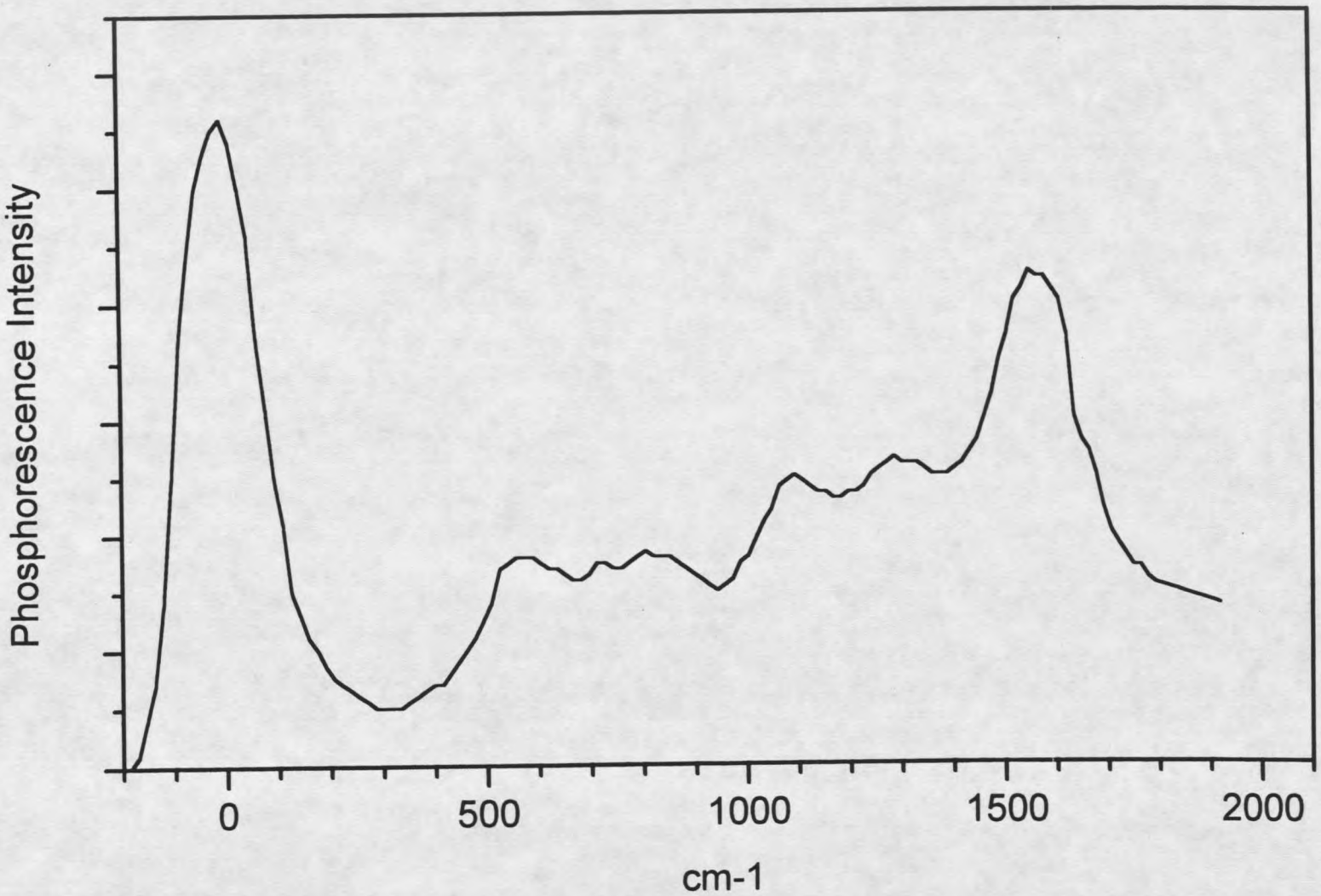

Figure 49. The phosphorescence spectrum of indole in N_2 at 30K.

3-Methylindole In N_2 At 30K

3MI has been found to have one of the smallest ^1L_a-^1L_b energy gaps of any indole studied (260 cm^{-1} in argon). The incorporation of 3MI into N_2 at 30K causes a substantial loss of fluorescence intensity. Because of this loss, the fluorescence excitation and the fluorescence spectra could not be obtained with sufficient accuracy to be reported.

The transmittance spectra (first 1000 cm^{-1}) of 3MI in argon at 20K and 3MI in N_2 at 30K are shown in Figure 50a and 50b respectively. The two spectra are on an absolute wavelength scale for comparison purposes. The argon spectrum in Figure 50a displays two discernable origins, the ^1L_a origin centered at 286.6 nm and the ^1L_b origin centered at 288.8 nm. However, the N_2 spectrum in Figure 50b displays only one broad origin centered at 286.9 nm. The data suggests that the ^1L_a and ^1L_b origins have converged and lie on top of one another. This convergence requires the N_2 to stabilize the ^1L_a origin 30 cm^{-1} and destabilize the ^1L_b origin 190 cm^{-1}, as compared with argon. Contrast this result with the indole case, where both ^1L_a and ^1L_b were more stabilized by N_2. The transmittance of 0.2 ±0.1 for the ^1L_b origin, proves that a good absorption of photons occurs. However, a strong non-radiative process is present and quenches the emission energy.

To make sure that the experimental setup was not causing the problem, the matrix gas was switched to argon and the system purged. During this time,

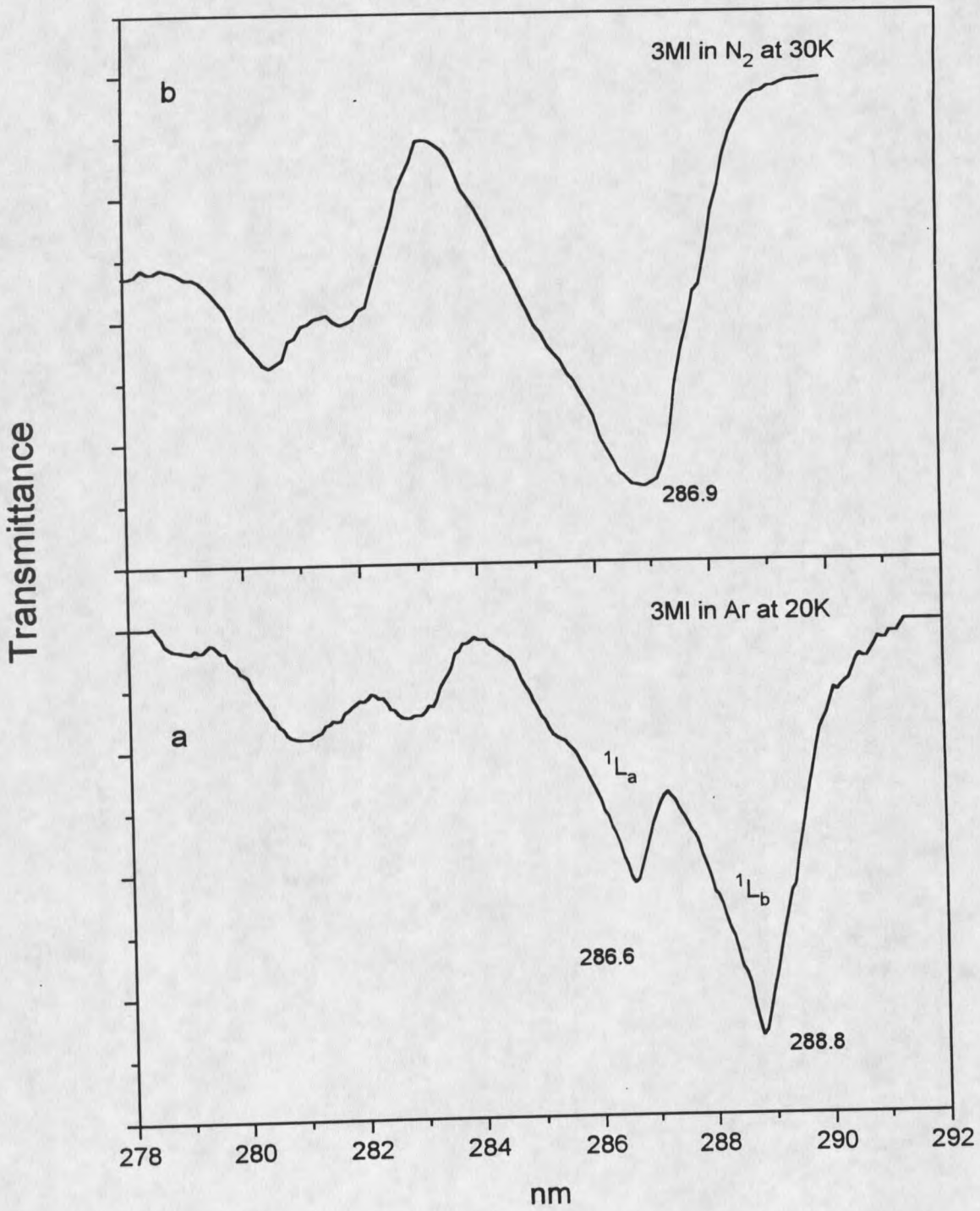

Figure 50. Transmittance spectra of 3MI in argon at 20K, (a), and N_2 at 30K, (b).

no adjustments were made to the experimental setup. The experiment was then run with argon at 20K, and the spectral data matched perfectly 3MI/argon data taken earlier. Several times, the matrix gas was switched back and forth, and the same respective data was obtained. Thus, the experimental setup was ruled out, but the non-radiative process is still a mystery. This non-radiative process must be intrinsic to 3MI in N_2 at 30K, possibly caused by the origin overlap.

3-Methylindole In Ethanol At 15K

There has been some discussion in the literature about the emission of tryptophan in ethanol at 2 K. Scott *et al.*[78] found sharper emission with red-edge excitation on the excitation manifold of tryptophan in ethanol at 2K. Friedman concluded that the sharp emission was coming from the ^1L_b state, where certain molecules on the red-edge had environments that preferentially lowered the ^1L_b over the ^1L_a state[78]. This prediction came as some surprise to us, due to our own understanding and recent literature on similar systems. On similar systems, Eftink and Callis[79] (working on 3MI in propylene glycol at -50^0 C) and Pierce *et al.*[80] (working on N-acetyl-L-tryptophanamide (NATA) in ethanol at 77K), found the fluorescence of both systems to be ^1L_a by anisotropy measurements.

Friedman's interpretation seems inconsistent, so similar experiments on 3MI in ethanol ($8X10^{-5}$ M) at 15K were carried out to end the debate. The room temperature fluorescence spectrum of 3MI in ethanol, shown in Figure 51a, is broad (60 nm) and structureless. The strong interaction between the molecular

dipole and the polar solvent field causes the large Stokes shift. The fluorescence spectrum of 3MI in ethanol at 15K, with excitation at 290 nm (which is 2000 cm^{-1} into the excited-state manifold), is shown in Figure 51b. The fluorescence spectrum blue-shifts and has much more structure than the room temperature spectrum. As the excitation wavelength moves to the red-edge of the excited-state manifold, the fluorescence spectrum red-shifts and displays more structure. Figure 51c displays the fluorescence spectra exciting at 303.5 and 307 nm. Excitation at 303.5 nm produces a fluorescence spectrum with an origin at 308.5 nm and a strong peak centered at 322.3 nm; excitation at 307 nm produces identical features at 310.6 nm and 325.1 nm. Moving the excitation wavelength from 303.5 to 307 nm produces a fluorescence red-shift of 4.0 nm, similar to shifts seen by Azumi[85,71] but no more observable sharpening of the spectra.

Distinguished by its main feature centered at 1500 cm^{-1}, the unresolved Franck-Condon active 8^0_1, 9^0_1, and 10^0_1 modes, the fluorescence is ^1L_a and can be distinguished from its ^1L_b counterpart that would be at 1350 cm^{-1}.

One interesting point to mention, is that the fluorescence spectra taken on the red-edge are not sharper than the fluorescence spectrum taken at 290 nm. This makes sense only if the fluorescence spectrum taken at 290 nm is composed of a superposition of ^1L_a and ^1L_b fluorescence, with the ^1L_b adding a narrow component to the spectrum. This would require the frozen solvent to have certain sites that destabilized the ^1L_a state so that the ^1L_b state emits, which

is possible in frozen ethanol. Also, the fluorescence spectra taken on the red-edge must exclusively emit from the ^1L_a state. Lastly, some of the broadness in Figure 51c could be coming from impurities, which become more influential on red-edge excitation.

The sharpening of the emission of 3MI is due to the red-edge excitation and is not due to the ^1L_b state. Excitation high upon the excited state manifold produces emission from origin excited molecules that are in blue sites (molecules not stabilized much by their environment) and electronic+ vibrational excited molecules that are in red sites (molecules more stabilized by their environment). Therefore, the fluorescence is broad because there are at least two different types of molecules emitting simultaneously. Red-edge excitation selectively excites molecules to their S_1 origin that are in red sites. The emission is sharpened because only one type of molecule emits. We can conclude that the sharp emission that Scott et al.[78] reported as ^1L_b is really just red-edge sharpened ^1L_a emission.

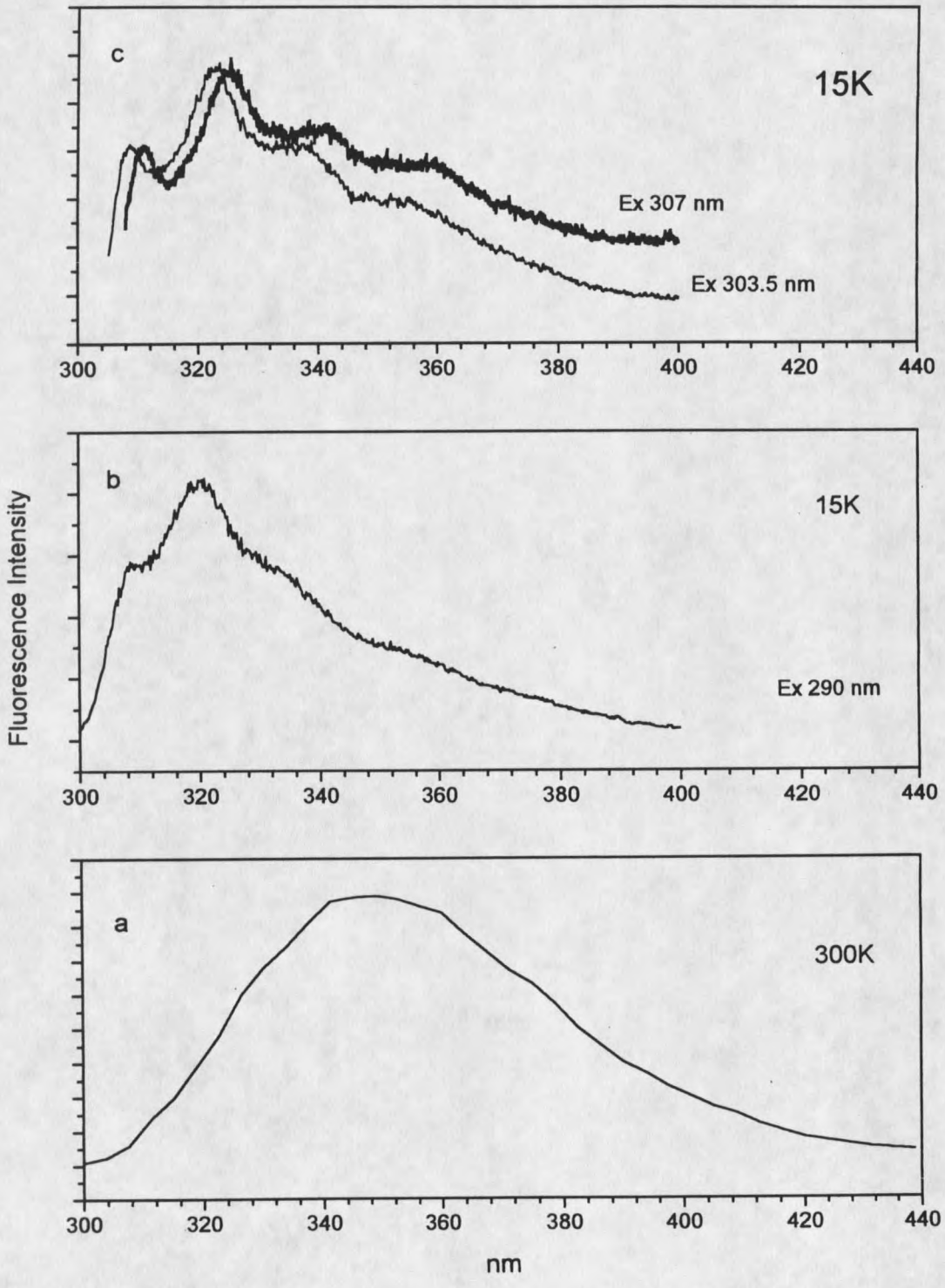

Figure 51. Fluorescence spectra of 3MI in ethanol at 300K, (a), 15K, (b), and red-edge excitation (307 and 303.5 nm) at 15K, (c).

3-Methylindole complexes in a supersonic jet

Water Complex

This experiment repeats work done by Sammeth and Siewart[9], to verify their results and to extend the work. In the jet, high H_2O complex signals (spectral lines) are difficult to achieve without also getting a high background signal caused by clustering. This low signal (intensity) may result from the split origin (2.8 cm^{-1}), giving an appearance of lower intensity since the intensity is distributed over two lines.

The ^1L_a origin for 3MI under jet conditions is within 500 cm^{-1} (from jet data[9] and argon data[81]) of the ^1L_b origin, and the ^1L_a origin is split into several lines. The ^1L_b origin is also affected. Its Ω value shifts from Ω=1.4 for indole to Ω=1.14 for 3MI. The fluorescence excitation spectrum of the 3MI$(H_20)_1$ complex, zeroed to the non-complexed 3MI origin, is shown in Figure 52. The lines all come from the 3MI$(H_2O)_1$ complex, as verified by Huang and Sulkes[17] with mass selection through two-photon ionization. The spectrum inexplicably appears to consist of only one type of complex (either σ or π), which contrasts indole$(H_2O)_1$ where both were present[21].

It is proposed that the complexity of the spectrum comes from a combination of intermolecular modes with the possible ^1L_a origin being in this vicinity. The complex origin is split into a doublet at -234.8 and -232.0 cm^{-1}. This doublet suggests a double well potential, possibly caused by torsion of the

water molecule. The lines at -213.7, -204.3, and -181.4 cm^{-1} are definitely intermolecular modes built off the complex origin (0) with frequencies of 21.8, 30.5, and 53.4 cm^{-1} respectively. The line at -118.4 cm^{-1} is another intermolecular mode (I) with a frequency of 116.4 cm^{-1} and with the same series of intermolecular modes built off the origin at -103.2, -90.0, -86.6, and -83.3 cm^{-1}. It is proposed that the line at -23.6 cm^{-1} is the second quanta of mode (I) and is red-shifted by the close proximity of the ^1L_a origin.

The above scenario is a valid argument; however, some of these lines may be from the ^1L_a origin, which could be in the vicinity. For a listing of the relative line frequencies, intensities, and the Ω values, see Table 8.

Two-photon data was taken to verify measurements made by Sammeth[9]. The two-photon spectrum of $3MI(H_20)_1$ is shown in Figures 53. The non-complexed origin is found to have an Ω=1.08 and the complex origin doublet is found to have an Ω=0.80. These values match Sammeth's data to within experimental error. The complex origin is known to be ^1L_b by inspection of the emission[67].

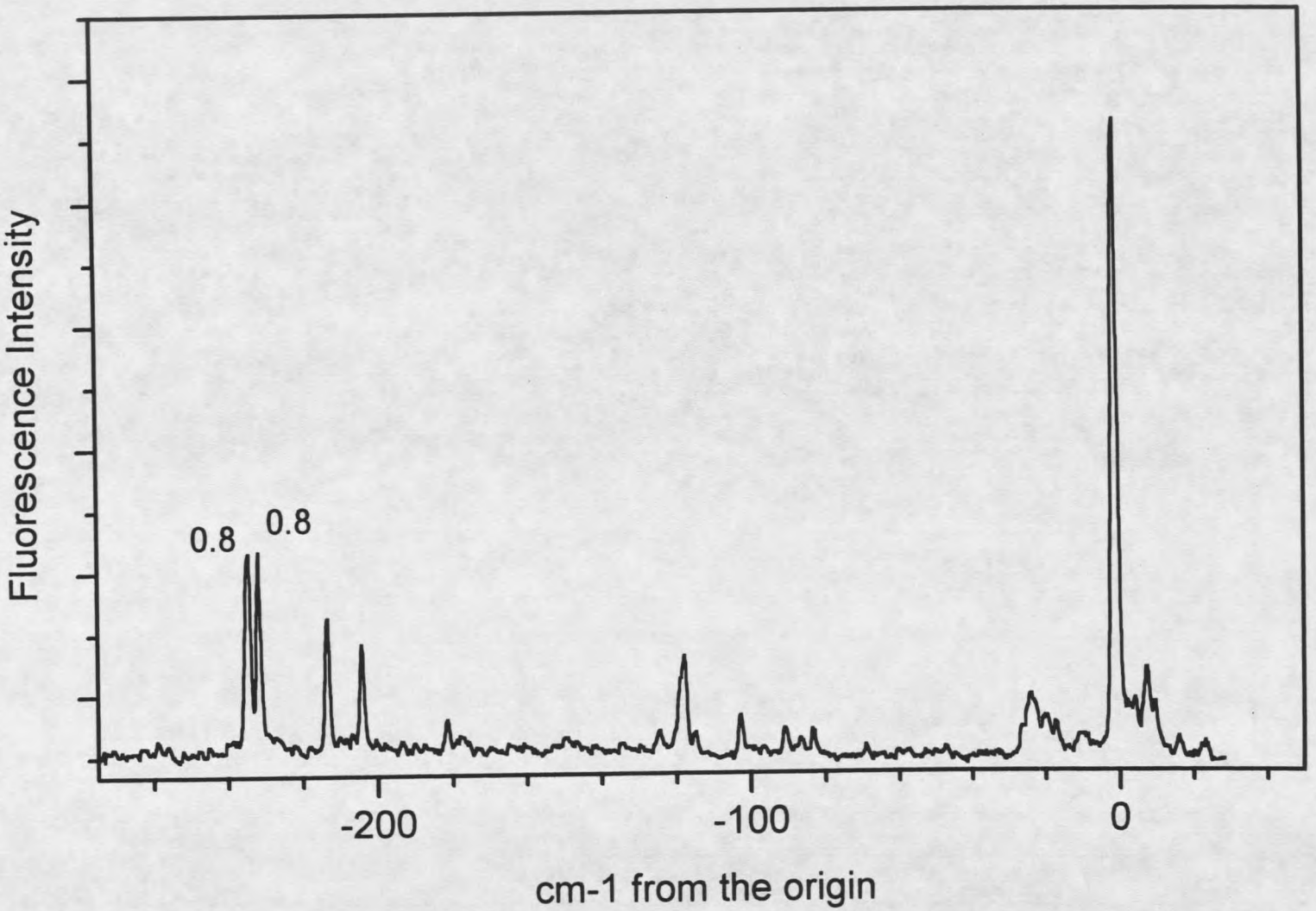

Figure 52. The fluorescence excitation spectrum of 3MI $(H_2O)_1$ in a supersonic jet (with Ω vlaues).

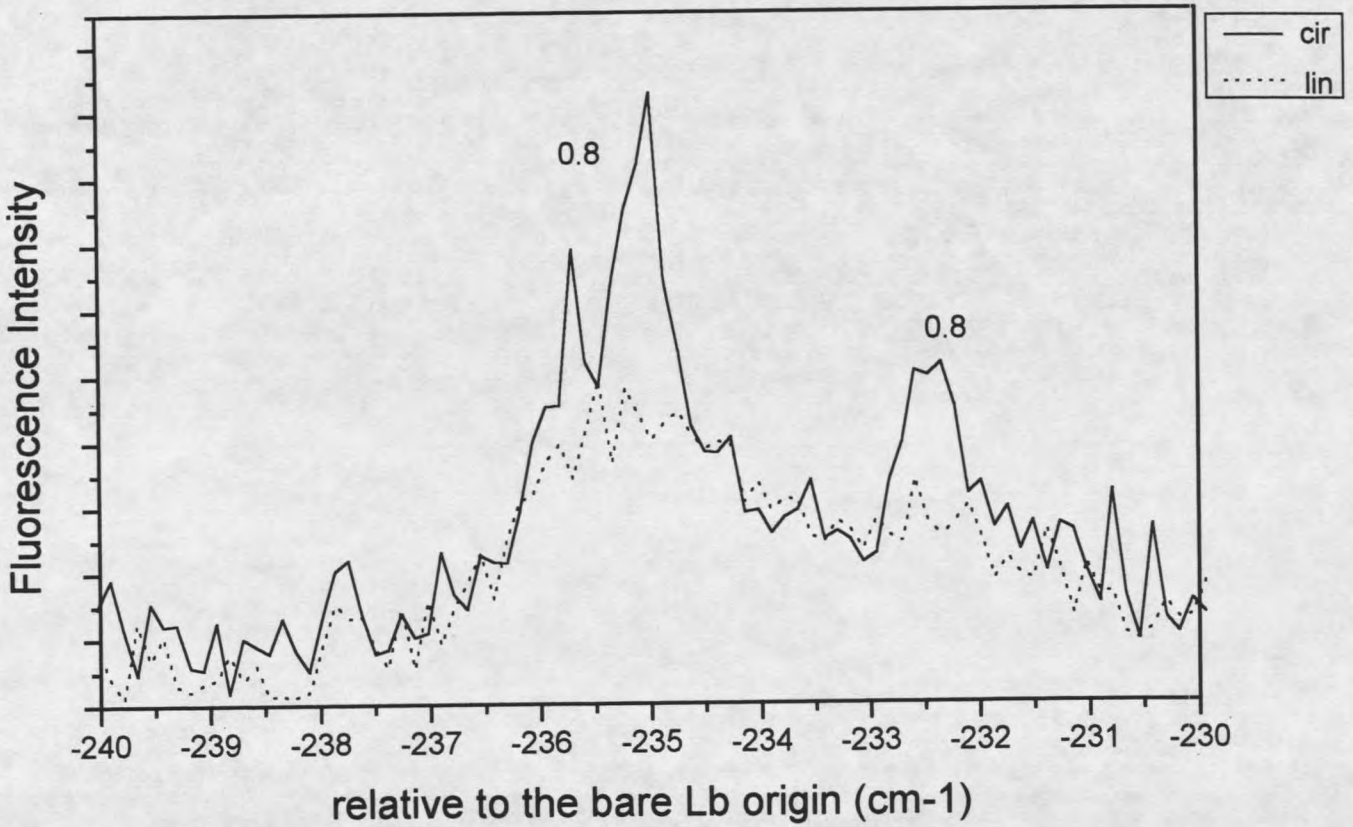

Figure 53. Two-Photon spectrum of $3MI(H_2O)_1$ complex origin (with Ω values).

Table 8. Indole + H_2O

Spectral shift (cm^{-1})	Intensity[a]	Ω^b	Assignment
-234.8	1.00	0.80	0
-232.0	0.84	0.80	0
-213.7	0.71		
-204.3	0.64		
-181.4	0.42		
-124.8	0.56		
-118.4	0.89		I
-103.2	0.38		
-90.9	0.38		
-86.6	0.27		
-83.3	0.35		
-23.6	1.85		2I
-10.0	0.50		
0.0	2.95	1.1	

a Relative to the origin of complex I
b Omega value uncertainty ±.1

Methanol Complex

Because Sammeth and Siewart[9] never experimented with this complex, and to obtain a more complete picture, the work was extended to methanol. Care had to be taken to limit the amount of methanol in the jet to achieve good complex formation, and residual water contamination in the system was observed and subtracted out.

The 3MI(methanol)$_1$ fluorescence excitation spectrum, zeroed to the non-complexed 3MI origin, is shown in Figure 54. Through mass resolved jet data[17],

the spectral lines are from the 3MI(methanol)$_1$ complex and the intermolecular progressions can be seen built off all 3MI molecular normal modes. The spectrum is also apparently made up of only one type of complex (either σ or π), which is contrasted with indole(methanol)$_1$ where both types were present[21]. The small lines sitting at -331.0 cm^{-1} and -312.9 cm^{-1} are most likely from contamination. The strong complex origin (0) lying at -289.6 cm^{-1} is nearly 40% of the non-complexed origin with a three-quanta progression of v_1 (21 cm^{-1}) at -268.3, -247.2, and -226.3 cm^{-1}. Intermolecular mode (I) is at -153.5 cm^{-1} with a frequency of 136.1 cm^{-1} and a two quanta of v_1 (21 cm^{-1}) progression at -132.1 and -111.3 cm^{-1}. Intermolecular mode (II) is at -87 cm^{-1} with frequency of 202. 6 cm^{-1}, and a two quanta v_1 progression at -65 and -41.6 cm^{-1}. Intermolecular mode (III) is at -82.2 cm^{-1} with a frequency of 207.4 cm^{-1} and a two quanta of v_2 (23 cm^{-1}) progression at -59.2 and -36.3 cm^{-1}. There may be some complications here in assignment because of the close proximity of the ^1L_a origin. The relative line frequencies, intensities, and the Ω values are found in Table 9.

The two-photon excitation spectra are shown in Figures 55 and 56. The complex origin at -289.6 cm^{-1} has an Ω=0.80, and the first 2 quanta at -268.3 and 247.2 cm^{-1} also have an identical Ω=0.80. The complex origin is believed to be ^1L_b by inspection of the fluorescence[67].

The data from the strong 3MI-methanol Franck-Condon progression at -289.6 cm^{-1} can be used to deduce the equilibrium geometry difference between the ground and excited states. The one assumption is that the vibration is

strictly an intermolecular vibration between the methanol and 3MI. The following derivation will follow the method used by Muino[21]. The Franck-Condon intensity distribution is given by the following equation:

$$I = \frac{\lambda^n}{n!} e^{-\lambda} = f_{0\to m} , \tag{19}$$

where λ is the spring energy induced by excitation(in units of hω) and is related to the intensity ratio between the origin and the first quanta of the progression:

$$\frac{f_{0\to 1}}{f_{0\to 0}} = \frac{\lambda e^{-\lambda}}{e^{-\lambda}} = \lambda . \tag{20}$$

From the data in Table 9, λ is measured to be 0.667. From λ, the dimensionless displacement, s, is calculated ($s=2\lambda^{1/2}$) to be 1.15. From s, the equilibrium geometry difference, ΔQ, can be calculated:

$$\Delta Q = S\sqrt{\frac{h}{\omega\mu}} = 1.15\sqrt{\frac{33.715 \text{Å}^2 amu\ cm^{-1}}{21 cm^{-1}\ 25.75 amu}} = 0.29 \pm 0.02 \text{Å} \tag{21}$$

where μ, 25.75 amu, is the reduced mass of the 3MI-methanol system. The uncertainty in the displacement in Equation 20 comes from uncertainty in the measured frequencies and the relative intensities. The calculated displacement of 0.29± 0.02 Å for 3MI(methanol)$_1$ complex is between the displacements values Muino calculated for the π-complex (0.42 ± 0.04 Å) and the σ-complex (0.15 ±

0.02 Å) of indole$(H_2O)_1$ complex[21].

Table 9. Indole + Methanol

Spectral shift (cm^{-1})	Intensity[a]	Ω^b	Assignment
-289.6	1.00	0.8	0
-268.3	0.73	0.8	$0,1v_1$(21 cm^{-1})
-247.2	0.31	0.8	$0,2v_1$
-226.3	0.14		$0,3v_1$
-153.5	0.40		I
-132.1	0.31		$I,1v_1$
-111.3	0.14		$I,2v_1$
-87.0	0.22		II
-82.2	0.37		III
-65.0	0.23		$II,1v_2$(23 cm^{-1})
-59.2	0.43		$III,1v_2$
-41.6	0.15		$II,2v_2$
-36.3	0.24		$III,2v_2$
0.0	3.41	1.1	

a relative to the origin of complex II
b Omega value uncertainty ±.1

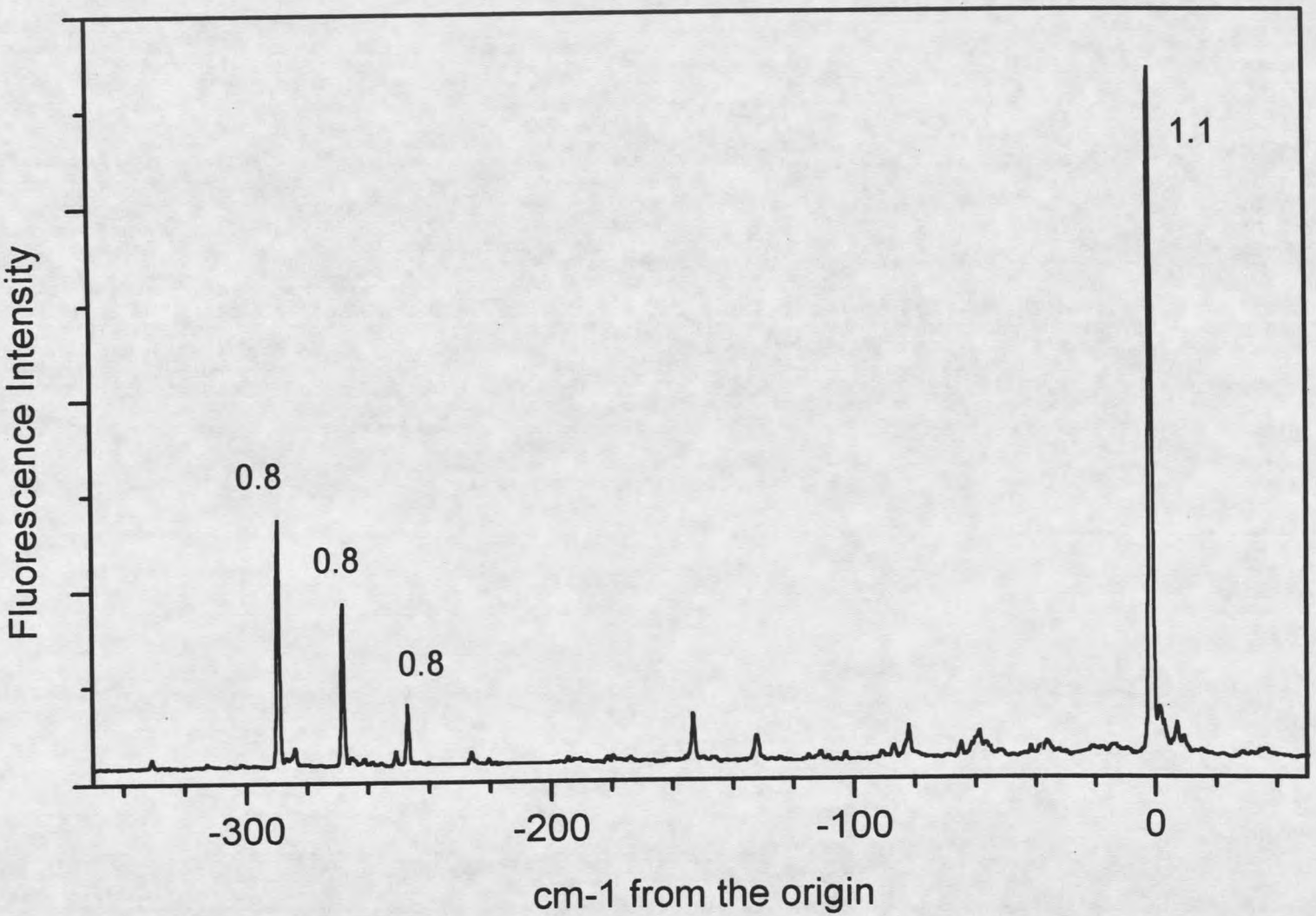

Figure 54. The fluorescence excitation spectrum of 3MI(methanol)$_1$ in a supersonic jet (with Ω vlaues).

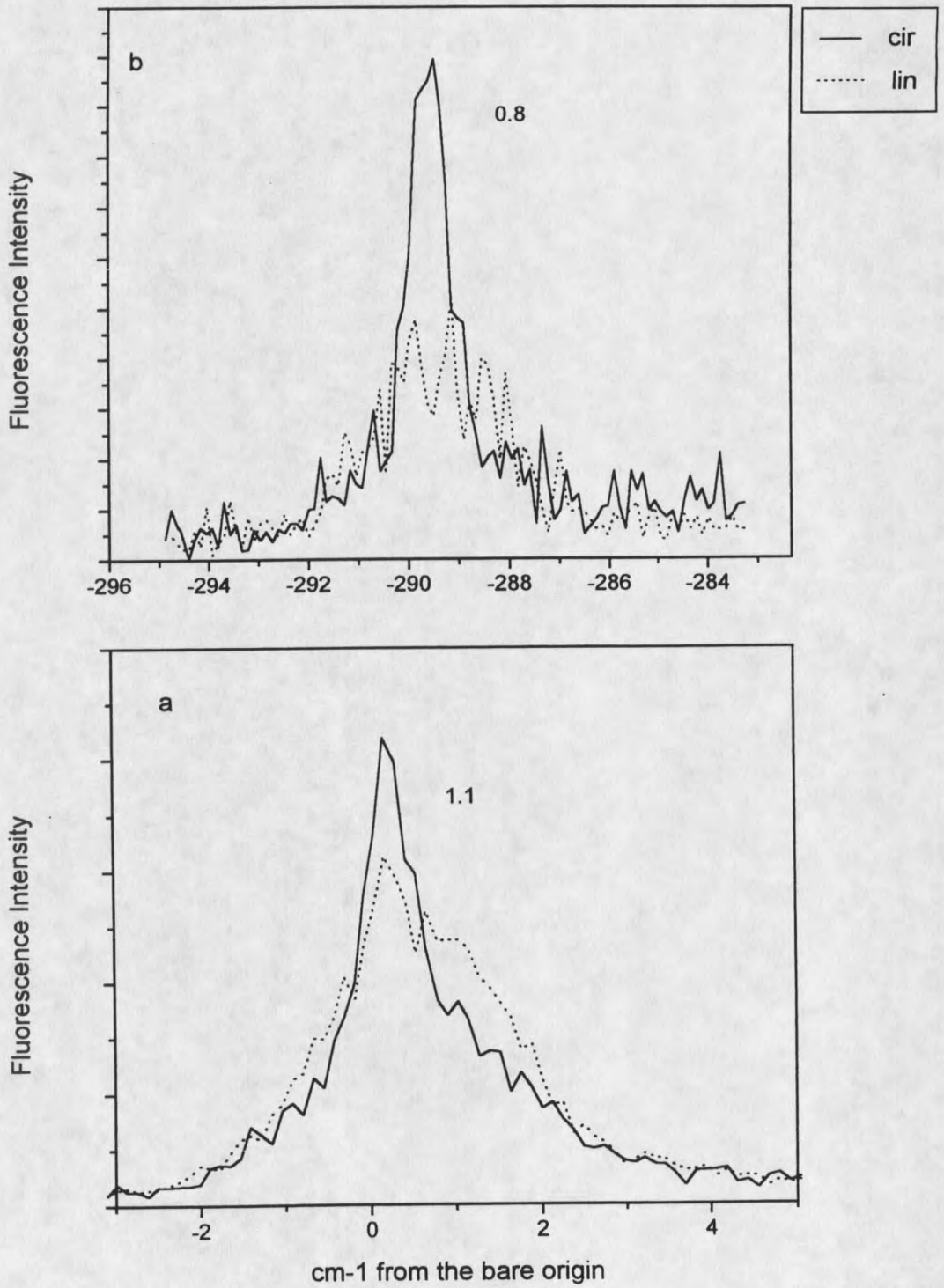

Figure 55. Two-photon spectra of the bare 3MI origin, (a) and 3MI(methanol)$_1$ complex origin, (b), (with Ω values).

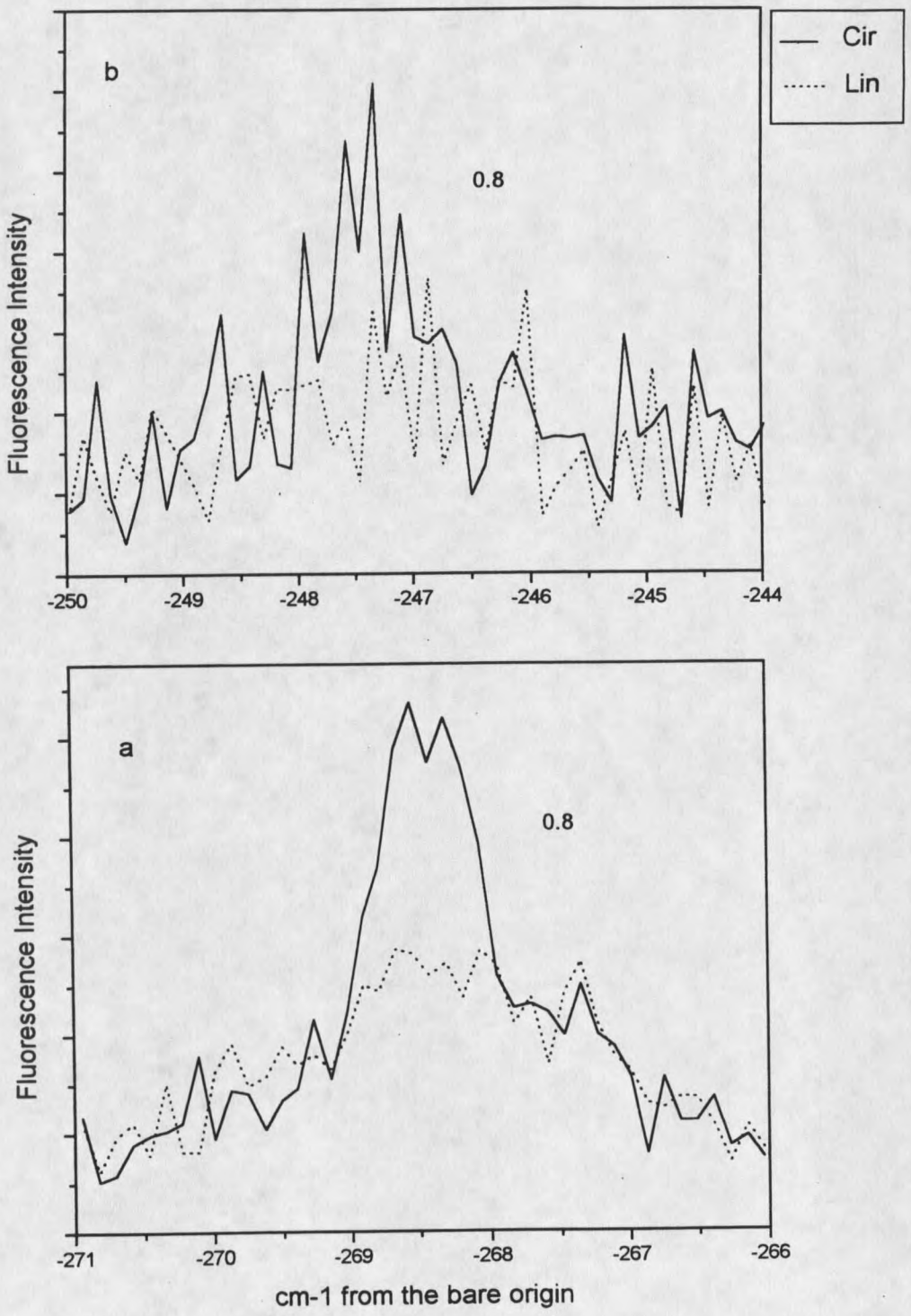

Figure 56. Two-photon spectra of the first quanta at -268.3 cm^{-1}, (a), and the second quanta at -247.2 cm^{-1}, (b), (with Ω values).

Chapter 5

SUMMARY

The purpose of this work was to identify the locations of the true ^1L_a origins. The ^1L_a origin of indole is 1100-1300 cm^{-1} above the ^1L_b origin in solid argon and is distinguished from the false origin at 455 and 480 cm^{-1} (jet) by differential solvent shifts in the matrix. The jet's false origin at 455 and 480 cm^{-1}, "the red herring", is a Fermi doublet and Herzberg-Teller vibronically coupled to the ^1L_a manifold. Incorporation into the argon also caused sharp phosphorescence giving the Franck-Condon factors for L_a emission, which helps complete the indole picture.

For 3-methylindole, which best represents tryptophan, the ^1L_a origin is 260 cm^{-1} above the ^1L_b origin and is not split. This energy separation is extremely small, and even changing the matrix environment from argon to N_2 causes the origins to converge. Therefore, in most proteins, tryptophan would emit exclusively from the ^1L_a state. However, if ^1L_b fluorescence is observed, then it could be deduced that a local electric field exists across the indole that blue-shifts the ^1L_a state.

For 2,3DMI, the combination of the methyl groups causes an inversion of the states, with the ^1L_a state being lowest in energy. This molecule is the only

indole studied here that gives ^1L_a fluorescence. The ^1L_a origin lies above the ^1L_b origin for the rest of the substituted indoles: 5MI (1800 cm^{-1}), 2MI (400-600 cm^{-1}), 1MI (430-600 cm^{-1}), and 4FI (1520 cm^{-1}).

This research included seven different substituted indoles forming a large data base on the electronic and vibrational energies (Tables 7, 8, and 9). There are a few outstanding examples: methylation in the 5-position stabilizes the ^1L_b state only, with an ^1L_b red-shift of 705 cm^{-1} and an ^1L_a shift of only 5 cm^{-1}. On the other hand, methylation in the 2-position almost exclusively stabilizes the ^1L_a state, with an ^1L_a red-shift of 725 cm^{-1} and an ^1L_b red-shift of 25 cm^{-1}: for 3MI, the ^1L_a is stabilized by 1193 cm^{-1}, three times greater than the ^1L_b stabilization; 1MI stabilizes the ^1L_a state by 1331 cm^{-1}, twice as great as the ^1L_b; and, 2,3DMI stabilizes the ^1L_a state by 1439 cm^{-1}, seven times greater than that of the ^1L_b. The addition of a fluorine to the 4-position causes the ^1L_b state to blue-shift by 495 cm^{-1} and the ^1L_a state by 915 cm^{-1}.

REFERENCES

1. S. V. Konev, Fluorescence and Phosphorescence of Proteins and Nucleic Acids, (Plenum Press, New York, 1967).

2. G. Weber, *Biochem. J.*, 75, 335(1960).

3. J. R. Platt, *J. Chem. Phys.*, 17, 484(1949).

4. B. Valeur and G. Weber, *Photochem. PhotoBiol.*, 25, 441(1977).

5. P. R. Callis, *J. Chem. Phys.*, 95, 4230(1991).

6. M. R. Eftink, Z. Chen, *J. Of Fluor.*, 4, 165(1994).

7. E.H. Strickland, C. Billup, E. Kay, *Biochemistry*, 11, 3657 (1972).

8. E.H. Strickland, J. Horwitz, C. Billups, *Biochemistry*, 9, 4914 (1970).

9. D.M. Sammeth, Ph. D. Thesis, Montana State University (1992).

10. G.A. Bickel, D.R. Demmer, E.A. Outhouse, S.C. Wallace, *J. Chem. Phys.*, 91, 6013(1989), and supplementary material.

11. D. R. Demmer, G. W. Leach, A. Outhouse, J. W. Hager, and S. C. Wallace, *J. Phys. Chem.*, 94, 582(1990).

12. J. Hager and S. C. Wallace, *J. Phys. Chem.*, 88, 5513(1984).

13. J. W. Hager, D. R. Demmer, and S. C. Wallace, *J. Phys. Chem.*, 91, 1375(1987).

14. J. Hager, S. C. Wallace, *J. Phys. Chem.*, 87, 2121(1983).

15. G. A. Bickel, G. W. Leach, D. R. Demmer, J. W. Hager, and S. C. Wallace, *J. Chem. Phys.*, 88, 1(1988).

16. D. R. Demmer, G. W. Leach, and S. C. Wallace, *J. Phys. Chem.*, 98, 12834(1994).

17. Y. Huang and M. Sulkes, *J. Phys. Chem.*,100, 16479(1996).

18. A.A. Rehms, Ph. D. Thesis, Montana State University, (1990).

19. D. Sammeth, S. Yan, L. Spangler, P. Callis, *J. Phys. Chem.*, 94,

7340(1990).

20. J. R. Cable, *J Chem. Phys.*, 92, 1672(1990).

21. P.L. Muino, Ph. D. Thesis, Montana State University (1993).

22. D. Sammeth, S. Siewert, P. Callis, L. Spangler, *J. Chem. Phys.*, 96 5771(1992).

23. M. Bronskill, J. Wong, *Biochem.*, 249, 305 (1988).

24. Y. Chem, R. L. Rich, F. Gai, and J. W. Petrich, *J. Phys. Chem.*, 97, 1770(1993).

25. F. Gai, R. L. Rich, and J. W. Petrich, *J. Am. Chem. Soc.*, 116, 735(1994).

26. R. L. Rich, Y. Chen, D. Neven, M. Negrerie, F. Gai, and J. W. Petrich, *J. Phys. Chem.*, 97, 1781(1993).

27. N. H. Ayachit, A. M. Huralikoppi, and M. A. Shashidhar, *Spectrochimica Acta.*, 42A, 781(1986).

28. T. L. O. Barstis, L. I. Grace, T. M. Dunn, and D. M. Lubman, *J. Phys. Chem.*, 98, 4261(1994).

29. L. Andrews, R.S. Friedman, and B. J. Kelsall, *J. Phys. Chem.*, 89, 4550(1985).

30. H. Riesen, E. Krausz, A. Zilian, and H. U. Gudel, *Chem. Phys. Lett.*, 182, 271(1991).

31. J. Agreiter, A. M. Smith, and V.E. Bondybey, *Chem. Phys. Lett.*, 241, 317(1995).

32. K. Palewski, E. C. Meister, and U. P. Wild, *J. Of Luminescence*, 50, 47(1991).

33. K. Palewski, J. Lipinski, J. Sworakowski, J. Sepiol, H. Gygax, E. C. Meister, U. P. Wild, *J. Phys. Chem.*, 99, 16835(1995).

34. A. Kawski, I. Gryczynski, Z. Gryczynski, *Z. Naturforsh*, 49A, 1091(1994).

35. P. Ilich and S. Sedarous, *Spectroscopy Lett.*, 27, 1023(1994).

36. M. Gutman, P.F. Schonzart, G. Hohlneicher, *Chem. Phys.*,140, 107(1990).

37. M.S. Gudipati, J. Paverkausen, G. Hohlmeicher, *Chem Phys.*, 173, 143(1993).

38. P.R. Callis, J.T. Vivian, L.S. Slater, *Chem. Phys. Lett.* (1995), in press.

39. A. Kawski, *Critical Review in Anal. Chem.*, 23, 459 (1993).

40. F. Perrin, *La Fluoresence des solution. Induction Moleculaire. Polarisotion et duree d'emission - Photochimie, Ann. Phys.* 12, 169 (1929).

41. A. Jablonski, *Postepy Fiz.*, 18, 663(1967).

42. L. Onsager, *J. Am. Chem. Soc.* 58, 1486 (1936).

43. Y. Ooshika, *J. Phys. Soc. Jpn.* 9, 594 (1954).

44. N. Mataga, Y. Kaifu, and M. Koizumi, *Bull. Chem. Soc. Jpn.*, 28, 690 (1955).

45. N. Mataga, Y. Kaifu, and M. Koizumi, *Bull. Chem. Soc. Jpn.*, 29, 465(1956).

46. E. Lippert, *Z. Naturforsch. Teil A*,10, 541 (1955).

47. E. Lippert, *Z. Phys. Chem.*, 6, 125 (1956).

48. E. G. McRae, *J. Phys. Chem.* 61, 562 (1957).

49. E. G. McRae, *Spectrochim. Acta*. 12, 192 (1958).

50. A. Penner, A. Amirav, J. Jortner, A. Nitzan, and J. Gersten, *J. Chem. Phys.*, 93, 147(1990).

51. R. Fraenkel, U. Samuni, Y. Haas, and B. Dick, *Chem. Phys. Lett.*, 203, 523(1993).

52. J. N. Murrell, The Theory of the Electronic Spectra of Organic Molecules, (John Wiley and Sons Inc., New York, 1963)

53. J. Wolf, G. Hohlneicher, *Chem. Phys.*, 181, 185(1994).

54. M. Goppert-Mayer, *Ann. Rev.*, 9, 273(1929).

55. W. M. McClain, *J. Chem. Phys.*, 57, 2264 (1972).

56. W. M. McClain, *J. Chem. Phys.*, 55, 2789 (1971).

57. P. R. Monson and W. M. McClain, *J. Chem. Phys.*, 53, 29(1970).

58. P. R. Callis, *J. Chem. Phys.*,99, 27(1993).

59. B. E. Anderson, Ph. D. Thesis, Montana state University, (1983).

60. R. Fraenkel and Y. Haas, *J. Chem. Phys.*, 100, 4324(1994).

61. R. Fraenkel and Y. Haas, *Chem. Phys.*, 186, 185(1994).

62. B. Meyer, Low Temperature Spectroscopy, (American Elsevier Pub.Co.,Inc., New York, 1971).

63. R. D. Jones and P. R. Callis, *J. Appy. Phys.* 64, 4301(1988).

64. S.R. Meech, D. Phillips and A.G. Lee, *Chem. Phys.* 80, 317(1983).

65. H. Lami and N. Glasser, *J. Chem. Phys.* 84,597(1986).

66. B.J. Fender, D.M. Sammeth, P.R. Callis, *Chem. Phys. Lett.*,239, 31 (1995).

67. K. Short and P. R. Callis, unpublished results.

68. D. K. Hahn and P.R. Callis, *J. Phys. Chem. A*, 101, 2686(1997).

69. R. L. Williamson and A. L. Kwiram, *J. Chem. Phys.*, 88, 6092(1988).

70. E. H. Strickland and C. Billups, *Bioploymers*, 12, 1989(1973).

71. T. Azumi, K. Itoh, and H. Shiraishi, *J. Chem. Phys.*, 65, 2550(1976).

72. L. Brand and M. L. Johnson, Methods of Enzymology, Vol 278 (Academic Press Inc., San Diego, 1997).

73. T. Barstis, L. Grace, T. Dunn, D. Lubman, *J. Phys. Chem.*, 98, 4261(1994).

74. R. C. Weast, M. J. Astle, W. H. Beyer, CRC Handbook of Chemistry and Physics, (CRC Press, Inc., Boca Raton, 1986).

75. R. W. G. Wyckoff, Crystal Structure, (Interscience Publisher, New York, 1963).

76. B. J. Fender and P. R. Callis, unpublished results.

77. J. Khademi, M. Fischer, B. Kapelle and V.A. Apkarian, *J. Phys. Chem.* 91, 6526 (1987).

78. T.W. Scott, B.F. Campbell, R.L. Cone, and J.M. Friedman, *Chem. Phys.*, 131, 63(1989).

79. M.R. Eftink, L.A. Selvidge, P.R. Callis, and A.A. Rehms, *J. Phys. Chem.*, 94, 3469(1990).

80. D.W. Pierce and S.G. Boxer, *Biophysical J.*, 68, 1583(1995).

81. B. Fender and P. R. Callis, *Chem. Phys. Lett.*, 262, 343(1996).

82. A. A. Rehms and P. R. Callis, *Chem. Phys. Lett.*, 140, 83(1987).

83. Y. Huang and M. Sulkes, *Chem. Phys. Lett.*, 254, 242(1996).

84. N. Glasser and H. Lami, *J. Chem. Phys.*, 74, 6526(1981).

85. K. Itoh and T. Azumi, *J. Chem. Phys.*, 62, 3431(1975).

86. P. L. Muino and P. R. Callis, *J. Chem. Phys.*, 100, 4093(1994).

MONTANA STATE UNIVERSITY LIBRARIES
3 1762 10293209 0